

RADC-TR-88-328
Final Technical Report
March 1989



AD-A208 521

**TIME DEPENDENT DIELECTRIC
BREAKDOWN OF SILICON DIOXIDE
UNDER CONSTANT TUNNELING
CURRENT STRESS**

DTIC
ELECTE
MAY 24 1989
S H D

SGS-Thomson Microelectronics, Inc.

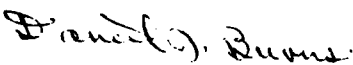
**Dr. Fu-Tai Liou, D.A. Tiffin, F.R. Bryant, R.L. Hodges, J.W. Staman III,
J.A. Michlowsky, W.A. Williams III**

APPROVED FOR PUBLIC RELEASE; DISTRIBUTION UNLIMITED.

ROME AIR DEVELOPMENT CENTER
Air Force Systems Command
Griffiss Air Force Base, NY 13441-5700

This report has been reviewed by the RADC Public Affairs Division (PA) and is releasable to the National Technical Information Service (NTIS). At NTIS it will be releasable to the general public, including foreign nations.

RADC-TR-88-328 has been reviewed and is approved for publication.

APPROVED: 
DANIEL J. BURNS
Project Engineer

APPROVED: 
JOHN J. BART
Technical Director
Directorate of Reliability & Compatibility

FOR THE COMMANDER:



JAMES W. HYDE III
Directorate of Plans & Programs

If your address has changed or if you wish to be removed from the RADC mailing list, or if the addressee is no longer employed by your organization, please notify RADC (RBRP) Griffiss AFB NY 13441-5700. This will assist us in maintaining a current mailing list.

Do not return copies of this report unless contractual obligations or notices on a specific document require that it be returned.

UNCLASSIFIED

SECURITY CLASSIFICATION OF THIS PAGE

REPORT DOCUMENTATION PAGE				Form Approved OMB No. 0704-0188	
1a. REPORT SECURITY CLASSIFICATION UNCLASSIFIED			1b. RESTRICTIVE MARKINGS N/A		
2a. SECURITY CLASSIFICATION AUTHORITY N/A			3. DISTRIBUTION/AVAILABILITY OF REPORT Approved for public release; distribution unlimited		
2b. DECLASSIFICATION/DOWNGRADING SCHEDULE N/A			4. PERFORMING ORGANIZATION REPORT NUMBER(S) N/A		
5. MONITORING ORGANIZATION REPORT NUMBER(S) RADC-TR-88-328			6a. NAME OF PERFORMING ORGANIZATION SGS-Thomson Microelectronics, Inc.		
6b. OFFICE SYMBOL (If applicable)			7a. NAME OF MONITORING ORGANIZATION Rome Air Development Center (RBRP)		
6c. ADDRESS (City, State, and ZIP Code) 1310 Electronics Drive Carrollton TX 75006			7b. ADDRESS (City, State, and ZIP Code) Griffiss AFB NY 13441-5700		
8a. NAME OF FUNDING/SPONSORING ORGANIZATION Rome Air Development Center		8b. OFFICE SYMBOL (If applicable) RBRP	9. PROCUREMENT INSTRUMENT IDENTIFICATION NUMBER F30602-85-C-0164		
8c. ADDRESS (City, State, and ZIP Code) Griffiss AFB NY 13441-5700		10. SOURCE OF FUNDING NUMBERS			
		PROGRAM ELEMENT NO 62702F	PROJECT NO 2338	TASK NO 01	WORK UNIT ACCESSION NO 44
11. TITLE (Include Security Classification) TIME DEPENDENT DIELECTRIC BREAKDOWN OF SILICON DIOXIDE UNDER CONSTANT TUNNELING CURRENT STRESS					
12. PERSONAL AUTHOR Dr. Fu-Tai Liou, D.A. Tiffin, F.R. Bryant, R.L. Hodges, J.W. Staman III, J.A. Michlowsky, W.A. Williams III					
13a. TYPE OF REPORT Final		13b. TIME COVERED FROM Jun 86 TO May 88	14. DATE OF REPORT (Year, Month, Day) March 1989		15. PAGE COUNT 152
16. SUPPLEMENTARY NOTATION PRDA Effort.					
17. COSATI CODES			18. SUBJECT TERMS (Continue on reverse if necessary and identify by block number)		
FIELD	GROUP	SUB-GROUP	Silicon Dioxide, Accelerated Life Testing, Constant Current, Wafer Level Testing, Trapping, Latent Defects, EB&C, Electron Beam, Induced Current, TEM, Transmission Electron (over)		
13	08				
20	12				
19. ABSTRACT (Continue on reverse if necessary and identify by block number) This report describes a study of the time dependent dielectric breakdown characteristics of oxides in the 200 Angstrom, 100 Angstrom, and 50 Angstrom thickness range, under constant current stress. Current level and temperature were the main stress variables used. The test vehicle was a small (less than .001 square centimeter) polysilicon/silicon dioxide/silicon capacitor fabricated with a process similar to that used in commercial dynamic random access memory (DRAM) products. The test matrix included 34 wafers of test capacitors, arranged in 17 cells, with about 1200 individual capacitors per cell. An automated wafer level system was used to control stress and log data. Sample voltage was monitored during stress, and C-V curves were taken initially and after partial stress. Life- time statistics, trapped charge density, and trap generation rate were extracted from the data. An attempt was made to correlate electrical test results with physical characteristics of the films, such as latent defect type, density and location, as determined by (over)					
20. DISTRIBUTION/AVAILABILITY OF ABSTRACT <input checked="" type="checkbox"/> UNCLASSIFIED/UNLIMITED <input type="checkbox"/> SAME AS RPT <input type="checkbox"/> DTIC USERS			21. ABSTRACT SECURITY CLASSIFICATION UNCLASSIFIED		
22a. NAME OF RESPONSIBLE INDIVIDUAL Daniel J. Burns			22b. TELEPHONE (Include Area Code) (315) 330-2868		22c. OFFICE SYMBOL RADC (RBRP)

DC Form 1473, JUN 86

Previous editions are obsolete.

SECURITY CLASSIFICATION OF THIS PAGE

UNCLASSIFIED

UNCLASSIFIED

Block 18. Subject Terms (Cont'd)

Microscopy, Surface Replication

Block 19. Abstract (Cont'd)

transmission electron microscope (TEM) surface replica imaging and electron beam induced current (EBIC) unbiased and biased sample current imaging techniques.

Qualitatively, the 50 Angstrom films exhibited about 10 times lower trap generation rates and correspondingly lower trapped charge densities at failure than the 200 Angstrom films. The 50 Angstrom films also had lower latent defect densities, especially at the gate/field oxide periphery.

Accession For	
NTIS CPA&I	<input checked="" type="checkbox"/>
DTIC TAB	<input type="checkbox"/>
Unannounced	<input type="checkbox"/>
Justification	
By _____	
Distribution/	
Availability Codes	
Dist	Avail and/or Special
A-1	

2
INSPECTED

UNCLASSIFIED

EVALUATION

This project was proposed to RADC by the former MOSTEK Corporation in response to a general PRDA announcement on Failure Mechanisms in Microelectronics. An important, attractive feature of the contractor's proposed effort was his intention to do a study of the "latent" physical defects in thin film silicon dioxide test capacitors, in addition to the usual electrical lifetime characterization. This he did, using TEM surface replica imaging and biased EBIC sample current imaging.

The effort involved study of the time dependent dielectric breakdown characteristics of oxides of 200 Angstrom, 100 Angstrom, and 50 Angstrom thickness under constant current stress. Current and temperature were the main stress variables used. The test vehicle was a small (less than .001 square centimeter) poly silicon/silicon dioxide/silicon capacitor fabricated with a process similar to that used in commercial dynamic random access memory (DRAM) products. The test matrix included 34 wafers of test capacitors, arranged in 17 cells, with about 1200 individual capacitors per cell.

An automated wafer level system was used to control stress and log data. Sample voltage was monitored during stress, and C-V curves were taken initially and after partial stress. Lifetime statistics, trapped charge density, and trap generation rate were extracted from the data. An attempt was made to correlate electrical test results with physical characteristics of the films, such as latent defect type, density and location, as determined by transmission electron microscope (TEM) surface replica imaging and electron beam induced current (EBIC) unbiased and biased sample current imaging techniques, which were done on both stressed (failed) and unstressed samples.

Qualitatively, the 50 Angstrom films exhibited about 10 times lower trap generation rates and correspondingly lower trapped charge densities at failure than the 200 Angstrom films. The 50 Angstrom films also had lower latent defect densities, especially at the gate/field oxide periphery. (Section 6 summarizes conclusions).

Most of the raw data from this experiment is available on mag tape. At another time, further analysis may be done to look more carefully at lifetime vs. wafer position, early vs. main population failure modes, and failed vs. surviving capacitor electrical characteristics.

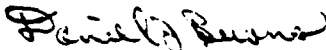

DANIEL J. BURNS
Project Engineer
RADC/RBRP

TABLE OF CONTENTS

Section	Title	Page
1.0	Introduction	1
2.0	Experimental Design	3
2.1	Scope of the Project	3
2.1.1	The Object of the Experiment	4
2.1.2	Background Research	4
2.1.3	Stress Factors	4
2.1.4	Evaluation of the Data	5
2.2	The Hadamard Matrix	6
2.3	Stress Factors	6
2.3.1	Electrical Stress -- Time Dependence	6
2.3.2	Radiation	6
2.3.3	Elevated Temperature	9
2.3.4	Electrical Stress -- Currents	9
2.4	Electrical Characterization	9
2.4.1	The Electrical Stress and Characterization Technique	9
2.4.2	Prober Hardware	9
2.4.3	Prober and Test Software	10
2.5	Physical Characterization	10
2.5.1	TEM Replicas	10
2.5.2	SEM Signal Current	11
3.0	Sample Preparation and Test Set-Up	13

TABLE OF CONTENTS

Section	Title	Page
3.1	Introduction	13
3.2	Wafer Fabrication	13
3.2.1	Capacitor Growth Cycle	16
3.3	Electrical Test Set-Up	18
3.4	Electrical Test Set-Up Software	21
4.0	Electrical Measurements and Stress Results	25
4.1.1	Electrical Measurement and Stress Results	25
4.1.2	Pre-Stress Testing	25
4.1.2.1	Pinhole Test	25
4.1.2.2	Pre C-V Testing	25
4.1.2.3	Oxide Thickness Determination	27
4.1.3	Oxide Stress Parameters	27
4.1.4	Post Stress Testing	30
4.1.5	Results and Discussions	32
4.1.5.1	Delta VFB	32
4.1.5.2	% BVT	32
4.1.5.3	PT	32
4.1.5.4	% Tot Fails	32
4.1.5.5	Ebd	32
4.1.5.6	T10, T16, T50	32
4.1.5.7	Time-to-Fail Dependence	32
4.1.5.8	Field Breakdown Dependence	34

TABLE OF CONTENTS

Section	Title	Page
	4.1.5.9 Time-to-Fail	34
4.2	Wafer Defect Mapping	34
	4.2.1 Introduction	34
	4.2.2 Analysis	36
	4.2.3 Discussion	38
4.3	Charge Trapping	38
	4.3.1 Theory and Methodology of Charge Trapping Analysis	38
	4.3.2 Analysis of Data Concerning Charge Trapping Characteristics	40
4.4	Statistical Analysis	54
	4.4.1 Factorial Analysis	57
	4.4.2 Characteristics of Factorial Experiments	57
	4.4.3 The Design and Analysis of 2-Level Full-Factorial Experiments	62
	4.4.4 Guidelines for Designing 2-Level Full-Factorial Experiments	63
	4.4.5 The Analysis of the Measured Data . . .	68
	4.4.6 The Design and Analysis of Screening Experiments	70
	4.4.7 The Matrix Applied to Cumulative Percent Fails and Charge Trapping	71
	4.4.8 Analysis of Cumulative Percent Fails in Time as an Output	72
	4.4.9 Analysis of Charge Trapping Properties Nt and G as Outputs	75

TABLE OF CONTENTS

Section	Title	Page
	4.4.10 Summary of Statistical Results	79
5.0	Physical Analysis	80
5.1	Electron Beam Induced Current Analysis.	80
5.1.1	Introduction	80
5.1.2	Analysis.	80
5.1.3	Observations.	82
5.1.4	Results and Discussions	93
5.2	Oxide/Si Surface Morphology Examination by TEM.	94
5.2.1	Introduction.	94
5.2.2	Analysis.	94
5.2.3	Results	96
5.2.4	Discussions and Summary	101
6.0	Conclusions	116
6.1	Conclusions from the Electrical Data	116
6.2	Conclusions from the Physical Data (TEM Replicas)	117
6.3	Conclusions from Physical Data (SEM Signal Current)	117
6.4	Recommendations	117
	References	119
	The Appendix	121

FIGURES LIST

Figure	Title	Page
3.1	Test Structure	15
3.2	Capacitor Growth Cycle	17
3.3	Test System	19
4.1A	Vg vs. Time (During Oxide Stress)	26
4.1B	Vg vs. Time (During Oxide Stress)	26
4.1C	Pre/Post Oxide Stress C-V Curves	26
4.2	I-V Plot of Oxide Tunneling Current	28
4.3	Voltage at Fail vs. Time of Fail	31
4.4	50% Failure vs. Breakdown Field	33
4.5	TTF Plot (Cumulative % Fail vs. Log Time)	35
4.6	200 Angstrom Wafer Map	37
4.7	50 Angstrom Wafer Map	39
4.8	Typical Delta Vg vs Time Data (200 Ang.)	42
4.9	Typical Delta Vg vs Time Data (50 Ang.)	43
4.10	Illustration of Heavy Electron Trapping Just Prior to Breakdown	44
4.11	Illustration of Instantaneous Hole Trapping	45
4.12	Example of the 10X Difference in the Density of Trapped Charge for 50 and 200 Angstrom oxides	47
4.13	Example of the 10X Difference in Trap Generation Probability for the 50 and 200 Angstrom Oxides	48
4.14	Effect of Temperature on Charge Trapping Properties of 50 Angstrom Oxides	49

Figure	Title	Page
4.15	Effect of Temperature on Charge Trapping Properties of 200 Angstrom Oxides	50
4.16a	Effect of Temperature on Charge Trapping for Different Current Densities for the 50 Angstrom Oxides-Density of Trapped Charge	51
4.16b	Effect of Temperature on Charge Trapping for Different Current Densities for the 50 Angstrom Oxides-Trap Generation Probability	52
4.17a,b	Effect of Temperature on Charge Trapping for Different Current Densities for the 200 Angstrom Oxides-Density of Trapped Charge and Trap Generation Probability	53
4.18	Effect of Injected Charge Density on Charge Trapping of 50 Angstrom Oxides	55
4.19	Effect of Injected Charge Density on Charge Trapping of 200 Angstrom Oxides	56
4.20	Depiction of Three Factor Experiment	60
4.21	Two Factor Example Showing Interaction Effects	61
4.22	Example of Curvature	64
5.1	Signal Current Circuit	81
5.2	Photo 1 Cell 4 Wafer 27 Secondary Electron Image	85
5.3	Photo 2 Cell 4 Wafer 27 Signal Current (EBIC) Image	86
5.4	Photo 3 Cell 3 Wafer 37 Secondary Electron Image	87
5.5	Photo 4 Cell 3 Wafer 37 Signal Current (EBIC) Image	88
5.6	Photo 5 Cell 5 Wafer 1 Secondary Electron Image	89

Figure	Title	Page
5.7	Photo 6 Cell 5 Wafer 1 Signal Current (EBIC) Image	90
5.8	Photo 7 Cell 1 Wafer 23 Secondary Electron Image	91
5.9	Photo 8 Cell 1 Wafer 23 Signal Current (EBIC) Image	92
5.10	Possible Propagated Crystal Defects Replica 55,714x	99
5.11	Cell 7 Unstressed Oxide No Radiation 50 Angstrom Tox - More Pitting Replica 55,714x	102
5.12	Cell 13 Unstressed Oxide Radiated 50 Angstrom Tox - Less Pitting Replica 55,714x	103
5.13	Cell 2 Unstressed Oxide No Radiation 200 Angstrom Tox - More Pitting Replica 55,714x	104
5.14	Cell 9 Unstressed Oxide Radiated 200 Angstrom Tox - Less Pitting Replica 55,714x	105
5.15	Cell 16 Unstressed Oxide 30 Degrees Celsius Stress 50 Angstrom Tox - More Pitting Replica 55,714x	107
5.16	Cell 11 Unstressed Oxide 125 Degrees Celsius Stress 50 Angstrom Tox - Less Pitting Replica 55,714x	108
5.17	Cell 2 Unstressed Oxide 30 Degrees Celsius Stress 200 Angstrom Tox - More Pitting Replica 55,714x	109
5.18	Cell 2 Unstressed Oxide 125 Degrees Celsius Stress 200 Angstrom Tox - Less Pitting Replica 55,714x	110
5.19	Shadowing Difference Replica 55,714x A. Projection B. Depression	114
5.20	General View of Overshadowing Replica 55,714x A. Bubble Artifact B. Acetate Contaminant	115

LIST OF TABLES

Table	Title	Page
1.1	Hadamard Experimental Matrix	7
3.1	Wafer Process Flow	14
3.2	Experimental Thickness Ranges Argon : Oxygen Ratios	16
3.3	Summary of Electrical Test Set-up	20
3.4	Electrical Test Routines	22
4.1	Input / Output Table	29
4.2	Coded Design Table	66
4.3	Decoded Design Table	67
4.4	Computation Table for Factor Effects Related to Cumulative Percent Fails at 1 Second	73
4.5	Values used in Calculating the MSF	74
4.6	Computation Table for Factor Effects Related to Charge Trapping for 50 Angstrom Oxides	76
4.7	Computation Table for Factor Effects Related to Charge Trapping for 200 Angstrom Oxides	78
5.1	Instrument Parameters	82
5.2	Thin Oxide EBIC Observations	83
5.3	EBIC Observation Summary	84
5.4	TEM Data and Trend Summary	111
5.4a	TEM Data and Trend Summary Continued	111a
5.5	Overall Pitting Trend for Unstressed 50 and 200 Oxides	112
5.5a	Overall Pitting Trend for stressed 50 and 200 Oxides	112a

ACKNOWLEDGEMENTS

This work was supported by Air Force Systems Command, Air Development Center, Griffiss Air Force Base, New York under Contract No. F30602-85-C-0164. The authors gratefully acknowledge Sharon Cummings for her work in producing the signal current micrographs, Chuck Davin for his modification of the Auger stage for use in the signal current work, Margaret Jarvis for her dark room work in printing the many TEM micrographs, Ric Stone for his help in the statistical analysis and Tim Turner for his input in the signal current analysis and other work. The authors would also like to thank Dennis Gonsalves and Bob Banks for their encouragement and management support in this project.

Time Dependent Breakdown of Silicon Dioxide under Constant Tunneling Current Stress

1.0 INTRODUCTION

The scaling of microcircuits in order to achieve higher packing densities and performance [1] has resulted in the introduction of scaled oxides on the order of 100 Angstroms thick or less. This document contains a study of time dependent breakdown characteristics of oxides in the 200 Angstrom, 100 Angstrom and 50 Angstrom thickness range under constant current stress.

A Hadamard matrix technique has been used to study the effects of constant current electrical stress, oxide thickness and its interdependence with the accelerating variables time dependence, radiation effects and elevated temperature on charge trapping and oxide breakdown. An attempt was made to gain some understanding of the fundamentals of the oxide-silicon interface characteristics; as well as, the nature of latent defects and their development in the oxide. A goal was to gain some understanding of oxide defect interaction with these acceleration variables. One of the main objectives of the study was to develop a mathematical model expressing the effects and interdependencies of the test variables on charge trapping and oxide breakdown.

An automated prober system with computer control of electrical stress, temperature stress and computerized data acquisition and analysis of the electrical data was used in this study. The system and software will be discussed in the experimental set-up section of this document.

The computerized acquisition and analysis of data and the use of the Hadamard matrix analysis technique allowed for the analysis of a large data base in a short period of time.

The test vehicle for this work included oxide test capacitors arranged with two test wafers per cell, 1200 test capacitors each cell. The test capacitors are of small area, less than 0.001 square centimeters in area and are oxide test vehicles of the type used for oxide feasibility studies. The fabrication process used to produce these test capacitors was that similar to the process used to produce commercially available dynamic

random access memories (N polysilicon/(silicon-dioxide)/P silicon).

Physical, as well as electrical analytical techniques were used in the characterization effort. These techniques included TEM replication [2] of the capacitor oxide surfaces of electrically good and failed test capacitors and SEM signal current (with and without negative bias) study of some of the good and failed oxides of the cell capacitors; the Si substrate under some of the cell capacitors was replicated to study any relationship between Si defects and defects in the capacitor oxides.

One of the objects of this investigation was to attempt to physically image latent defects or the physical effects of these latent defects in the oxides using TEM replicas and/or the SEM signal current technique and to relate what was detected in the physical data to what is observed in the electrical data. Other techniques, such as liquid crystal detection of high current points, can be used to image areas drawing high current in thin oxides; [3] however, it was hoped that signal current imaging would provide lower current detection limits than other methods.

Another object was to study the effects of and interactions of the several stress variables on the rate of trap generation and oxide breakdown and to study the relationship between this and the development of and/or activation of early life failures and latent defects in the oxides and to draw a mathematical conclusion expressing the effects and interdependencies of these test variables on charge trapping and oxide breakdown.

The replica technique has been used with the voltage ramp method of stressing oxides to image defects in the oxides in the past [4]; therefore, it is a logical technique to use in the evaluation of oxides under constant current stress. Differences between what was detected with oxides stressed using the voltage ramp method and oxides stressed under constant current were observed.

Some of this data was presented to RADC in the two oral presentations [5]. Three physical defects could be detected using this technique, round pin holes, larger areas that seemed to be thin areas in the oxide and oxide defects that looked like two small marks in the oxide. When the substrate Si under the oxide was replicated, it was seen that the "two mark" defects were related to material defects in the Si substrate [6].

One might expect the constant current stress method to yield different results, and it did. In general, the three physical defects seen in the voltage ramp method were not seen in the constant current stress method.

It was determined that signal current with no bias would not show the oxide defects; therefore, a variable negative bias was applied to the substrate so that the image of the oxide defects was enhanced (the technique will be expounded upon in the experimental set-up and physical analysis sections).

This work represents the effort of several persons in the Advanced Technology Group and Reliability Group at SGS-Thomson Microelectronics over a 2 year period. Thanks are expressed to all persons involved in the effort over the last two years.

We hoped to explore some new areas in this study and develop a clearer understanding of the physics of these ultra-thin oxides.

2.0 EXPERIMENTAL DESIGN

The experiment was designed to be run using standard VLSI test vehicles of a type used in development work involving DRAMs. The test vehicles have been designed to be tested with an automated stress and characterization system to yield data for evaluation of the effects of the several stress factors used in this experiment on the integrity of the thin oxides in the test vehicles. The development of latent defects in these test vehicles was monitored using analytical methods that can provide relationships between the integrity of the oxides under test and the stress factors.

The fabrication and structure of the test vehicles will be more fully covered in the sample preparation section of this technical report.

2.1 SCOPE OF THE PROJECT

The scope of the project is the study of defects produced in thin oxides in the three thickness ranges, 50 Angstroms, 100 Angstroms and 200 Angstroms, under constant current stress, and the evaluation of the processes involved in ultra-thin silicon dioxide breakdown.

The effects of and interaction of oxide thickness, constant current stress, temperature, time and radiation exposure on the rate of trap generation and oxide breakdown were to be studied. The development of latent oxide defects was electrically and physically monitored in the ultra-thin oxide of the capacitors.

Three characterization techniques were used in the study of these ultra-thin oxides: electrical characterization (I-V and C-V), TEM replica imaging and SEM imaging using unbiased and negative biased signal current and secondary electron imaging.

2.1.1 The Object of the Experiment

The object of the experiment was to gain knowledge of the effects of several stress factors on the production of defects in these ultra-thin oxides and the development of latent defects and to produce a mathematical model for the interrelation between these stress factors and oxide quality, latent oxide defects and charge trapping.

2.1.2 Background Research

Scaling of VLSI design dimensions has occurred in recent years in order to provide for higher packing density and better circuit performance; therefore, reliability of oxides in the 30-300 Angstrom thickness range is of deep concern.

Concerns include the reliability of such oxides under radiation exposure, electric field stress and tunneling current leakage. Study of the tunneling characteristics and dielectric breakdown modes of oxides in this range of thickness may provide an understanding of the dielectric strength and oxide-silicon interface characteristics of these oxides. The relationship between these stress factors and stress time-to-fail, charge trapping and charge trap generation was investigated.

2.1.3 Stress Factors

The stress factors that were evaluated included: temperature, constant current stress, stress time and radiation dose. The relationship of these stress factors to oxide time-to-fail, charge trapping and charge trap generation was investigated.

2.1.4 Evaluation of the Data

The automated electrical stress and characterization system was used to study the largest number of experimental test vehicles in the shortest time.

The Hadamard matrix evaluation technique [7] was used to analyze the data and evaluate mathematical relationships between the input variables and the several output variables.

In one-at-a-time experiments, only one factor in each run is changed, while the other factors are held constant. In an experiment with five factors, this would require 32 runs to determine the relationships between those factors. Obviously, this may lead to incomplete coverage of the experimental space, missing relationships between factors, and the possibility of erroneous assumptions.

In factorial experiments, the use of factorial arrangements for the factors in an experiment make each run yield information concerning every factor. The Hadamard matrix makes use of one such design involving factorial experiments.

Our experimental matrix is a Hadamard arrangement which is designed as a two-level, half-factorial matrix (i.e. $2^5 = 32$ runs for five factors), we have elected to use a half-factorial matrix which involves 16 runs plus one center point run for a total of 17 runs. In this way, our responses no longer contain information about a single main or interaction effect. However, they contain response information from two or more effects. This is known as confounding. These special cases of factorial matrix design will be discussed more extensively in the specific section concerning our experimental matrix design and analysis.

Micrographs documenting defects observed were made in the signal current mode, secondary electron mode and TEM micrographs were made on the replicas of the areas on the test vehicles to be evaluated and 8X10 TEM prints were produced for evaluation of this physical defect data.

An effort was made to relate physical data to electrically observed effects and it was found that there was some relationship between the physical observed data and electrical data.

2.2 THE HADAMARD MATRIX

The Hadamard matrix was used to obtain the most information with few experimental splits. The Hadamard matrix technique will be discussed in more detail in the Statistical Data Analysis and Discussions section. The experimental matrix consisted of 17 cells of two semiconductor wafers each having 600 test dice for a total of 1200 test dice per experimental cell (see Table 1.1).

The following were experimental matrix input variables: cell, wafer, oxide thickness, stress temperature, stress current, stress time and radiation exposure dose.

The following were the main electrical output: time-to-fail data, charge trapping data, I-V data and C-V data; these, as well as, the physical data were evaluated in the Electrical Measurements and Stress Results section, the Physical Analysis section and Statistical Data Analysis and Discussions section of this report.

The output variables for the physical data included: TEM replica trends observed on the micrographs and SEM signal current trends observed on the micrographs. These data will be covered in the Physical Analysis section of this report.

2.3 STRESS FACTORS

The effects of each of the stress factors have been evaluated using the Hadamard matrix technique and this is covered in detail in the Statistical Data Analysis and Discussions section of this report.

2.3.1 Electrical Stress -- Time Dependence

Three stress times were used in the experiment, 1 sec., 10 sec., and 60 sec.

2.3.2 Radiation

The wafers to be exposed to radiation were exposed according to the schedule of the experimental matrix and were electrically stressed and characterized within one week of the exposure. After the electrical stress and characterization, physical analysis was conducted on the wafers.

<u>CR.</u> <u>0</u>	<u>LOT</u> <u>0</u>	<u>WAFERS</u> <u>0</u>	<u>THICKNESS</u> <u>ANGS.</u>	<u>GAMMA DOSE</u> <u>(KRAD)</u>	<u>STRESS</u> <u>CURRENT</u>	<u>TEMPERATURE</u> <u>CELSIUS</u>	<u>STRESS</u> <u>TIME</u>
1	P50-328	23.47	200	500	-2.E-4	30	1 SEC
2	"	25.46	200	0	-5.E-4	30	1 SEC
3	"	37.38	200	500	-5.E-4	125	1 SEC
4	"	27.43	200	0	-5.E-4	125	60 SEC
5	"	01.27	50	500	-5.E-4	125	60 SEC
6	"	33.42	200	500	-2.E-4	125	60 SEC
7	"	02.16	50	0	-5.E-4	30	60 SEC
8	"	34.41	200	0	-2.E-4	125	1 SEC
9	"	35.40	200	500	-5.E-4	30	60 SEC
10	"	03.15	50	0	-5.E-4	125	1 SEC
11	"	04.14	50	0	-2.E-4	125	60 SEC
12	"	36.39	200	0	-2.E-4	30	60 SEC
13	"	05.23	50	500	-5.E-4	30	1 SEC
14	"	06.21	50	500	-2.E-4	125	1 SEC
15	"	08.10	50	500	-2.E-4	30	60 SEC
16	"	09.01A	50	0	-2.E-4	30	1 SEC
17	"	20.30	100	50	-3.EE-4	70	10 SEC

TABLE 1.1 HADAMARD EXPERIMENTAL MATRIX

Radiation-induced defects in MOS oxides have been the object of several studies and hydrogen atoms have been considered to have a role to play in the generation of these defects; however, their role in the process or other areas of the process are not yet clear. SIMS and FT-IR measurements have indicated results consistent with a model where free hydrogen atoms generated by the irradiation move toward the interface and attack a Si-Si bond forming a SiH bond and an Si dangling bond or a Si-O-Si bond forming an SiOH and a hole trap. It has been determined by SIMS and FT-IR that under irradiation, hydrogen atoms do move toward the interface and that SiH and SiOH bonds increase at the interface giving credence to this model; therefore, it may be necessary to limit the exposure of ultra-thin oxides to hydrogen in the fabrication process [8]

The radiation exposure was performed at Texas A and M University, Nuclear Science Center, College Station, Texas. The radiation source at Texas A and M is calibrated using a traceable Mdh electronic ion chamber. The following conversions were used to determine the proper irradiation times necessary for this work: from the Radiological Health Handbook the conversions were found:

$$1 \text{ RAD} = 100 \text{ erg/g} \quad (1.1)$$

$$1 \text{ R} = 86.9 \text{ erg/g air} \quad (1.2)$$

Readings at the surface of the source where the samples were placed were calibrated to be 1454 R/min.; therefore, for 500 KRAD irradiation, the time was found by first converting rads to roentgen 575 KR and then dividing by 1454 R/min. The time for irradiation of the 500 KRAD sample wafers was found to be 6 hours, 35 minutes (for example).

An assumption that had to be made here was that the silicon wafer has the same dose factor as for air; from this the conversion factor from rad to roentgen is made [9]:

$$1 \text{ R} = 1 \text{ Rad} = 100 / 86.9 = 1.15 \text{ R/rad} \quad (1.3)$$

Cells were exposed to one of three doses of Co 60 radiation, 0 KARD, 50 KRAD, 100 KRAD and 500 KRAD. Co 60 produces gamma radiation and the energies of the modes of decay for Co60 are the following: Beta -- 0.315 MeV (99.7%), 0.67 MeV (0.2%) and 1.49 MeV (0.1%) with a decay Q

value of 2.82 MeV; gamma -- 1.33 MeV (100%), 1.17 MeV (99.9%) and 2,200 m/sec neutron absorption cross section (barns) = 2.0 [10].

2.3.3 Elevated Temperature

Cells were temperature stressed at one of three temperatures 30 degrees Celsius, 70 degrees Celsius and 125 degrees Celsius

2.3.4 Electrical Stress -- Currents

Three stress currents were used in this experiment: $-2.0E-04$ amp, $-5.0E-04$ amp and $-3.5E-04$ amp. These currents were selected after indications of data taken before the start of the experimental matrix electrical stress (the area of each test capacitor was $6.35E-4$ cm**2).

2.4 ELECTRICAL CHARACTERIZATION

Fully automated stressing, electrical measurement and data analysis techniques were used in this work. Measurements of current-voltage (I-V) and capacitance-voltage (C-V) characteristics of each test die was made and recorded using our computerized system.

The electrical analysis included continuous monitoring of and recording of voltage as a function of time during constant tunneling current stress.

2.4.1 The Electrical Stress and Characterization Technique

The technique used in this study was constant current stress for the three different current splits and three different time splits as detailed above. The experimental stress was completed using an automatic stressing system.

2.4.2 Prober Hardware

A PDP-11/73 computer is interfaced with a Keithley S-350 test system through a DMA interface. The Keithley is used for the constant current stress and to connect the measurement cables of two Hewlett Packard Instruments to the device under test. The H.P. 4192A and H.P. 4104B are controlled by a General Purpose Interface Bus which is connected to the PDP-11/73. The PDP-11/73 provides control of the capacitance data taken on the H.P. 4192A and controls the I-V measurements taken on the H.P. 4140B. The

2001X Auto Prober is used to step the wafer during testing. The manual hot chuck keeps the temperature at the proper setting (30, 70 or 125 deg. C). All data collected is transmitted across the Ethernet to a MicroVAX 3600 for data analysis. The outputs are printed on a LNO3 Plus Laser Printer.

2.4.3 Prober and Test Software: the following is a list of software used in this work -- Main Program: OXIDES - Calls all supporting subroutines; Subroutines: INIT1 - Initializes all general auto prober parameters, INITOA - Initializes all device specific parameters, CVZERO - Loads opens and shorts registers in HP 4192A, OXSET - Allows default set points of all stress and measurement parameters to be changed, STRTO - Allows input of wafer information, LOKATE - Returns wafer position, SHORTS - Checks for shorted capacitors, CVLOW - Controls the HP 4140B for I-V measurements, CVHIGH - Controls the HP 4192A for C-V measurements and STRESS - Controls the Keithley S-350 for current stress measurements.

2.5 PHYSICAL CHARACTERIZATION

The physical analysis was not automated and was very labor intensive. Two physical characterization techniques were used in this work. TEM C-Pt/Pd two-stage replicas of the oxide surfaces and substrate surfaces to be evaluated were produced, examined and photographed in the TEM and the SEM unbiased and negative biased signal current technique with an scanning Auger microprobe providing the signal current was used to image areas with possible oxide defects. Secondary electron images were also used. It was determined that bias on the test capacitor was needed in order to image defect and latent defect areas; therefore the signal current technique with bias (EBIC) was used in this study.

It was thought that the use of the TEM replica technique would provide needed resolution to image surface defects in the ultra-thin oxides and would have the advantage over SEM techniques not only in providing more resolution, but also in the fact that the replicas would provide a charge free surface; whereas one might run into charging problems in the close examination of the ultra-thin oxide surfaces in the SEM mode.

2.5.1 TEM Replicas

The TEM replica technique used in this study is an old technique having been used for over 30 years; however, it provides enough resolution for a study of this type. The replica sample preparation technique will be covered in detail in the physical analysis section of this report.

Replicas of the oxide surfaces and substrate surfaces that were under study were made, optical maps were made for each replica sample and the replicas were examined and photographed in the Philips EM420T in the TEM mode using an accelerating voltage of 120 KV.

Stressed versus unstressed oxides were adjacently located and were analyzed using the TEM replica technique.

The oxide surface at the oxide/polysilicon interface was replicated and TEM examinations of this surface was conducted on five test vehicles from each cell. Earlier work at UTC-Nostek had seen a correlation between physical defects observed using the TEM replica technique in ultra-thin oxides and materials defects in the Si substrate of test vehicles of the same type used in this study; however, the voltage ramp method of electrical stress was used in that work [11].

The silicon surface at the silicon/oxide interface was replicated and TEM examinations of this surface were conducted on two test vehicles per cell.

The instrument used for the TEM replica study of the oxide and Si substrate surfaces is a Philips EM420T analytical electron microscope. The instrument provides about 2 Angstrom resolution in the TEM mode, about 15 Angstrom resolution in the STEM mode and about 25 Angstrom resolution in the high resolution SEM mode.

An accelerating voltage of 120 KV was used for the replica work on this instrument.

2.5.2 SEM Signal Current

In SEM signal current work, the electron-beam-induced current is intensity modulated on the viewing screen to show the location of local areas in the oxide drawing high current. Signal current is one of several techniques which can be used to localize defects in MOS capacitor oxide structures.

Three test vehicles from each cell were physically analyzed using SEM techniques including sample current and secondary imaging and detected defects in the oxide were documented; as well as, the minimum bias required to show the defects was documented.

Stressed versus unstressed test vehicles were adjacently located and were analyzed using this SEM signal current and secondary electron imaging technique.

The minimum negative bias voltage required to cause an image of the oxide defect area in the test vehicles was also recorded.

This technique makes use of a rastered and focused electron beam striking the surface of the sample while the substrate current induced by the beam is monitored. The substrate current is used to intensity modulate the SEM CRT so that local defect sites can be recorded.

In this case, an external negative bias was used to enhance the intensity of the defect area image. It was observed that the minimum negative bias required to cause a signal current image to be detected was changed with different samples.

A scanning Auger microprobe was used to provide the electron beam and viewing circuits for the signal current work.

This system was used only because of the availability of the sample current preamplifier attached to the instrument. The samples were mounted on a miniature probe station and then attached to a modified sample mounting stub and a simple voltage divider circuit was used to apply negative bias to the structures (see Figure 5.1 for illustration of the technique).

3.0 SAMPLE PREPARATION AND TEST SET-UP

3.1 Introduction

The MOS capacitors used in this investigation were all fabricated on (100) oriented p-type silicon wafers. The starting resistivity was 7-9 ohm-cm, the wafer thickness was 25 +/- 2 mils, and the wafer diameter was approximately 100 millimeters. The silicon substrate forms the bottom capacitor plate with edges defined by an isolation oxide. The dielectrics under investigation are grown in the areas between the isolation oxide. The top capacitor plate is formed from deposited polysilicon capped with Al. The top capacitor plate is patterned and etched in such a manner that the plate edges are over the thick isolation oxide to avoid localized high electric fields at the edges of the polysilicon. This means that only the silicon substrate/oxide/polysilicon capacitor structure is under study and the investigation is generally free from any influence of a mechanical edge structure. Although this is the best structure to study only the dielectric, about 15% of the defect locations (using EBIC analysis) are on the isolation to capacitor oxide edge. This means that some mixed failure modes are present in the data. The top plate material is patterned into lines which lead to probe pads also located over the thick isolation oxide so that during testing no pressure from the probe pins is transferred to the thin dielectrics under investigation. The capacitor size used in this investigation were 6.35E-4 centimeters squared. FIGURE 3.1 is an illustration of the test structure.

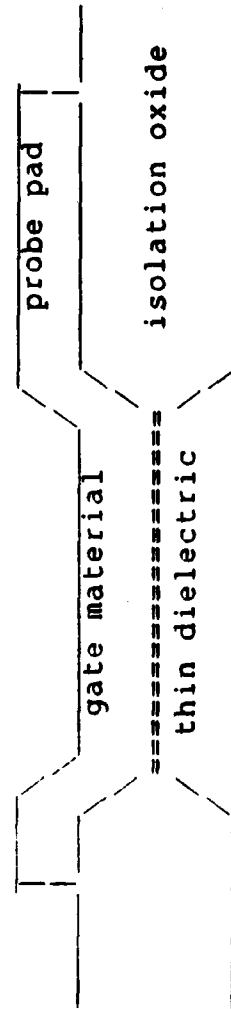
3.2 Wafer Fabrication

The process flow outlined in TABLE 3.1 below and the process traveler contained in addendum A were used to prepare the wafer samples. The process basically involves the use of a standard type LOCOS active area isolation with a field isolation implant, a sacrificial oxide before the capacitor oxide, the capacitor oxide grown to various thicknesses, and a top capacitor plate of n-type doped polysilicon capped with Al. The Al cap over the polysilicon plate is used to promote charge dispersion through out the plate. The Al is doped with ~ 0.5% Cu and ~ 1.0% Si. The capacitor oxides were grown in a Bruce induction heated horizontal furnace fitted with a standard type gas jungle. The ambient for growing the capacitor oxides was a mixture of argon, oxygen, with 1,1,1-trichloroethane (TCA) added during the main oxidation portion of the growth cycle.

WAFER PROCESS FLOW TOA rev. A (Thin Oxide Analysis)

1. LASER SCRIBE
 SCRIBE LOT NO., REV. NO. AND WAFER NO.
2. DIFFUSION PIRANHA (H₂SO₄/H₂O₂)
3. 10/1 (H₂O/49% HF) 20 SEC
4. INITIAL NITRIC ACID CLEAN
5. INITIAL OXIDE
 THICKNESS SPEC 600-700 A
6. NITRIDE DEPOSITION
 THICKNESS SPEC 900-1000 A
7. LP III BAKE
8. SPIN BAKE 6K RPM 1400-27 RESIST
9. ALIGN LEVEL 1
10. BATCH DEVELOP 45 SEC
11. PLASMA SILICON NITRIDE ETCH
12. IMPLANT 8.00X10⁺¹³ 30 KV BORON
13. ACETONE STRIP
14. INJECTION PIRANHA (H₂SO₄/H₂O₂)
15. 10/1 (H₂O/49% HF) 5 SEC
16. PRE GATE NITRIC ACID CLEAN
17. FIELD OXIDATION
 THICKNESS SPEC 5.0-6.0 KA
18. 10/1 (H₂O/49% HF) 1 MIN
19. WET SILICON NITRIDE ETCH 45 MIN
20. 10/1 (H₂O/49% HF) 2 MIN 30 SEC
21. PRE GATE NITRIC ACID CLEAN
22. STRIP GATE OXIDE
 THICKNESS SPEC 600-700 A
23. CAPACITOR OXIDATION
 THICKNESS VARIABLE
24. FIRST POLY DEPOSITION
 THICKNESS SPEC 4.5-5.5 KA
25. PHOS DEPOSITION 900C
 RS SPEC 30-40 OHM/SQ
26. 10/1 (H₂O/49% HF) 20 SEC
27. LP III BAKE
28. SPIN BAKE 5K RPM AZTOPLATE RESIST
29. BAKE 155C 30 MIN
30. WET POLY TILL BACKS CLEAR
31. WET OXIDE ETCH LOT
 7/1 (NH₄/HF) 38C TILL BACKS CLEAR +5 SEC
32. ACETONE STRIP
33. INJECTION PIRANHA (H₂SO₄/H₂O₂)
34. PRE EVAP PIRANHA (H₂SO₄/H₂O₂)
35. METALLIZATION
 THICKNESS SPEC 5.5-6.5 KA
36. LP III BAKE
37. SPIN BAKE 4K RPM 1318 SFD RESIST
38. ALIGN LEVEL 2
39. POST EXPOSURE BAKE
40. BATCH DEVELOP 100 SEC
41. PLASMA DESCUM
42. BAKE 125C 30 MIN
43. WET METAL ETCH LOT
 ETCH TILL CLEAR + 20 SEC
44. PLASMA POLY ETCH LOT
45. ACETONE STRIP
46. PLASMA RESIST STRIP
47. BACKSIDE METALLIZATION
 THICKNESS SPEC 5.5-6.5 KA

TABLE 3.1. WAFER PROCESS FLOW



p-type Si substrate

back of Si wafer

FIGURE 3.1. TEST STRUCTURE

The same ambients were used to grow all of the oxide thickness ranges. The polysilicon was doped n-type at 900 degrees C using a POCl₃ source. The POCl₃ carrier gas was N₂ and the source temperature was 24.0 +/-1.0 degrees C. The polysilicon doping step was the only high temperature step that the oxides under study saw after growth. The Al/polysilicon sandwich was patterned using typical photoresist techniques and etch in phosphoric acid metal etch followed by a polysilicon plasma etch. After resist removal Al was sputtered onto the back of the Si substrates to reduce the chuck to wafer resistance.

3.2.1 Capacitor Growth Cycle

The capacitor growth cycle shown in FIGURE 3.2, illustrates graphically the changes in temperature and ambient with time. The argon to oxygen volume ratio was modified to attain the oxide thickness spread defined by the experiment and yet maintain as many growth conditions as possible constant. The time of the central portion of the oxidation cycle was also adjusted to aid in reaching the target thicknesses once the range had been reached with gas ratio modifications. The chlorine to oxygen ratio was held at 3.0 +/- 0.2% by volume for all of the oxide thickness ranges grown. The chlorine source used was 1,1,1-trichloroethane at 23.0 +/-1.0 degrees C with oxygen as the carrier gas. The ratios of argon to oxygen used to adjust the partial pressure to provide different oxide ranges using approximately the same oxidation rate are shown in TABLE 3.2.

oxide thickness range	argon : oxygen
200 angstrom	2 : 1
100 angstrom	3 : 1
50 angstrom	5 : 1

TABLE 3.2 EXPERIMENTAL THICKNESS RANGES
ARGON : OXYGEN RATIOS

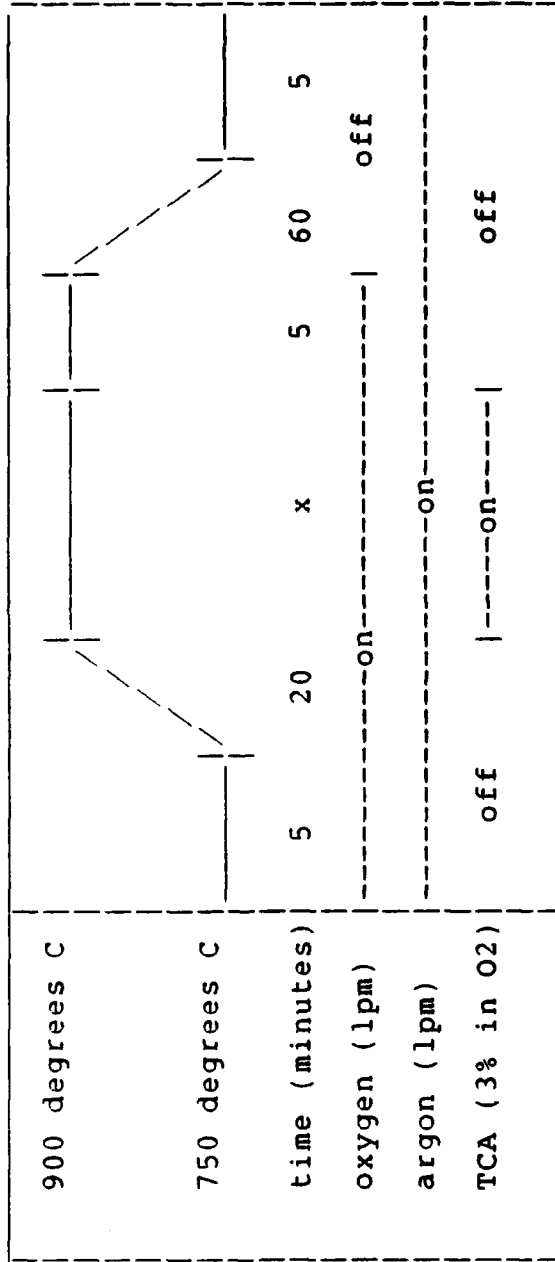


FIGURE 3.2. CAPACITOR GROWTH CYCLE

3.3 ELECTRICAL TEST SET-UP

FIGURE 3.3 is a diagram of the test system and TABLE 3.3 is a summary of the electrical test parameters that were used to test the wafers.

The Keithley S 350 Parameteric Tester is the base system selected for forcing current and measuring voltage. This system includes: The PDP11/73 computer, the Keithley instruments and the 2001X Auto Prober.

The digital PDP11/73 computer has 4 mega-bytes of memory, the RAM Disc uses 2.0 mega-bytes of the memory, Fujitsu 2351 Eagle Disc drive (474 mega-bytes unformatted), a G.P.I.B. (General Purpose Interface Bus) board, DMA (Direct Memory Access) board and an Ethernet (a network interface) board. The operating system used was RSX 11m Ver. 4.1 and all test routines were written in Fortran 77 Ver. 5.0.

The Keithley has Current/Voltage sources, a Voltage meter, a Current meter and Relay matrices. The Relay matrices are used to connect the Current source to the proper D.U.T. pin on the 2001X Auto Prober via a coaxial cable and probe card.

The 2001X Auto Prober is a cassette to cassette automated wafer handler. The TC 2000 Thermal Chuck was added to the 2001X Auto Prober to control the temperature of the wafer during test.

The Hewlett Packard 4192A was added to the system to provide Capacitance curves. The measurement cables are connected to the D.U.T. via the Keithley Relay matrices. The PDP11/73 is used to control the H.P. 4192A via the G.P.I.B. board (IEEE).

The Hewlett Packard 4140B was added to the system to provide Fowler-Nordheim curves. The measurement cables are connected to the D.U.T. via the Keithley Relay matrices. The PDP11/73 is used to control the H.P. 4140B via the G.P.I.B. board (IEEE).

Due to the amount of raw data generated for each wafer a digital MicroVAX 3600 system with a LN03 Plus Laser Printer was chosen for data analysis, manipulation and reduction. The operating system used was VMS Ver. 4.7 and

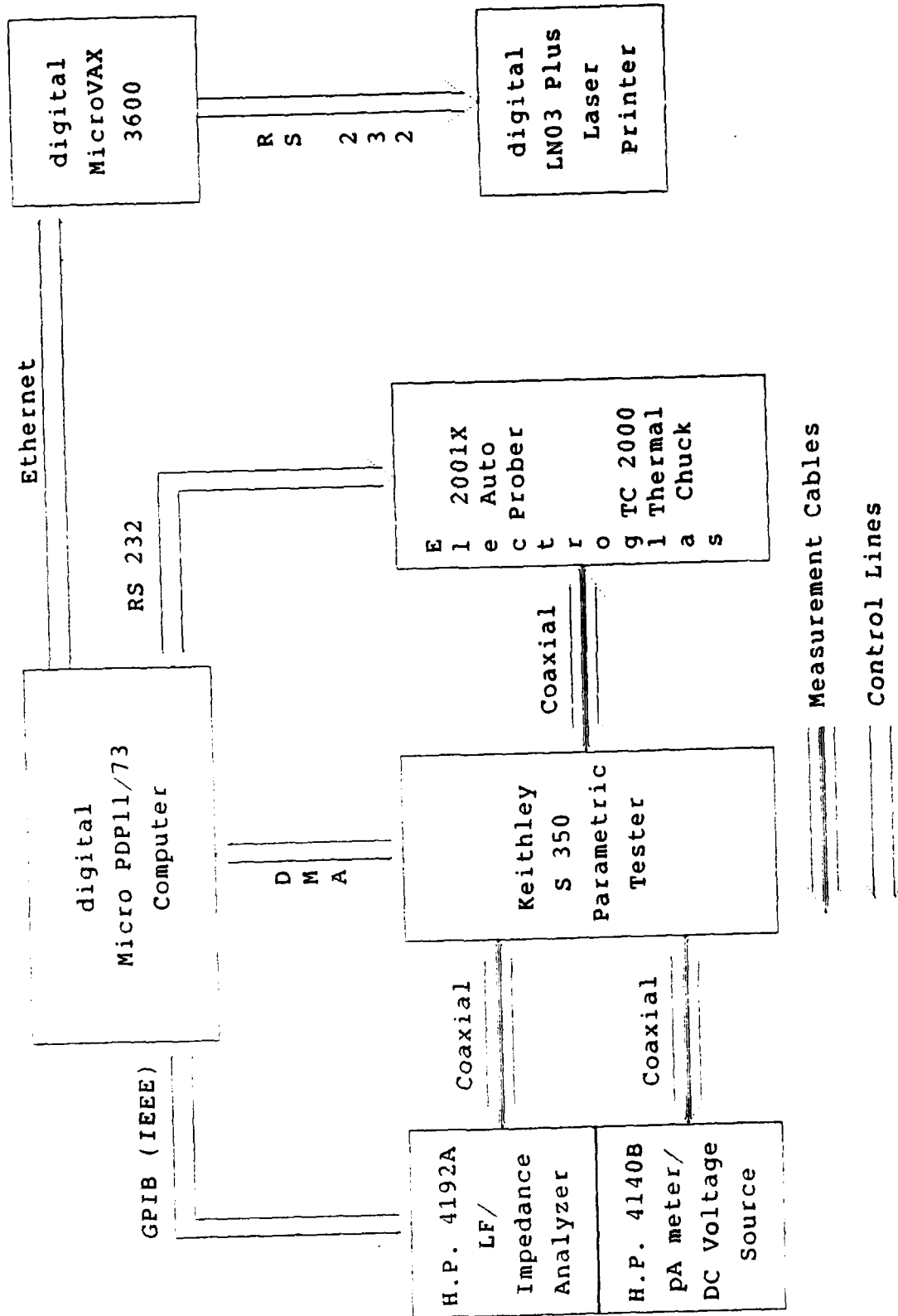


FIGURE 3.3. TEST SYSTEM

TABLE 3.3 SUMMARY OF THE ELECTRICAL TEST SET-UP

TEST #	PURPOSE	ELECTRICAL TEST												
1.	Check for initial pinholes in the oxide.	Measure continuity between gate and substrate. Leakage current must be less than 100nA at -5. volts to pass test. (-5. is 2.5 Mv/cm for a 200 Angs. oxide)												
2.	Obtain tunneling current curve to breakdown on the two center die.	Using H.P. 4140B measure current while ramping voltage from 0.0V to -35.0 volts. 0.5 volt per sec true ramp, measuring current at 0.5 volt increments.												
3.	Perform a pre-stress capacitance curve measurement on all die except two center die.	<p>Using the H.P. 4192A and using the following criteria:</p> <table border="1"> <thead> <tr> <th>Tox</th> <th>Start Voltage</th> <th>Stop</th> </tr> </thead> <tbody> <tr> <td>200A</td> <td>-10.0</td> <td>+3.0</td> </tr> <tr> <td>100A</td> <td>- 6.0</td> <td>+5.0</td> </tr> <tr> <td>50A</td> <td>- 4.0</td> <td>+4.0</td> </tr> </tbody> </table> <p>****1.0Mhz frequency ****0.1 volt oscilator level Measure capacitance every step interval where</p> $\text{step} = \frac{\text{stop-start}}{100}$	Tox	Start Voltage	Stop	200A	-10.0	+3.0	100A	- 6.0	+5.0	50A	- 4.0	+4.0
Tox	Start Voltage	Stop												
200A	-10.0	+3.0												
100A	- 6.0	+5.0												
50A	- 4.0	+4.0												

all output software was written in RPL Command Language, RS/1 Ver. 3.0.

3.4 Electrical Test Software

Refer to TABLE 3.4 for a summary of the Testing software.

The purpose of the testing software was to have a Menu driven program that would allow you to make easy changes to the input parameters.

The main program name is "OXIDES", the purpose of the main program is to coordinate the calling of all of the subroutines. Each subroutine performs a portion of the overall wafer testing task. The main program flow and the flow of all of the test subroutines are explained in detail in the following paragraphs. "OXIDES" The main program flow:

- 1) Declare all input and output variables.
- 2) Initialize all input variables to the default settings.
- 3) Call "INIT1" and "INITOA" to setup all the parameters in the 2001X Auto Prober and to attach the communication line of the 2001X Auto Prober to LUN (Logical Unit Number) file number. This allows the PDP11/73 computer to communicate with the 2001X Auto Prober without any interruption.
- 4) Call "CVZERO" to remove any stray capacitance between the H.P. 4192A and the D.U.T. This is accomplished by taking several readings with the probe pin about 10 mils. From the wafer chuck. Then taking several readings with the probe pin touching the wafer chuck. The location of the chuck (X and Y coordinates) and the open and short positions of the motor that raises or lowers the wafer chuck are saved in the program. Every 25 die the program will stop testing and return the chuck to this same position to rezero the H.P. 4192A, then resume testing.
- 5) Display the default settings of all of the input parameters. If there are any changes to be made, then call "OXSET". This subroutine allows you to change the input parameters and then re-displays the input parameters.
- 6) Call "STRTO" to request wafer information, auto align the wafer and prepare for testing to begin.
- 7) Setup a generic output file name to be used in the subroutines "STRESS", "CVHIGH", "CVLOW" and "SHORT".
- 8) Search the disk for old data files for the same wafer number as the wafer number being tested. If any old data files are found they are opened and read in to input the die

Main Program: OXIDES - Calls all supporting subroutines.

Subroutines: INIT1 - Initializes all general Auto Prober parameters.

INITQA - Initializes all device specific parameters.

CVZERO - Loads Opens and Shorts registers in the H.P. 4192A.

OXSET - Allows default set points of all stress and measurement parameters to be changed.

STRTO - Allows input of wafer information.

LOKATE - Returns wafer position.

SHORTS - Checks for shorted capacitors.

CVLOW - Controls the H.P. 4140B for I.V. measurements.

CVHIGH - Controls the H.P. 4192A for C.V. measurements.

STRESS - Controls the Keithley S 350 for Current Stress measurements.

TABLE 3.4 TABLE OF ELECTRICAL TEST ROUTINES

number to restart testing. The wafer is stepped to the last die tested and testing resumes. (the output software does not use any duplicate data, only the first file is used.)

9) The testing loop is entered at this time and the program will loop until all of the die on the wafer have been tested.

10) Call "LOKATE" to find the wafer chuck position.

11) Check to see if 25 die have been tested since the last time the H.P. 4192A has been zeroed. If so, call "CVZERO" to rezero the H.P. 4192A.

12) Enter a nested testing loop to test the four capacitors on each die.

13) Call "SHORT" to check for shorted capacitors, if shorted jump to Step 18.

14) Check die number, if equal to 79 or 80 then call "CVLOW". After taking the I.V. curve move to the next capacitor to be tested and jump to Step 18 or to Step 10 if the last capacitor on this die has been tested.

15) Call "CVHIGH" to take a pre-stress capacitance curve.

16) Call "STRESS" to stress capacitor.

17) Call "CVHIGH" to take a post-stress capacitance curve.

18) Move to the next capacitor to be tested.

19) Loop to Step 13 if there are more capacitors to be tested on this die.

20) Move to next die to be tested.

21) Loop to Step 10 if there are any more dies to be tested.

22) Unload the tested wafer from the wafer chuck.

23) End of testing program.

"CVHIGH" Subroutine flow:

1) Declare all input and output variables.

2) Encode all voltages and frequency into internal form for the capacitance curve to be taken on the H.P. 4192A.

3) Connect the H.P. 4192A to the D.U.T.

4) Move the probe pin to the zero pad on the die.

5) Load the opens and shorts data gathered when the H.P. 4192A was zeroed.

6) Load all parameters previously encoded into internal form to the H.P. 4192A.

7) Measure capacitance of the zero pad on the die.

8) Move back to the capacitor to be measured.

9) Enter the measurement loop to take the capacitance curve.

10) Take the capacitance measurement.

11) Store the reading and loop to step 10 until the capacitance curve is complete.

12) Calculate the oxide thickness.

- 13) Write the output file.
 - 14) Return to the main program
- "CVLOW" Subroutine flow:
- 1) Declare all input and output variables.
 - 2) Connect the H.P. 4140B to the D.U.T.
 - 3) Encode all voltages into internal form for the I.V. curve to be taken on the H.P. 4140B.
 - 4) Load all parameters previously encoded into internal form to the H.P. 4140B.
 - 5) Enter the measurement loop to take the I.V. curve.
-
- 6) Take the I.V. measurements.
 - 7) Write the output file.
 - 8) Return to the main program
- "SHORT" Subroutine flow:
- 1) Declare all input and output variables.
 - 2) Connect Keithley voltage source and current meter to the D.U.T.
 - 3) Force 2.5 Megavolt per centimeter and measure the current.
 - 4) If absolute current is less than 100 nanoAmps, then set pass flag true and return to the main program.
 - 5) Write blank files for the stress file and for the two C.V. curves for this capacitor.
 - 6) Return to main program
- "STRESS" Subroutine flow:
- 1) Declare all input and output variables.
 - 2) Connect the Keithley current source and voltage meter to the D.U.T.
 - 3) Reset the clock to zero.
 - 4) Force the stress current on the capacitor.
 - 5) Enter the measurement loop.
 - 6) Measure the voltage and the time that has elapsed.
 - 7) Write the data to the RAM disc and loop to Step 6 until the stress length time is reached.
 - 8) Write the data collected from the RAM disc to the hard disc output file.
 - 9) Return to main program.

4.0 ELECTRICAL MEASUREMENT AND STRESS RESULTS

4.1.1 Electrical Data Measurement Introduction

From the test routines in TABLE 3.4 in section 3.4, data was taken from each tested capacitor. Data for each capacitor consisted of pre-stress data testing, oxide stress, and post-stress data testing. Originally the pre-stress data testing included a pinhole test, an I-V, and a CV. It was found that the I-V needed to be in the measureable tunneling current range to be of any validity and that these current levels amounted to a stress on the oxide whose stress amount could not be quantified and therefore yielded results out of context. For this reason the initial and post-stress I-V test was dropped. After the pre-stress testing, each capacitor received a constant negative current stress for a prescribed time. The current densities and stress times were determined under the conditions of the contract to acquire the necessary data from the number of parameters being examined. The cells which required radiation exposure were treated before the electrical testing began. Radiation levels were determined for levels discussed in the literature which gave changes great enough to detect (David Fisch). During the electrical constant current stressing the voltage levels required to maintain the prescribed current were monitored (FIGURES 4.1A and 4.1B) and recorded. After the constant current stress, post CV plots were generated.

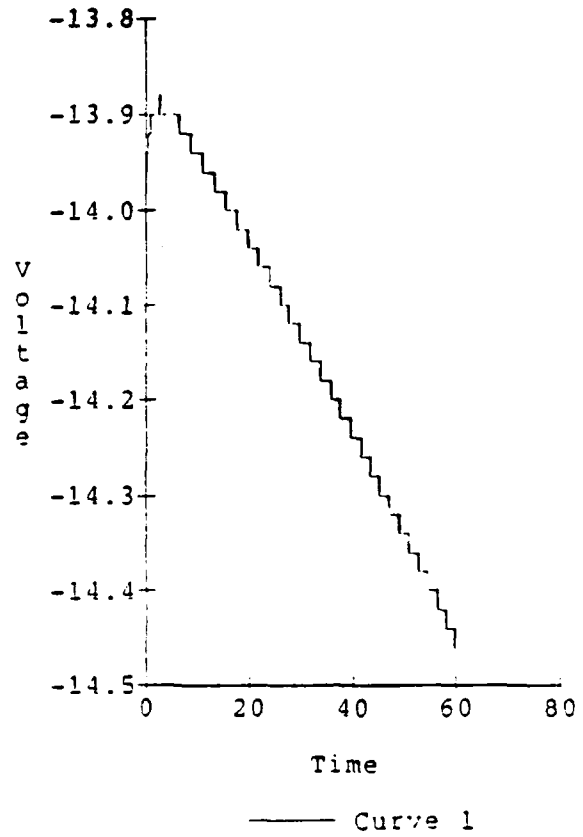
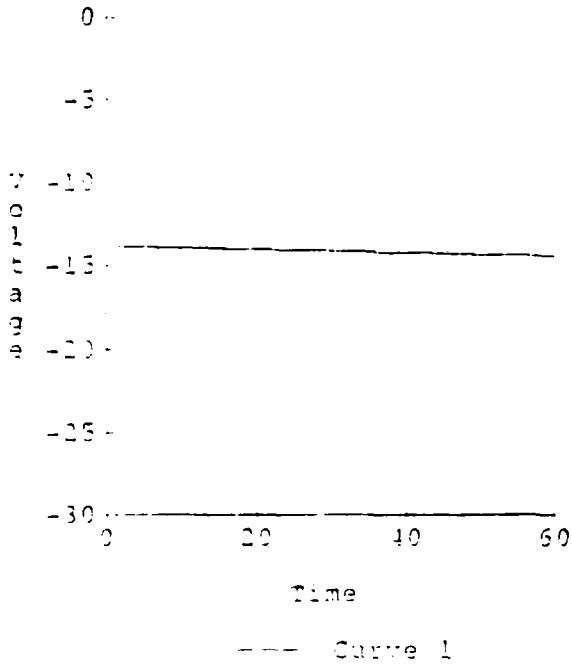
4.1.2 Pre Stress Testing

4.1.2.1 Pinhole test

Pinhole tests were taken on each capacitor at various voltage ranges according to the oxide thickness range. -5 volts was used on the 200 angstrom oxide range, -2.5 volts was used on the 100 angstrom oxides and -1.25 volts on the 50 angstrom oxide range of oxide thickness. A -100.0 nanoamp current flag signified a pinhole at the specified voltage. The capacitors used in this study were of $6.34E-4$ cm squared area. The total area per wafer tested was $3.8E-1$ cm squared and no die were found to be failing the pinhole test for any oxide thickness. This finding is consistent with typical pinhole densities at SGS-Thomson Americas. The pinhole density is low enough to require larger test areas to make a significant determination

4.1.2.2 Pre C-V testing

Lot# Wafer# 22 Die# 62
 X = 0 Y = 6 Pin# 47
 I = -0.0002 T = 60
 Test Date = 21-MAY-88



Lot# Wafer# 22 Die# 62
 X = 0 Y = 6 Pin# 47
 req = 1000 Volt = 0.1 Tox = 106.4283
 C> = 201.940006pF C< = 3.946pF
 Test Date = 21-MAY-88

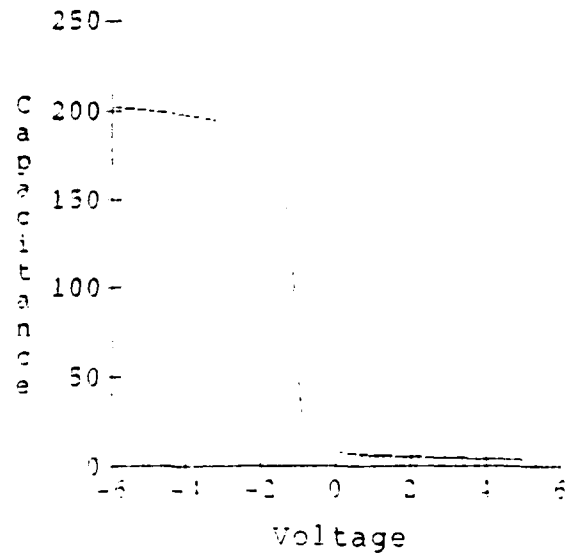


FIGURE 4.1.0 - PRE/POST OXIDE STRESS
 C-V CURVES

Due to the variation in oxide thickness the magnitude of the sweep voltage was modified to prevent unintentional stress. The 200 angstrom range of oxide thickness used a sweep voltage of -10.0 volts to +3.0 volts. The 100 angstrom range of oxide thickness used a sweep range of -6.0 to +5.0 volts. The 50 angstrom range of oxide thickness used a -4.0 volts to +4.0 volts sweep. Preliminary tests were performed to insure that maximum capacitance was attained at the sweep starting voltage for each range of thickness. The pre-stress C-V was plotted for each capacitor as shown in FIGURE (4.1C). After the current stress, the post-stress C-V is taken in the same manner as the pre C-V and plotted with the pre stress C-V. It was found that the initial capacitance of the test sites was undependable due to the equipment set-up. Therefore, oxide thickness calculations from the initial capacitance was inaccurate. Because of this and the necessity for accurate oxide thicknesses in the analysis of the matrix, selected die were used to determine the wafer oxide thickness from Fowler-Nordheim tunneling current. These die were not used in the stress matrix and on the wafer map they are labeled "untested".

4.1.2.3 Oxide Thickness Determination

Eight capacitors per wafer were selected in the interior portion of each wafer and used for thickness determination. A constant, 0.5 volts/second, voltage ramp was applied until oxide breakdown occurred on these capacitors (FIGURE (4.2)). This ramp rate has been determined, from previous studies, to be fast enough to avoid trapping induced errors. A 3 point fit at $\sim 10^{-9}$, 10^{-7} , 10^{-5} amps to Fowler-Nordheim tunneling probability EQUATION (4.1) was made to the resulting I-V plots:

$$I(FN) = A (1.4 \times 10^{-6})(E^{*2})e(\text{EXP}(-2.35 \times 10^{-8}/E)) \quad (4.1)$$

These thicknesses were used in the calculation of Ebd and the results were included in the Input/Output Table (TABLE 4.1).

4.1.3 Oxide Stress Parameters

The current densities for oxide stressing were determined by sample wafers run previous to the actual matrix wafers. In accordance with time restrictions for the completion of the matrix testing and the necessity to have representations of pre and post C-V data for $\Delta V(fb)$ for each cell, levels of current density were chosen. The

Lot# Wafer# 36 Die# 79
X = 4 Y = 7 Pin# 47
Step V = 0.5 Ramp = 0.5
Test Date - 13-MAR-88

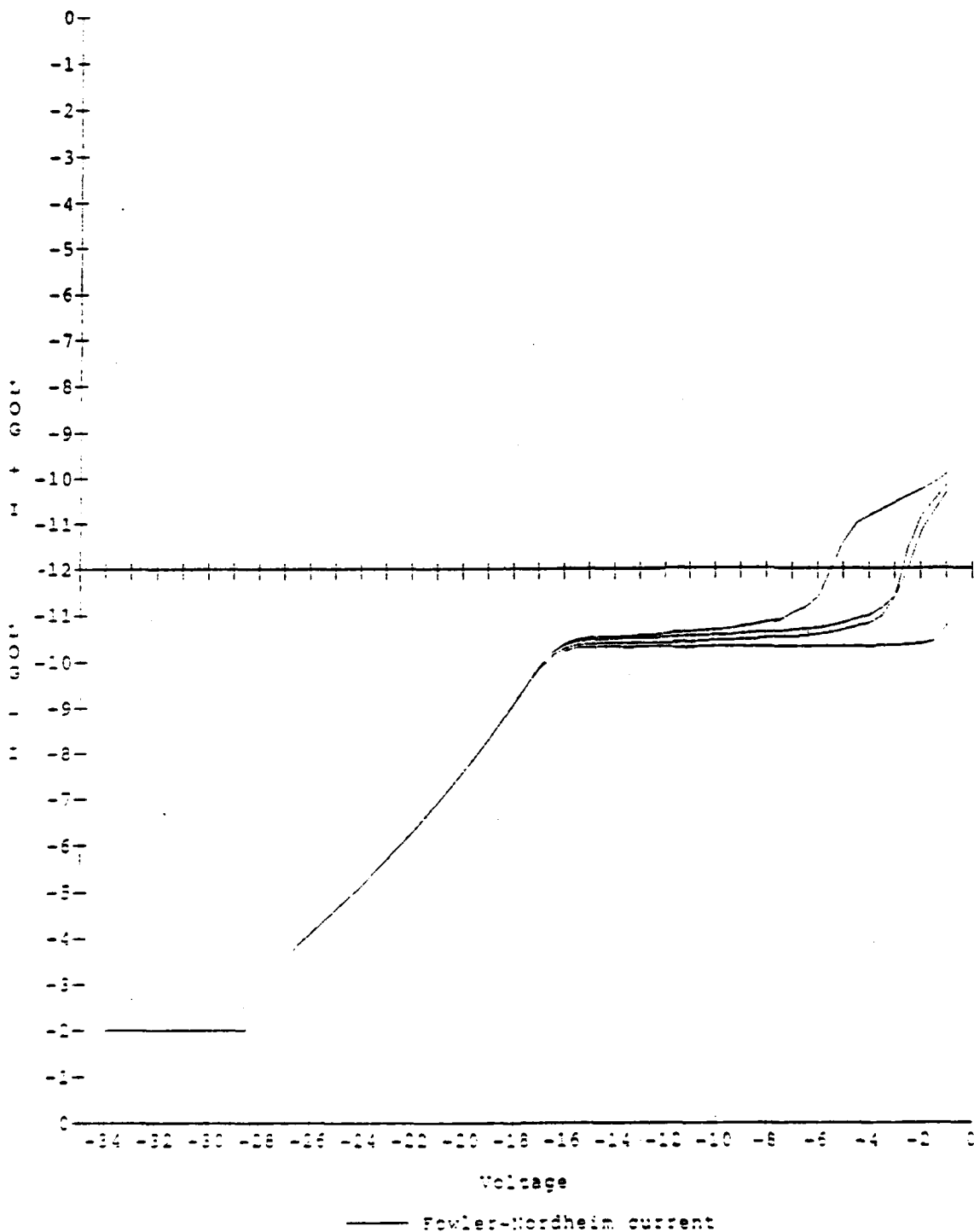


FIGURE 4.2. - I-V PLOT OF OXIDE TUNNELING
CURRENT FOR THICKNESS DETERMINATION

Cell (#)	WATER (#)	Temp (°F)	I (Amps)	Stress Time (Sec)	DOSE (KRADS)	DVFB (Volts)	k (%)	BVT (%)	# PT	k TOT (%)	Fail (%)	Ebd (MV/cm)	T10 (sec)	T16 (sec)	T50 (sec)
09	61.3	10	2.E-4	1	0	-0.21	2%	573		5%		13.13			
16	61.0	10	2.E-4	1	0	-0.21	19%	388		15.3%		13.21			
17	219.0	10	2.E-4	60	0	-0.5	1%	110		81%		11.10	0.45	1.43	17.01
17	219.5	10	2.E-4	60	0	-0.5	4%	106		81%		11.31	0.39	1.11	13.01
15	59.6	30	2.E-4	60	500	-0.34	1.2%	0		100%		13.89	7.67	10.0	14.25
15	50.3	30	2.E-4	60	500	-0.30	3%	10		98.3%		15.40	5.38	8.38	15.57
01	271.7	30	2.E-4	1	500	ND	10%	273		55%		11.22	0.03	0.05	0.77
01	233.1	30	2.E-4	1	500	ND	10%	461		23%		11.26	0.03	0.35	
07	59.7	50	5.E-4	60	0	-0.26	19%	0		98%		15.97			3.16
07	61.0	30	5.E-4	60	0	-0.28	1.9%	0		98%		11.90	1.86	2.12	4.51
02	280.6	30	5.E-4	1	0	ND	21%	2		98%		11.55			0.11
02	233.1	30	5.E-4	1	0	ND	7%	302		50%		11.67	0.04	0.19	0.81
13	57.9	30	5.E-4	1	500	-0.31	1.9%	573		5%		14.90			
13	61.5	30	5.E-4	1	500	-0.31	10%	514		14%		14.04	0.03		
09	219.5	30	5.E-4	60	500	ND	5%	0		100%		11.69	0.08	0.21	1.09
09	218.5	30	5.E-4	60	500	ND	5%	0		100%		11.74	0.08	0.21	1.09
11	55.2	125	2.E-4	60	0	-0.16	12%	1		99.8%		ND		0.29	1.86
11	51.3	125	2.E-4	60	0	-0.19	4%	0		100%		ND	0.03	0.92	1.7
08	237.9	125	2.E-4	1	0	1.5	4%	513		15%		11.35	0.33	1.0	
08	229.5	125	2.E-4	1	0	-4.94	4%	534		11%		ND	0.77		
14	57.0	125	2.E-4	1	500	-0.19	8%	480		20%		14.36	0.04	0.77	
11	65.6	125	2.E-4	1	500	ND	15%	452		24.6%		13.28		0.04	
06	232.1	125	2.E-4	60	500	0.29	4%	0		100%		11.58	0.32	0.70	7.67
06	236.0	125	2.E-4	60	500	ND	5%	1		99.8%		11.47	0.12	0.70	10.0
10	56.5	125	5.E-4	1	0	-0.18	3%	181		70%		14.91	0.41	0.54	0.84
10	54.7	125	5.E-4	1	0	-0.17	24%	89		85%		15.41			0.61
01	269.4	125	5.E-4	60	0	ND	16%	2		99.7%		11.68		0.03	0.39
01	233.9	125	5.E-4	60	0	ND	7%	0		100%		11.93	0.06	0.49	1.49
05	58.0	125	5.E-4	60	500	-0.16	15%	0		100%		14.50		0.03	0.64
05	58.0	125	5.E-4	60	500	-0.19	15%	0		100%		15.56		0.03	0.64
01	219.5	125	5.E-4	1	500	-5.72	5%	363		39.5%		11.48	0.05	0.23	
01	214.2	125	5.E-4	1	500	-5.63	7%	369		38%		11.95	0.08	0.28	
17	124.2	70	3.5E-4	10	50	-2.0	2%	539		10%		11.35	10.0		
17	123.9	70	3.5E-4	10	50	ND	2%	494		17.7%		11.30	8.4	9.8	

DVFB = Delta V Flat Band

k BVT = k Below Valid Time

PT = # that Passed Test

k TOT = Total k that failed on Cum k Fail vs. Time plot

ND = No Data

T10, T16, T50 Time in seconds for 10, 16, and 50% failures respectively

current density also would not only dictate the magnitude of the delta V(fb), but also the percentage of failed oxides to be used in TTF calculations. In order to meet these demands, current density magnitudes were chosen to yield significant data in all categories. This meant that some holes in the data outputs would naturally exist. Stress levels to attain data in the categories above for 200 angstrom oxides would over stress the 50 angstrom oxides and result in large failure percentages and no post stress C-V results. Likewise, current densities to yield results in the 50 angstrom thickness ranges would not fail enough capacitors to have significant TTF data. Therefore, a compromise in the current density ranges was made to yield data in all categories at some level of stress for each cell, all within a timely fashion.

Current densities chosen were: -0.79, -0.55 and -0.31 amps/cm squared (500 uA, 350 uA, 200 uA respectively for an area of $6.35e-4$ cm**2.) The times of stress chosen not only needed to be timely in order to test all of the wafer in the matrix, but also needed to complement the current densities in yielding data in all the output categories. Times chosen using the pre-matrix samples wafers were: 1, 10 and 60 seconds.

Stress temperatures were chosen to complement the typical industry standard testing temperatures. Temperatures chosen were: 30, 70 and 125 degrees C. Thirty degrees was chosen for the "room temperature" measurement because of the ability to have a stable temperature while using a chuck equipped with only a heater element. Ambient room temperature during the testing was in the 24 degrees C range.

During the stress of each oxide, the voltage to sustain the specified current density was monitored. The time between voltage sampling was in the range between 5.0-16.7 milliseconds. This time was dictated by the DMA (Direct Memory Access) internal to the Keithley tester being used. Plots were generated of voltage vs. time as shown in FIGURE (4.1A and 4.1B). Also, from this data, outputs of delta Vg at failure times and failure voltage (Vbd) were generated.

4.1.4 Post Stress Testing

C-V plots were generated after the stressing of the oxides. The C-V sweep ranges were the same as those used in the pre-stress C-V test. The frequency and oscillator level used during the C-V sweep were 1.0 MHz and 0.1 volts

Voltage at Fail vs Time at Fail

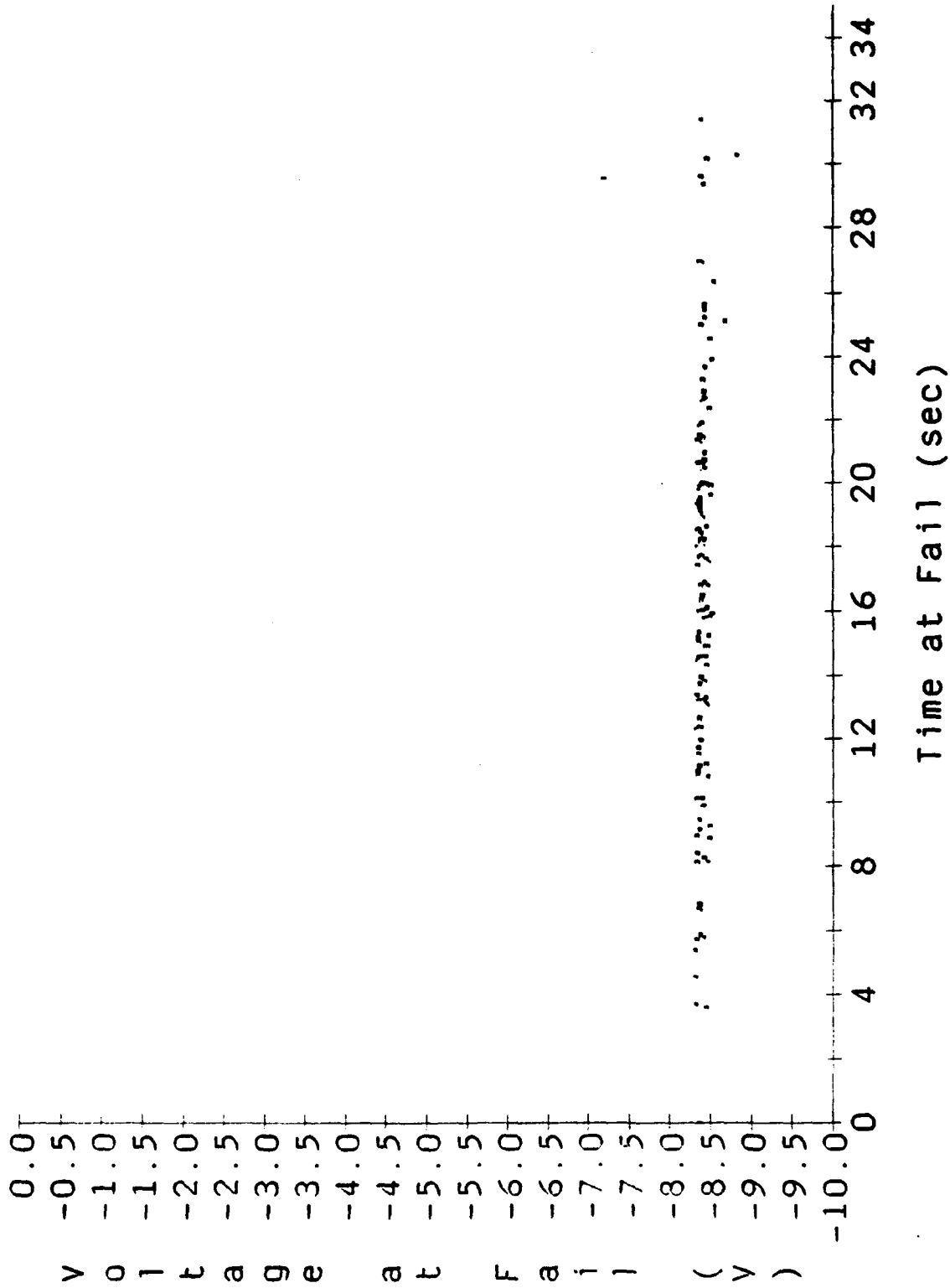


FIGURE 4.3 - Voltage at Fail vs Time of Fail

respectively. Delta Vfb values from the pre and post sweeps were of little value in some cases because of the large amounts of fluctuation in the data. We could not clearly distinguish between oxides near breakdown and oxides which could withstand longer stress times. This had the tendency to automatically build in large deviations. Nevertheless, where the data is good it has been used in the analysis.

4.1.5 Results and discussions

The Input/Output Table (TABLE (4.1)) gives a cursory view of the inputs and outputs of the test matrix. Output categories include:

4.1.5.1 Delta Vfb - the delta of the pre stress C-V and the post stress C-V at the half Cmax value. Post C-V data was taken at the end of the stress time for the cell. Where delta Vfb data occurs when % total fails is 100%, data is from < 25 of the tested caps which have acceptable post Vfb, but are "failed" capacitors.

4.1.5.2 % BVT - % of capacitors failing below the equipment valid measurement time of 34 milliseconds.

4.1.5.3 PT - number of good capacitors at the end of the stress time.

4.1.5.4 % TOT Fails - % of failed capacitors on the cumulative % fail vs. time plot. Note that these failures do not include probe pick-up failures.

4.1.5.5 Ebd - electric field at oxide failure. This value is calculated from the voltage (Vg) at fail vs. time plots for each wafer as shown in FIGURE (4.3). The voltage value used to calculate the Ebd comes directly off of the plot using the minimum threshold voltage illustrated. The extraction is done manually.

4.1.5.6 T10, T16, and T50 - are time in seconds that correspond to 10 percent, 16 percent and 50 percent cumulative failures.

4.1.5.7 Time to Fail Dependence

A strong time to fail dependence is seen in relation to the stress current. FIGURE (4.4) is a plot of Time for 50% failure vs Breakdown Field. FIGURE (4.4) illustrates, for both the 50 and 200 angstrom ranges of thickness, that the

oxides stressed to 500 microamps failed much sooner than the oxides stressed at 200 microamps. This plot also the 200 angstrom, 500 microamp current group (lower left group of data). The 30 degree test temperature has a longer time to fail for the 200 angstrom, 200 microamp stress, and the 50 angstrom, 500 microamp stress conditions.

Radiation effect is random in all the data groups illustrated in FIGURE (4.4) except the 200 angstrom, 200 microamp group. This is probably because the temperature stress is grouped to trend with the radiation magnitude. Therefore we assign a smaller or no significance to the effects of radiation on the TTF. It should be noted that the oxides were not biased during exposure to radiation and this result is consistent with findings of other researchers [12], [13].

The fact that the oxides stressed with 200 microamps lasted consistently longer than the 500 microamp stressed oxides appears to be entirely independent of the oxide thickness. The same trend was seen in the Time for 10% and 15% failure vs Breakdown Field characteristics.

4.1.5.8 Field Breakdown Dependence

A Field Breakdown (Ebd) dependence on oxide thickness can be seen in FIGURE (4.4). Also the difference in slope of the 50 angstrom oxides dependence on field from the slope of the 200 angstrom oxides indicates a change in the field acceleration factor with changing Ebd.

4.1.5.9 Time To Fail

Cumulative % failures in time plots (TTF) were generated directly from the monitor of voltage in time during stress. FIGURE (4.5) is an illustration of the TTF plot. The vertical line at a time between $10E-2$ and $10E-1$ represents the limit of the equipment to accurately measure the time to fail. From these plots, which were generated for each wafer, were extracted data for the T10, T16, and T50 columns of the Input/Output Table (TABLE 4.1).

4.2 WAFER DEFECT MAPPING

4.2.1 Introduction

Wafer defect mapping is an effective analysis tool for location of defect sensitive areas of a wafer. The

Lot# P50328 07 Pl 08
Material 07 08
Stress Current -0.0005A
Stress Time 60 Sec
1 Die Passed
T16 = 2.582422
T50 = 5.251302
SIGMA TIME = 0.709748

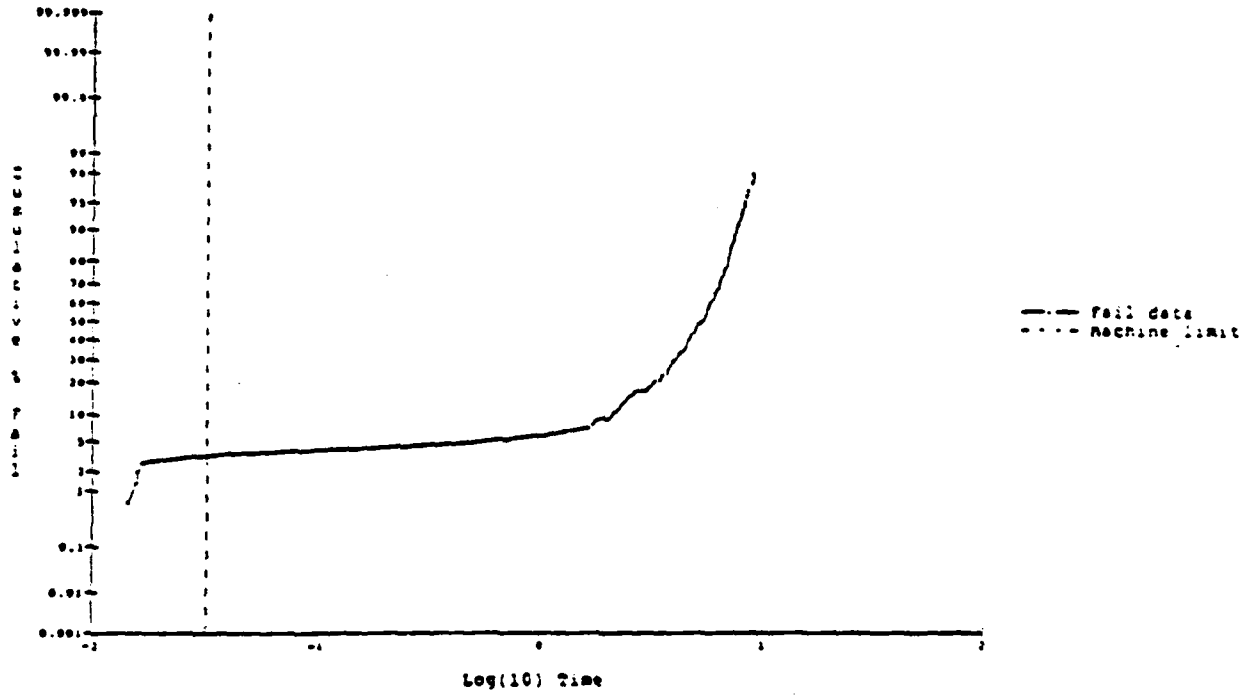


FIGURE 4.5 - TTF PLOT (CUMULATIVE & FAIL vs LOG TIME)

illustrates that although the time to fail is dictated first order by current density, and that temperature is a second order effect. This is clear in all the categories except technique can elucidate problems such as process induced effects, wafer orientation effects, and substrate defect locations. Process effects can be caused by etch rate non-uniformity, uneven oxidation rate or contamination level due to furnace wall proximity in the gate or capacitor oxide growth cycle, to name a few. Defect mapping can also highlight surface stacking faults (SSF) densities from oxygen concentrations in silicon substrate or crystal slip caused by thermal stress from heating non-uniformity. Therefore, this type of analysis is very important to determine the randomness of the defects under investigation and to help elucidate any defects created by effects from the above mentioned sources. The randomness of the defects insure that the defects being studied are of an inherent nature to the process and therefore "intrinsic" to the production of devices.

4.2.2 Analysis

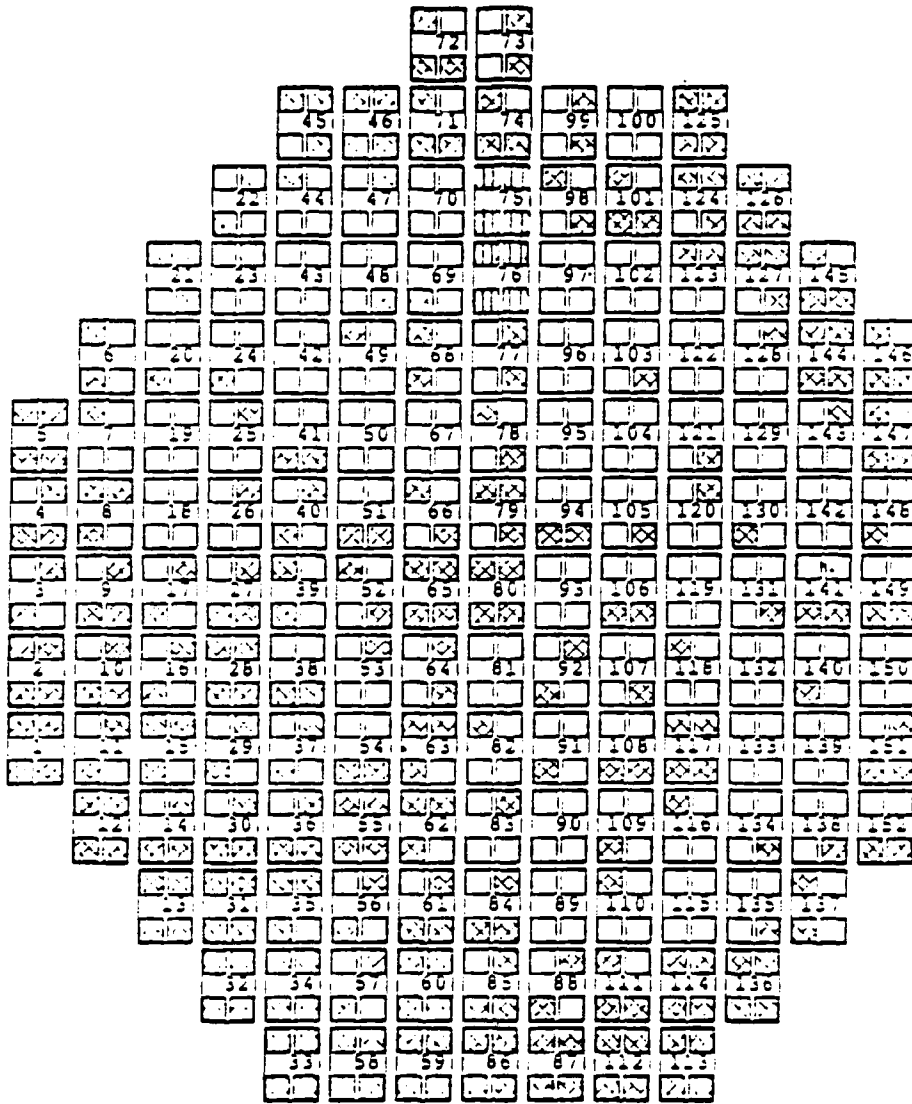
At the completion of wafer testing each die tested was mapped and labeled into categories, refer to FIGURE 4.6. There were four capacitors on each die, and 152 die per wafer. The die on the map were numerically labeled in the same order they were tested. The four squares within the larger squares (die) represent the individual capacitors and they are orientated as they are in each die. The categories that the capacitors were sorted into are: good capacitors, shorted capacitors, untested capacitors, and failed capacitors. Good caps are capacitors that had not ruptured at the end of the stress, that is, they passed the criteria of greater than 7.0 volts to sustain the current density of the test at the end of the test time. The 7.0 volt criterion applies to all the current densities and thicknesses in the matrix. Shorted caps are capacitors which failed a 100 nanoamp/ pinhole test criterion previous to the current stress. The pinhole test voltage was 5.0 volts for the 200 angstrom range oxides, 2.5 volts for the 100 angstrom oxides, and 1.25 volts for the 50 angstrom oxides. These caps would have been used to determine the pinhole density, but the densities were found to be too low for the area studied. Untested capacitors were capacitors not used in the constant current stress testing because they were used for I-V comparisons or oxide thickness determinations. Failed caps are capacitors which have failed the voltage criteria mentioned above for good caps at the end of the stress time.

LOT # - P50328

WAFER # - 46

MAP DATE - 14-JAN-88

- GOOD CAP
- UNTESTED CAP
- SHORTED CAP
- FAILED CAP



WAFER FLAT

FIGURE 4.6 200 ANGSTROM WAFER MAP

4.2.3 Discussion

Where a large percentage of the capacitors have failed at the end of the stress time (above 85 %) and likewise when a small percentage of the caps have failed (5-20%) it is easy to visually establish emerging trends in the maps. Fifteen of the 34 wafers in the test have effectively all the caps in the failed category and 2 wafers failed below 5% of the caps. This eliminates 50% of the generated maps from any trend analysis. Of the remaining maps it is evident that no radial or quadrat type trends are present. To illustrate this two examples are shown in FIGURES 4.6 and 4.7. FIGURE 4.6 is a map of a 200 angstrom wafer where 50% of the caps had failed after stress. FIGURE 4.7 is a map of a 50 angstrom wafer with 20% of the caps failed. It can readily be seen that no trends exist. Some edge die in the map (Figure 4.7) should be ignored because, by consensus we believe them to be caused by tweezer handling. This information gives evidence that the defects under investigation in this study are of a random nature.

4.3 Charge Trapping in 50 and 200 Angstrom Oxides Under Constant Current Stressing.

There have been many reports of fast hole trapping or donor trap generation followed by electron trapping or acceptor trap generation in stressed oxides [14]-[16]. Most reports agree that under a negative gate constant current injection, holes are trapped first, and eventually electron trapping dominates. In addition to this, most reports agree that the generation of traps increases with temperature, but there are conflicting reports concerning the effect of temperature on the density of trapped charge. In order to discuss charge trapping, we must first understand the method of characterization.

4.3.1 Theory and Methodology of Charge Trapping Analysis

We choose the method using the gate voltage change versus time necessary to maintain a constant current. The change in gate voltage (DV_g) for a single trapping mechanism is related to the electric field associated with that trap by EQUATION (4.2),

$$DV_g = E t_i + T_c \quad (4.2)$$

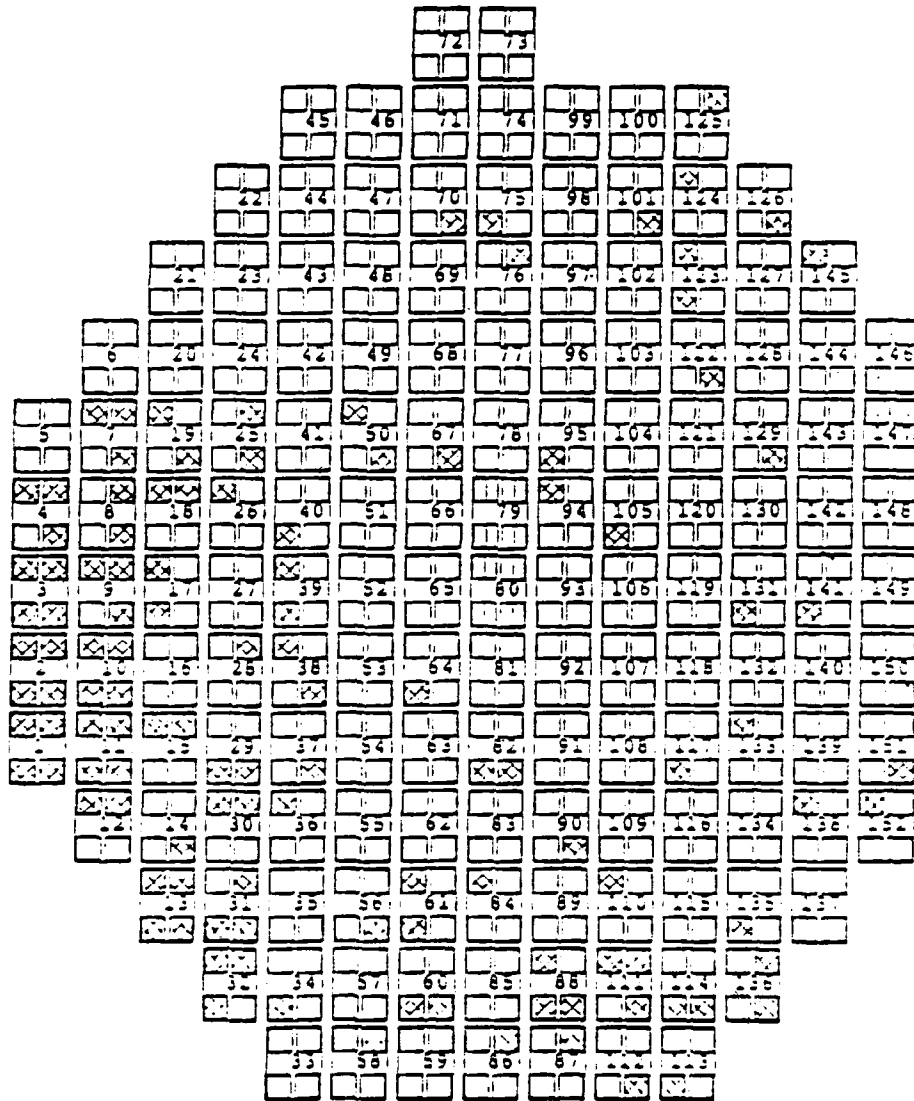
where T_c is the centroid of trapped charge measured from the non-injecting electrode and $E t_i$ is the trapping

LOT # - P50328

WAFER # - 06

MAP DATE - 07-APR-88

- GOOD CAP
- UNTESTED CAP
- SHORTED CAP
- FAILED CAP



WAFER FLAT

FIGURE 4.7 50 ANGSTROM WAFER MAP

field for that ith trap. The flatband voltage shift due to a single trapping mechanism is given by EQUATION (4.3),

$$DV_{fb} = E_{ti} * (T_{ox} - T_c). \quad (4.3)$$

From EQUATIONS (4.3) and (4.4), the centroid of trapped charge can be found for a single trapping mechanism as,

$$T_c = [DV_g / (DV_g + DV_{fb})] * T_{ox}. \quad (4.4)$$

The density of trapped charges for a single trap is related to the corresponding electric field as EQUATION (4.5),

$$E_{ti} = N_t * C \quad (4.5)$$

where $C = 2 * q / \epsilon$ and ϵ is the dielectric constant of SiO₂. From EQUATIONS (4.2) and (4.5), the density of trapped charge can be found to be EQUATION (4.6)

$$N_t = DV_g * C / T_c. \quad (4.6)$$

For traps with very small cross sections, the trap generation probability (G) is related to the density of trapped charge by EQUATION (4.7),

$$N_t = G * Q / q \quad (4.7)$$

where Q is the integrated leakage charge flux. Taking the derivative of EQUATION (4.7) with respect to time gives EQUATION (4.8),

$$dN_t / dt = G * J / q \quad (4.8) \quad \text{where } J \text{ is the current density.}$$

It is important to note here that the gate voltage change with time is made up of various components, each of which is related to a different trapping mechanism. Therefore, each DV_{gi} will correspond to a centroid of trapped charge and a trap generation probability. The trap generation probability, which may be defined as the number of traps per unit volume generated by one passing electron in cm⁻², is in units per electron. With these considerations in mind, we will now proceed with an analysis in general and an analysis designed to produce the outputs to be used in the Hadamard matrix.

4.3.2 Analysis of Data Concerning Charge Trapping Characteristics FIGURES 4.8 and 4.9 show some typical curves

for DVg vs time data for 50 and 200 Angstrom oxides respectively. The decrease in the magnitude of gate voltage change ($DVg > 0$ for negative gate injection) indicates hole trapping, while an increase in the magnitude of gate voltage change ($DVg < 0$ for negative gate injection) indicates electron trapping. It is obvious from the figures that initially both oxides are trapping holes, however, the hole traps for the 50 Angstrom oxide become saturated almost immediately while the hole traps for the 200 Angstrom oxides showed a much longer time until saturation of DVg with time, if saturation was observed at all. In fact, only one cell which was stressed at the lower current and for 60 seconds showed an eventual saturation of the DVg vs TIME curve which led a linear decrease of DVg with time, as observed in all of the 50 Ang. oxides, indicating a very large amount of electron trapping ($\sim 1e+13/cm^{**2}$) or a large amount of acceptor trap generation ($\sim 1e-06/e-$) as shown in FIGURE 4.10, However, these curves are not indicative of the data in general.

The initial hole trapping in the 50 Angstrom oxides occurs so fast that, for most of the wafers, there are only a few points or less which illustrate this effect, and for several it is as if the initial gate voltage change just appears between 10 and 50 millivolts above zero (FIGURE 4.11). It is for this reason, that we will concentrate on electron trapping or acceptor trap generation for the 50 Angstrom oxides; and hole trapping or donor trap generation for the 200 Angstrom oxides.

In order to be able to obtain a response for the Hadamard matrix analysis, it was necessary to determine a specific time at which the density of trapped charge (Nt) and the trap generation probability (G) should be analyzed. The trapping mechanism at that point in time would be the determining factor for the two quantities of interest. In determining a time at which to perform the analysis, two considerations had to be taken into account: 1) The time had to be one for which we had data for each cell and 2) We wanted to observe the effect, if any, that the charge trapping had on fails in time. From these two considerations it was clear that the most appropriate time to do the analysis was at the one second point.

It should be noted that all graphs of DVg Vs. Time are plotted Vs. Time of fail. That is, DVg is actually voltage at fail - initial voltage at the beginning of stress. This is a valid method due to the wide distribution of failures

Typical Delta Vg vs Time Curve

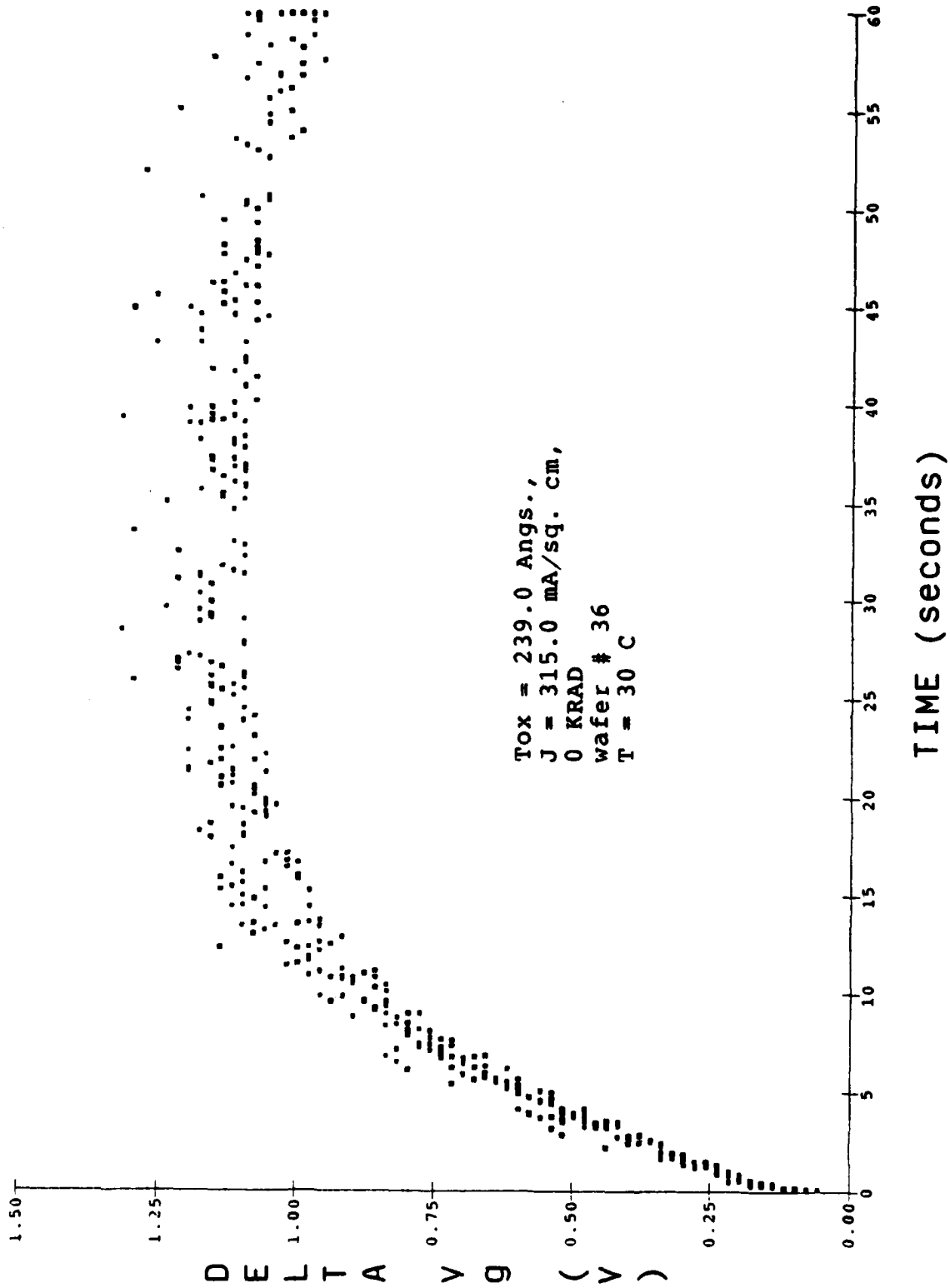
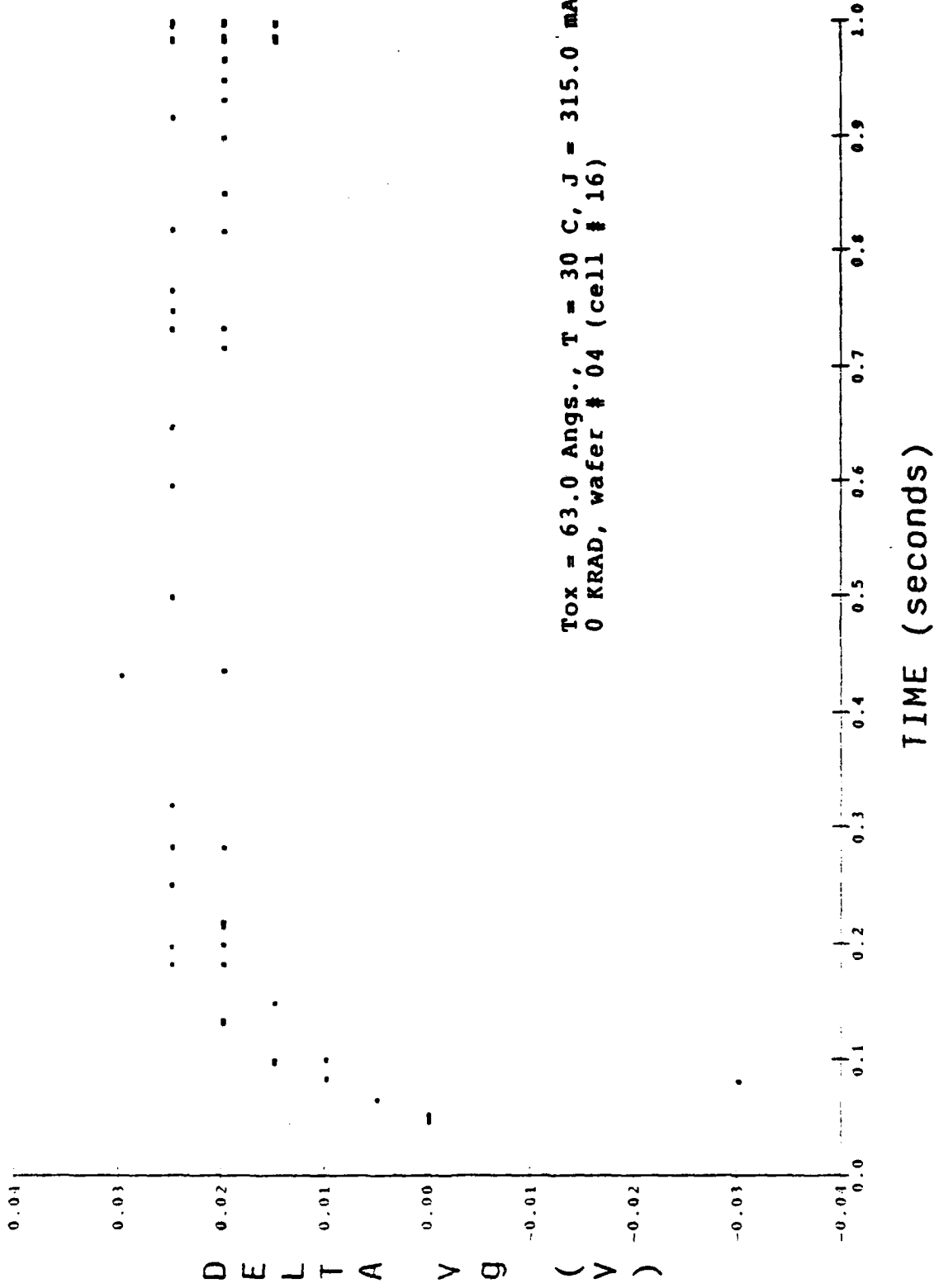


FIGURE 4.8. TYPICAL DELTA Vg vs TIME DATA (200 ANGS.)

Typical Delta Vg vs Time Curve.



Tox = 63.0 Angs., T = 30 C, J = 315.0 mA/sq.
 0 KRAD, wafer # 04 (cell # 16)

FIGURE 6.9. TYPICAL DELTA Vg vs TIME DATA (50 ANGS)

Electron Trapping Prior to
Breakdown for wafer # 42

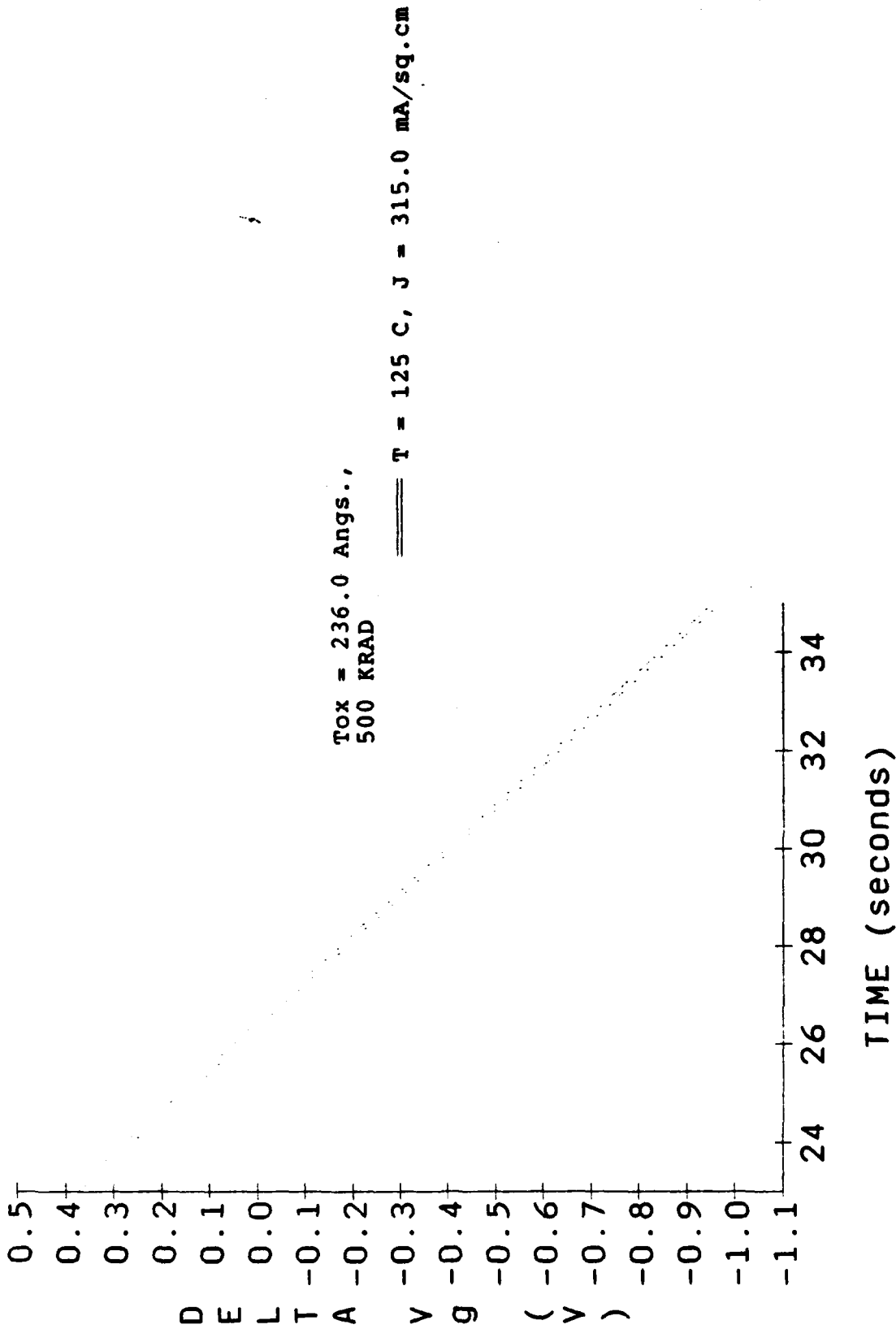


FIGURE 4.10. ILLUSTRATION OF HEAVY ELECTRON TRAPPING JUST PRIOR TO BREAKDOWN

Fast Hole Trapping for a 50 Angs.
 Illustrated by Wafer # 08

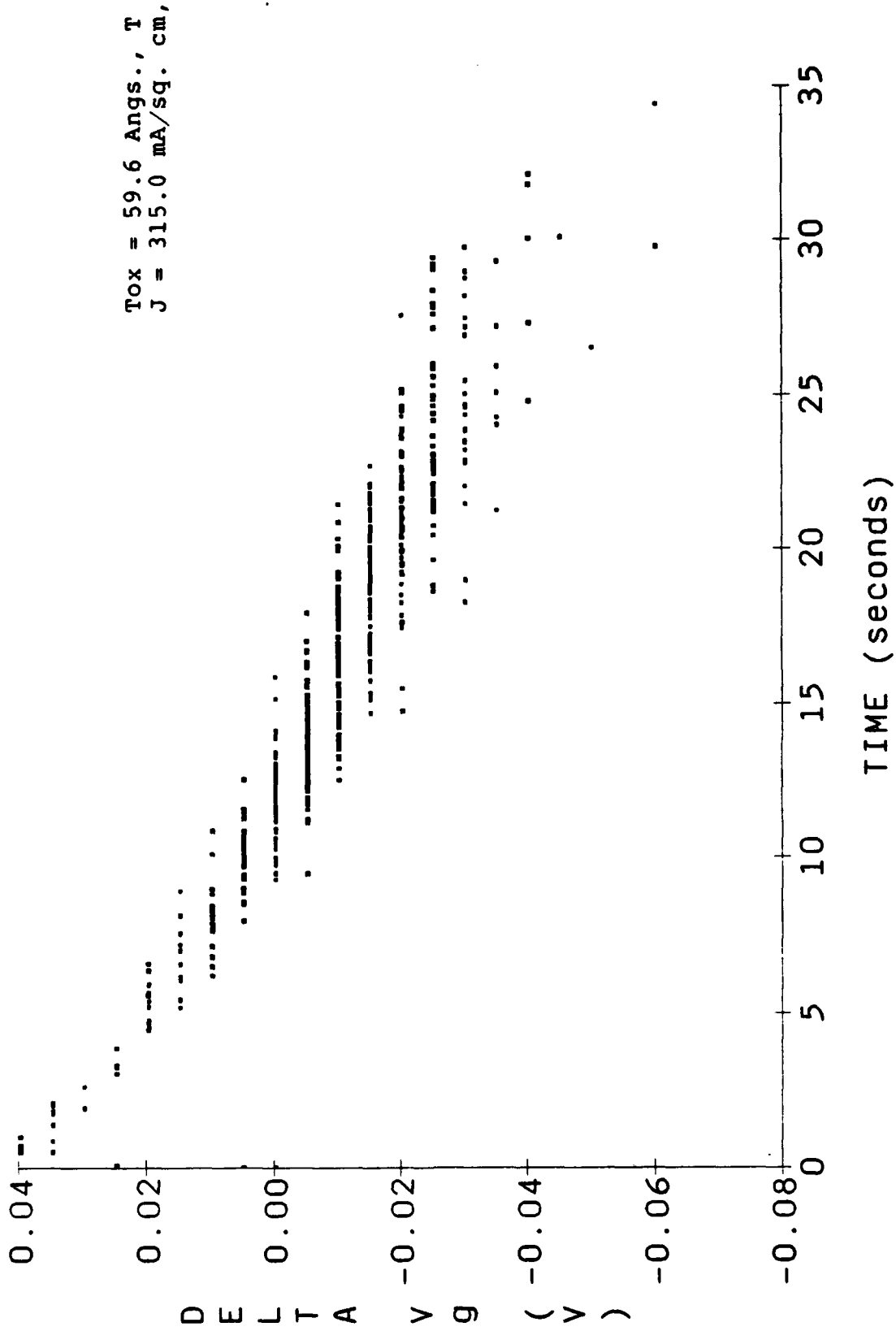


FIGURE 4.11. ILLUSTRATION OF INSTANTANEOUS HOLE TRAPPING IN THE 50 ANGS. OXIDES

in Time. Therefore, we do not have data for any one capacitor.

The analysis was performed by determining the dominant trapping mechanism, and then isolating that mechanism. In order to do this, only points which showed intrinsic breakdown characteristics and were related to that specific trapping mechanism were plotted. Also, for wafers which were stressed for one second, all points which indicated failure at the one second point were eliminated. This was because the probe, upon completion of the test, quickly ceases contact with the gate. When this happens, a voltage spike often occurs which blows the capacitor (and consequently causes a breakdown to be recorded.) Therefore, a somewhat large distribution of breakdowns occur at that point in time. To avoid any tainted conclusions, these points needed to be eliminated. Also, any points which showed failure at times below three one-thousandths of a second were eliminated due to machine limitations. The plots were then generated and least squares fits were obtained. From the equation of those fits the density of trapped charges and trap generation probability were obtained using EQUATIONS (4.6) and (4.8) respectively.

As stated previously, the analysis showed that for both thicknesses holes were being trapped initially with the eventual trapping of electrons. For the 50 Angstrom oxide, the trapping of holes became saturated very quickly while for the 200 Angstrom oxide, the hole trapping did not saturate for much longer times as was illustrated previously with the use of FIGURES 4.8 and 4.9. This is to be expected due to a smaller probability of electron collision in the thinner oxide.

Also, it was determined that for the different thicknesses, the trap density and trap generation probability differed by a factor of ten, and consequently the thicker oxide had the higher values for both. This is typified in FIGURES 4.12 and 4.13. Noyori et al., [17] has shown this to be true also.

FIGURES 4.14 and 4.15 show that the effect of temperature was to increase both the density of trapped charge and the trap generation probability for both electron and hole trapping in both thicknesses. This is illustrated even more effectively in FIGURES 4.16 (A and B) and 4.17 (A and B). It has been reported that at higher temperatures, the density of trapped charge actually decreases, however,

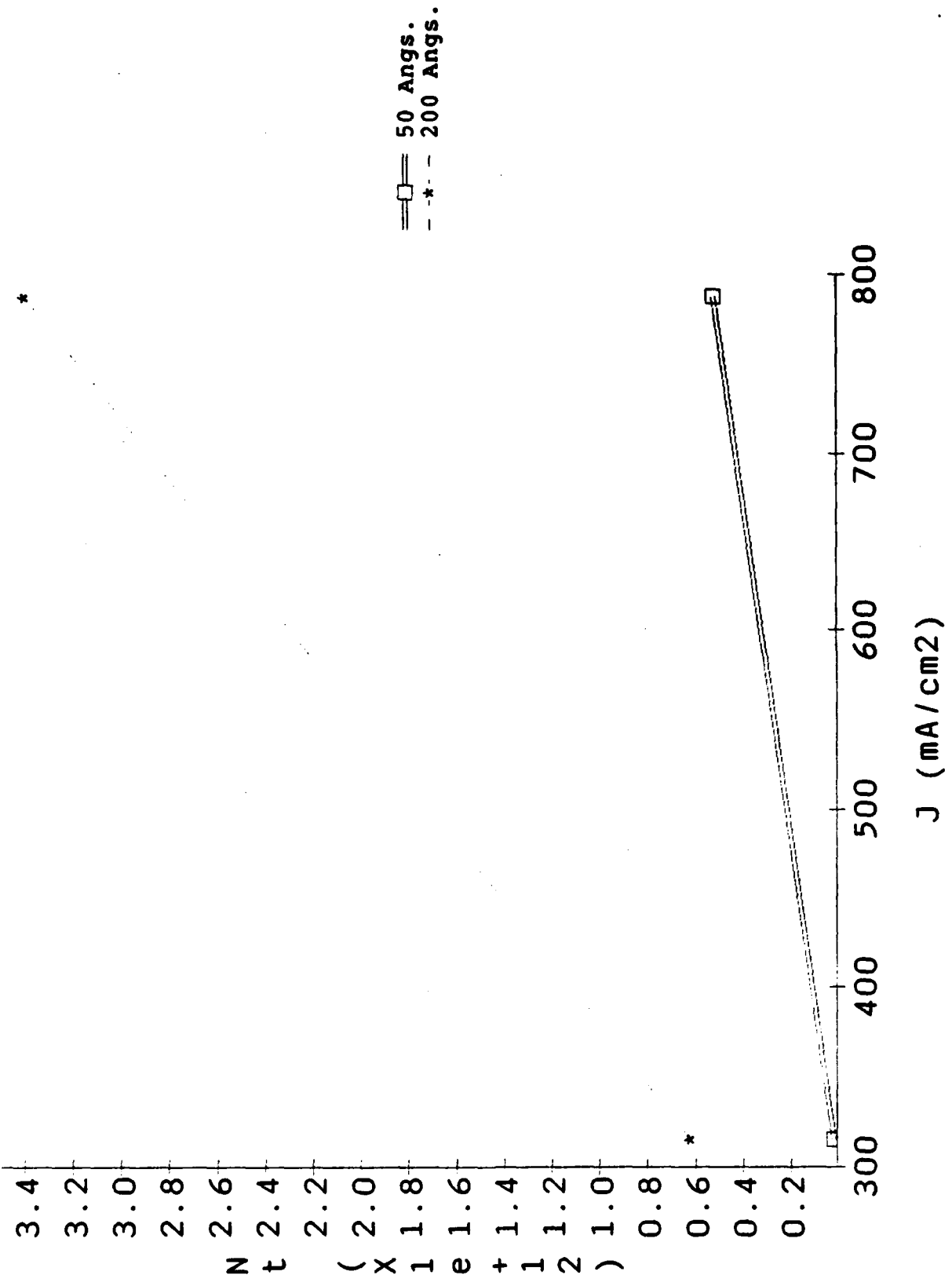


FIGURE 4.12. EXAMPLE OF THE 10X DIFFERENCE IN THE DENSITY OF TRAPPED CHARGE FOR 50 AND 200 ANGS. OXIDES

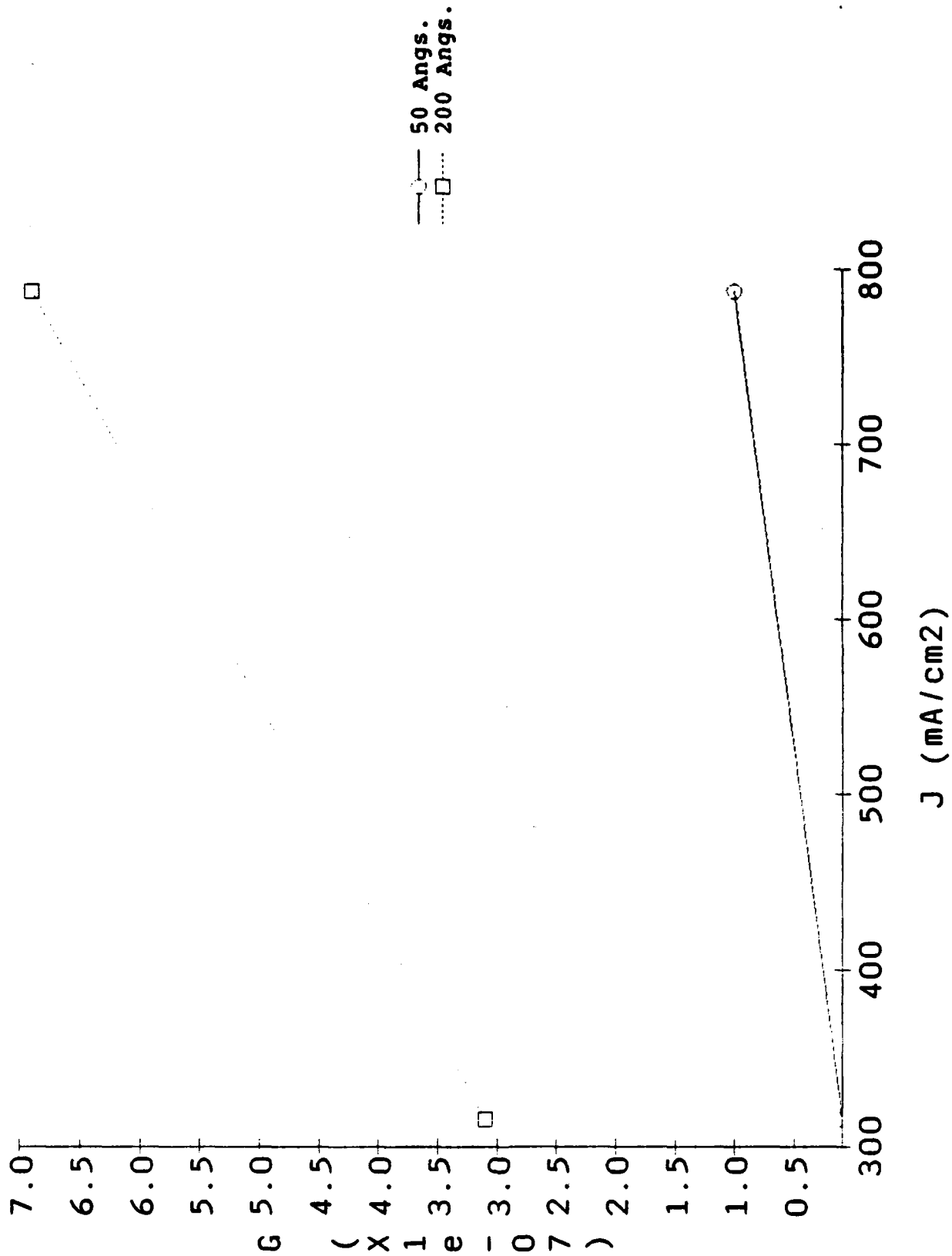
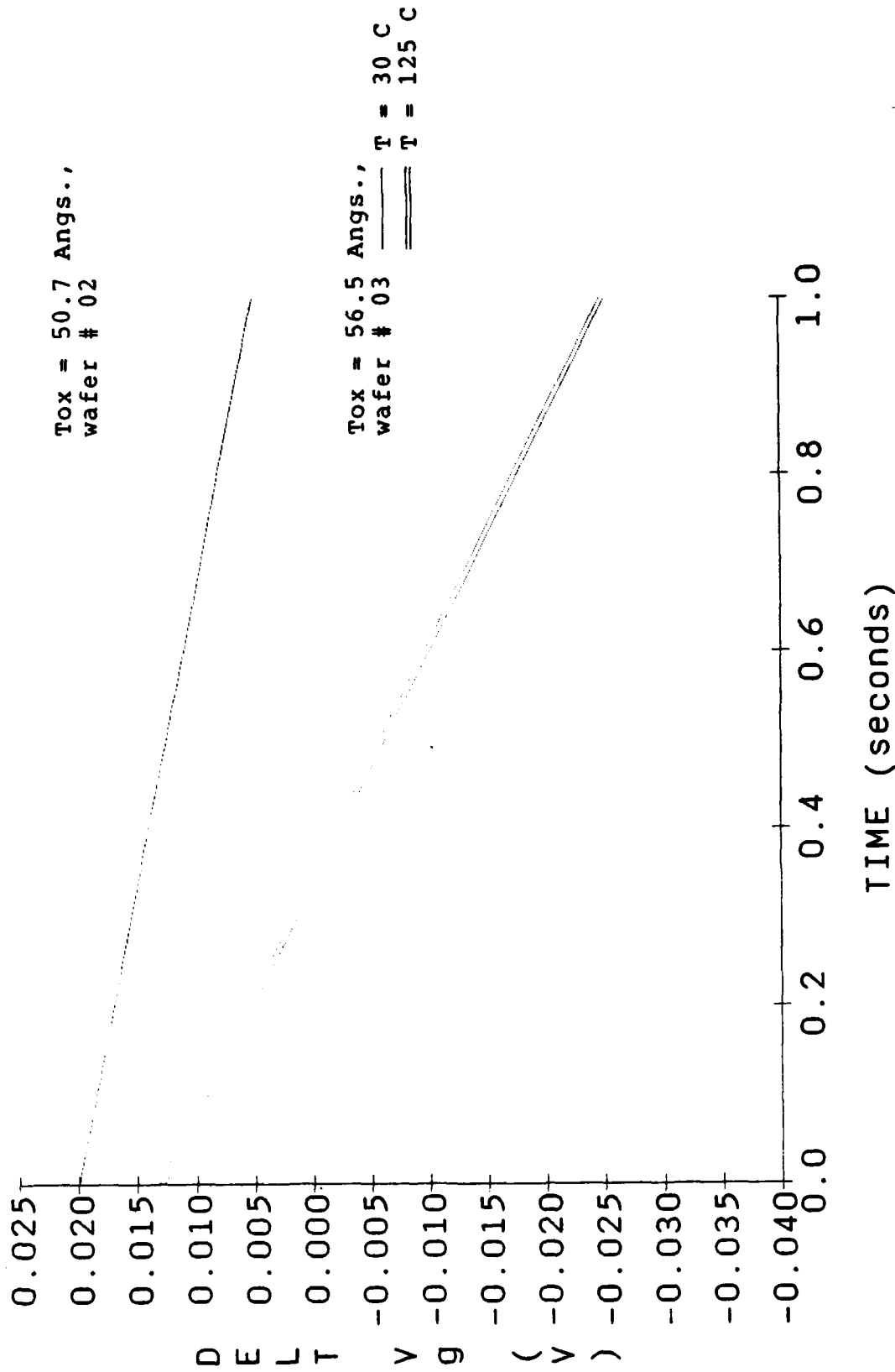


FIGURE 4.13. EXAMPLE OF THE 10X DIFFERENCE IN TRAP GENERATION PROBABILITY FOR THE 50 AND 200 ANGS. OXIDES

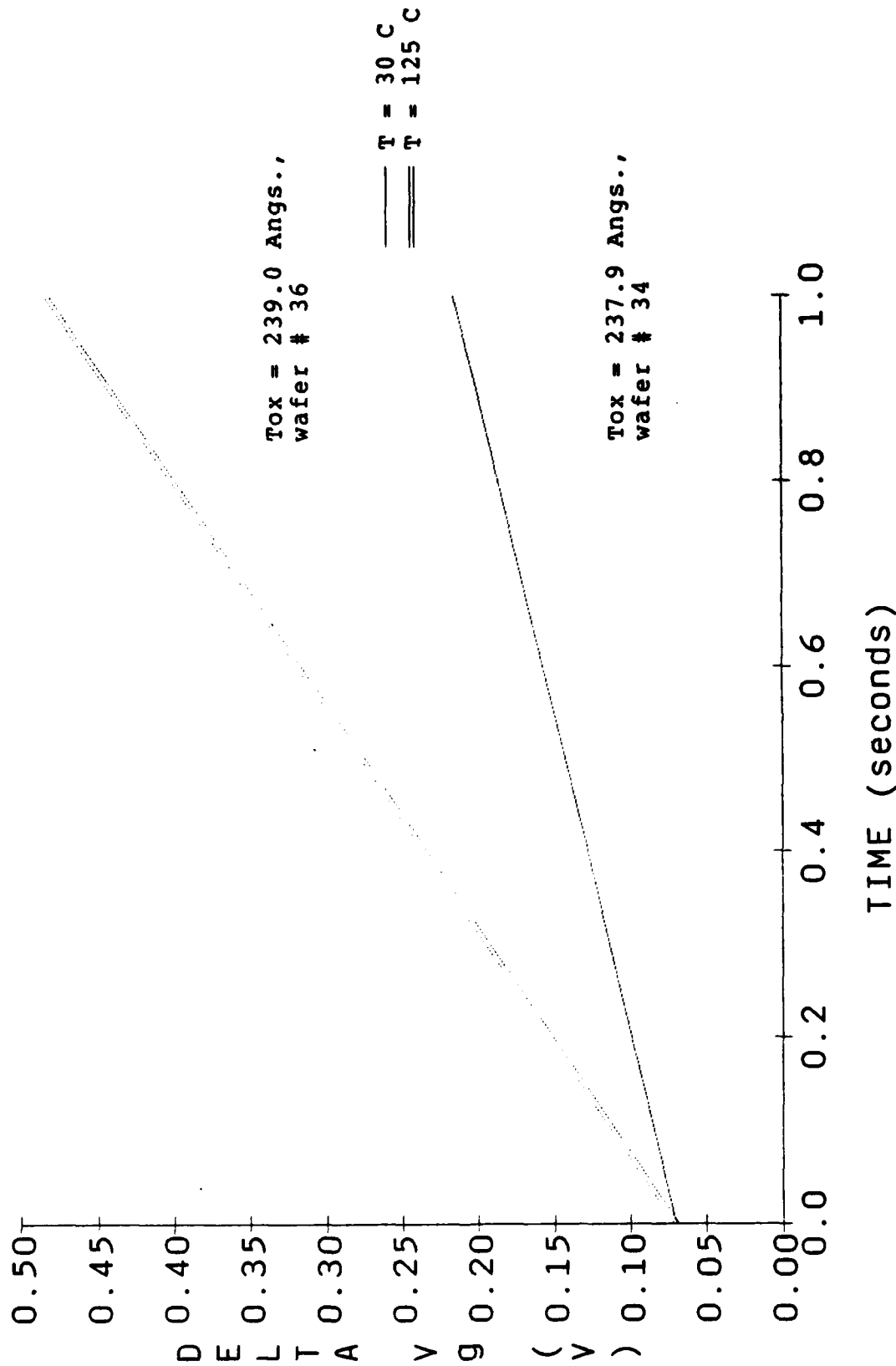
Effect of Temperature on 50 Angs. oxides.



J = 787.5 mA/sq. cm with 0KRAD for both wafers.

FIGURE 4.14. EFFECT OF TEMPERATURE ON CHARGE TRAPPING PROPERTIES OF 50 ANGS. OXIDES

Effect of Temperature on 200 Angs. Oxides.



J = 315.0 mA/sq. cm with 0 KRAD for both wafers.

FIGURE 4.15. EFFECT OF TEMPERATURE ON CHARGE TRAPPING PROPERTIES OF 200 ANGS OXIDES

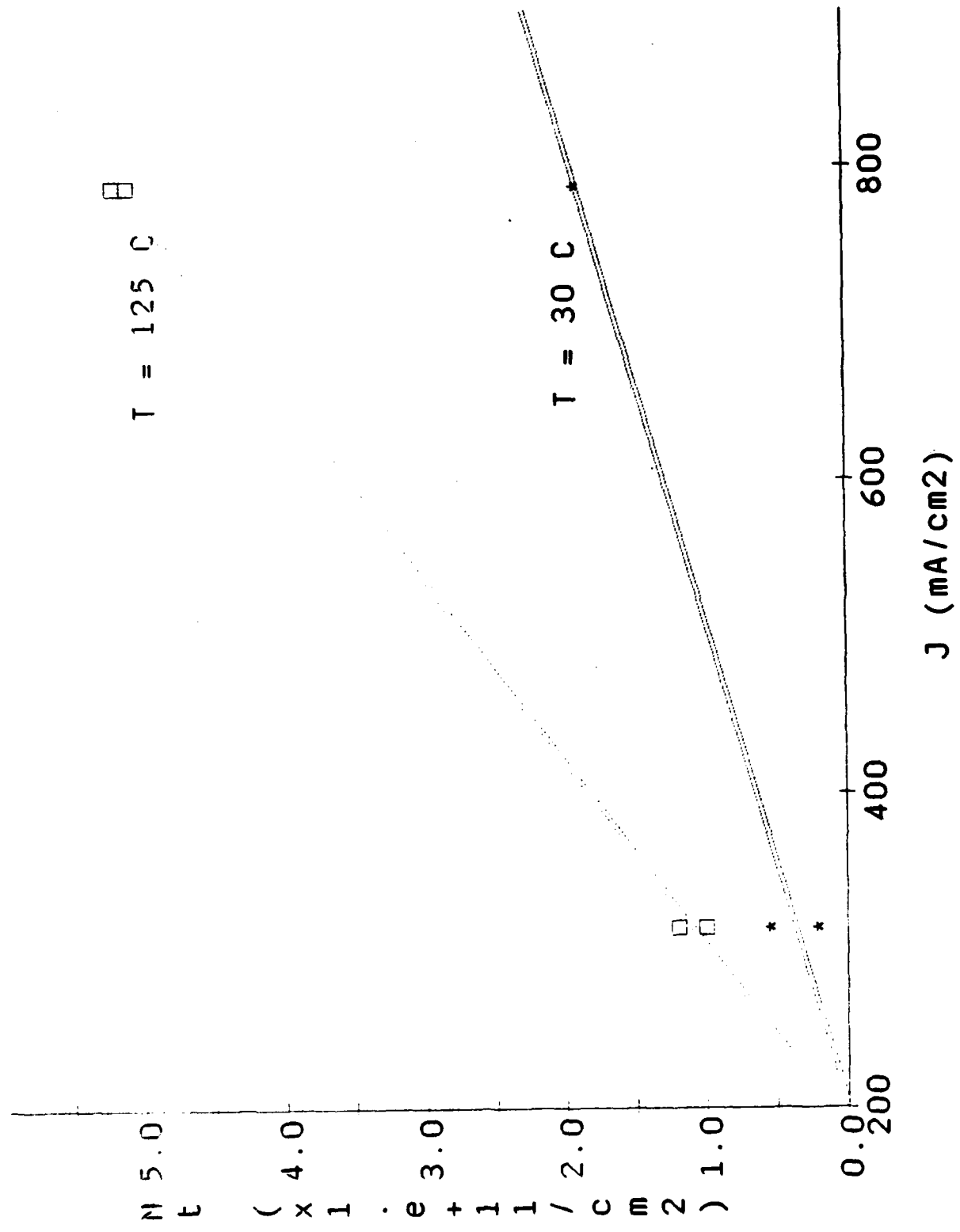


FIGURE 4.16A EFFECT OF TEMPERATURE ON CHARGE TRAPPING FOR DIFFERENT CURRENT DENSITIES FOR THE 50 ANGS. OXIDES

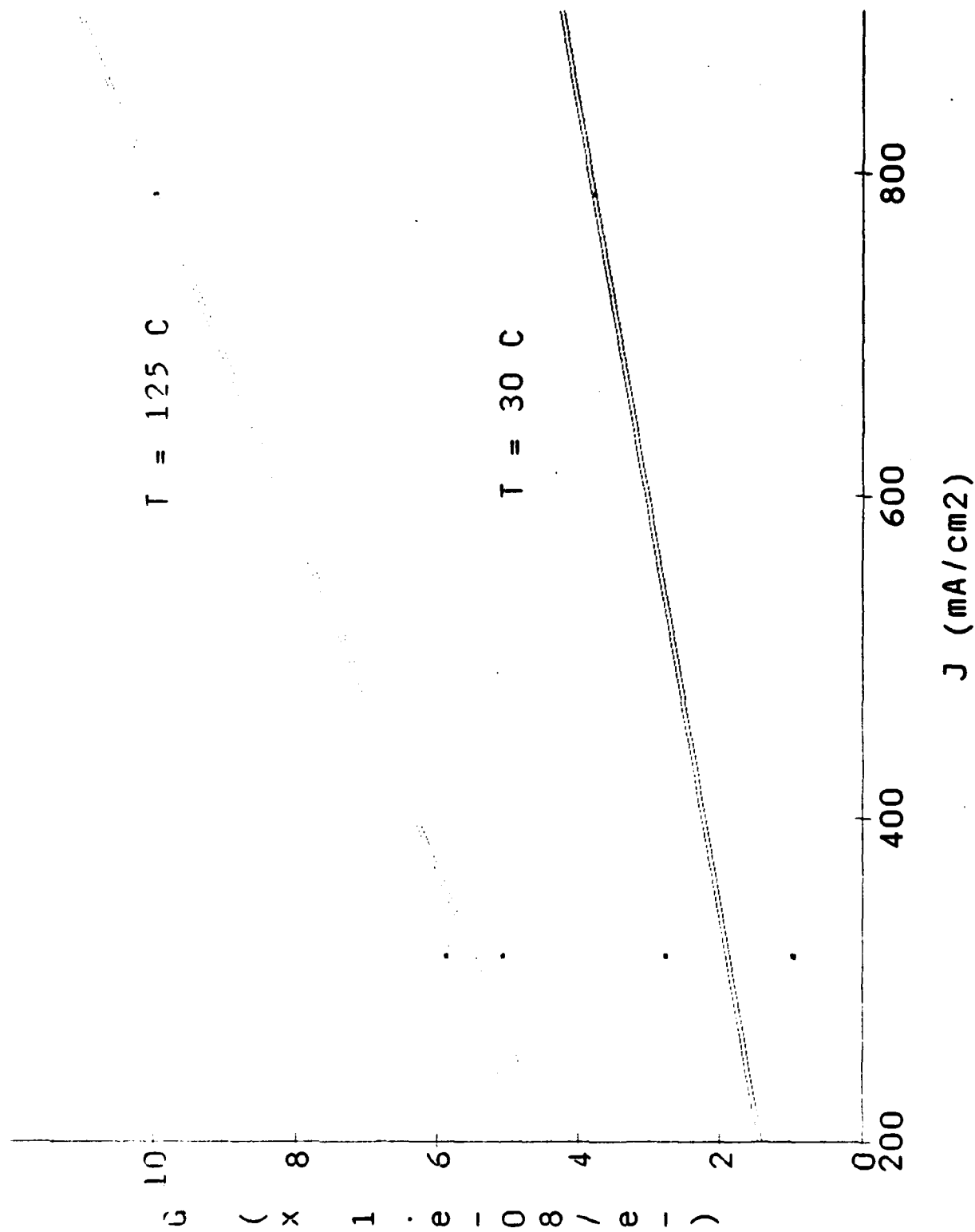


FIGURE 4.16B EFFECT OF TEMPERATURE ON CHARGE TRAPPING FOR DIFFERENT CURRENT DENSITIES FOR THE 50 ANGS. OXIDES

Nt vs J vs T For 200 Angs. Oxides.

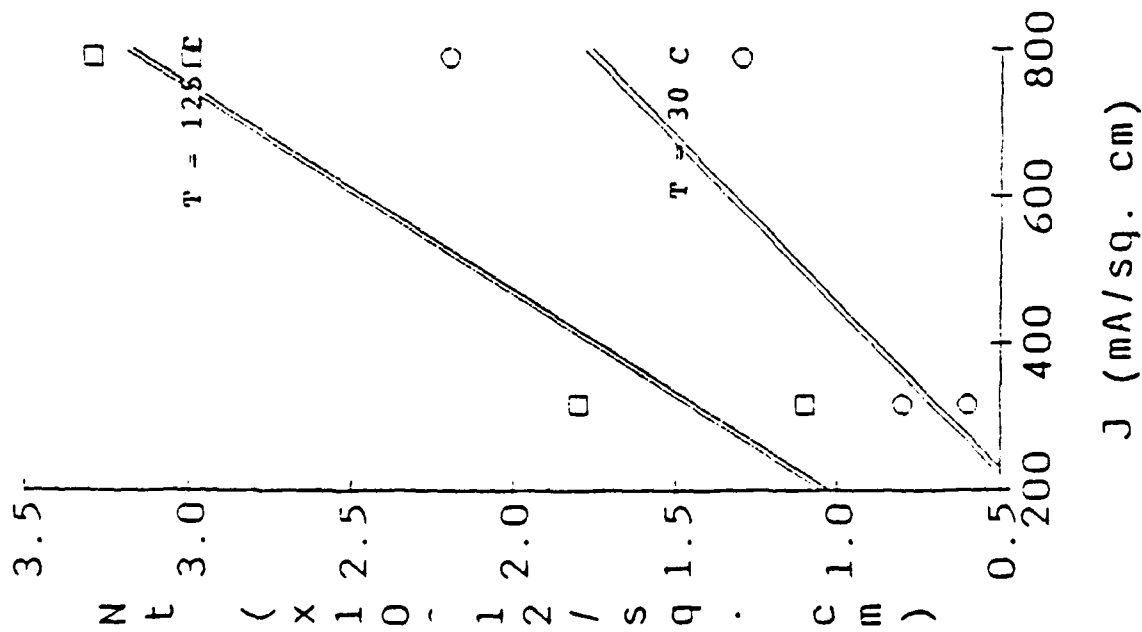


Figure A

G vs J vs T For 200 Angs. Oxides.

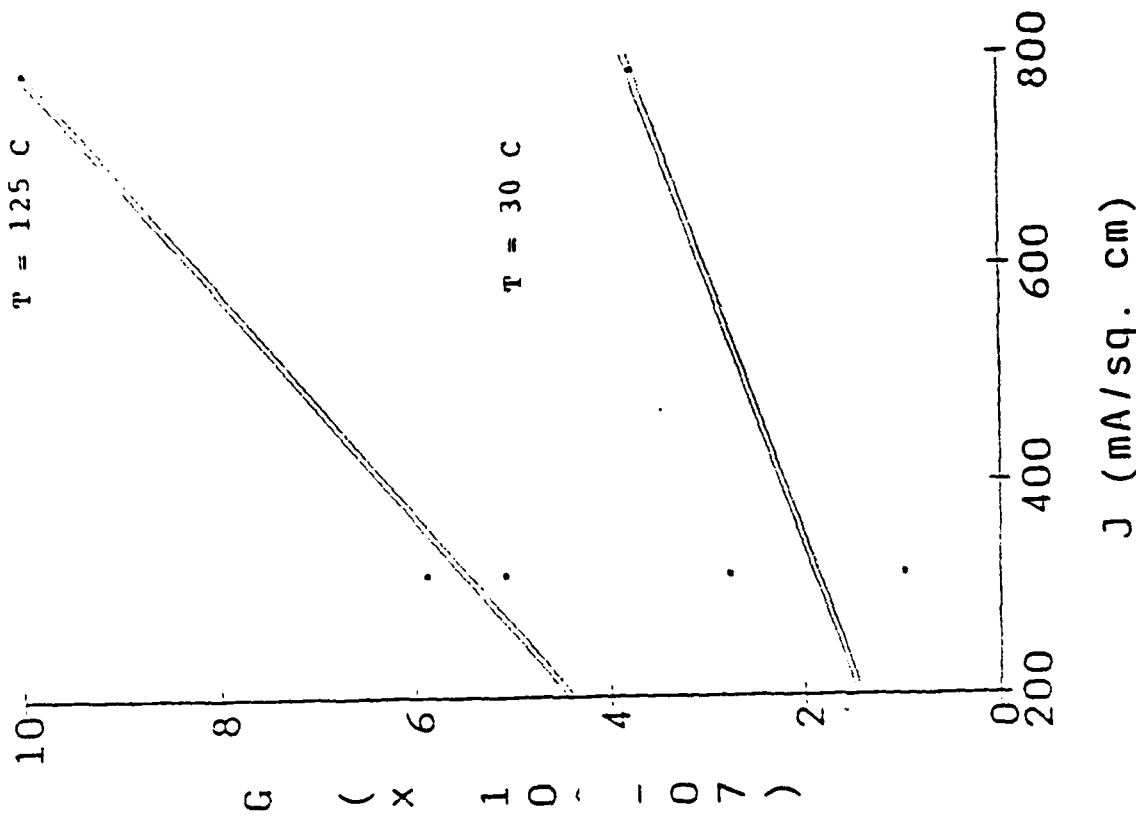


Figure B

FIGURE 4.17. EFFECT OF TEMPERATURE ON CHARGE TRAPPING FOR DIFFERENT CURRENT DENSITIES FOR THE 200 ANGSTROM OXIDES

we have not observed this phenomenon. Tatsuuma et al., [18] reported a transition temperature of 125 C from the low temperature region into the higher temperature region. Above 125 C, they reported that the electrons cannot gain enough energy to cause impact ionization due to phonon scattering effects. Our highest temperature was 125 C, so that a decrease in trapped charge may not have been observed due to the fact that we were right at the reported threshold. However, the possibility exists that the phenomenon does not exist at such high current densities (315 mA/cm**2 and 787.5 mA/cm**2).

Also, FIGURES 4.16 and 4.17 along with FIGURES 4.18 and 4.19 indicated a strong dependency of trapped charge and trap generation on the amount of the total charge density injected into the oxide. This is in agreement with much of the literature [14], and caters to physical intuition when one takes into account that we are injecting particles, which contain both a mass and a volume, through an amorphous solid.

Actual calculated values for each cell will be shown in the next section in tables 4.6 and 4.7.

4.4 Statistical Analysis

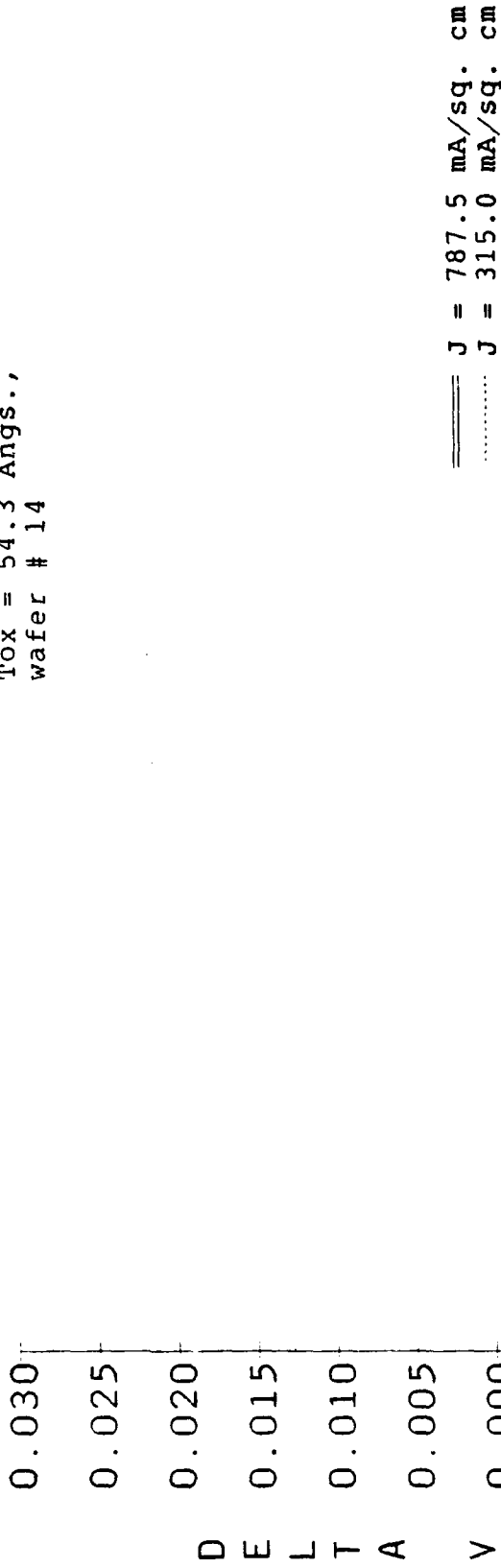
This section will be concerned with the choosing of the factorial matrix which we have used, along with the underlying concepts of factorial matrices. Then, a discussion of the statistical results will be given which will include a discussion of the electrical data. Some models to explain our observations and some suggestions for further study will be given to conclude this section.

An introduction and summary of factorial matrices, in general, will be presented in 4.4.1. Next, the characteristics of factorial matrices will be discussed with the help of some examples which show how we obtain the resulting relationships between factors and responses. This will be given in 4.4.2.

An overview of the design and analysis of two-level full factorial experiments will be given in 4.4.3. This will be followed by some guidelines for designing 2-level full-factorial experiments which will be laid out in 4.4.4.

Effect of Current Density on 50 Angs. Oxides

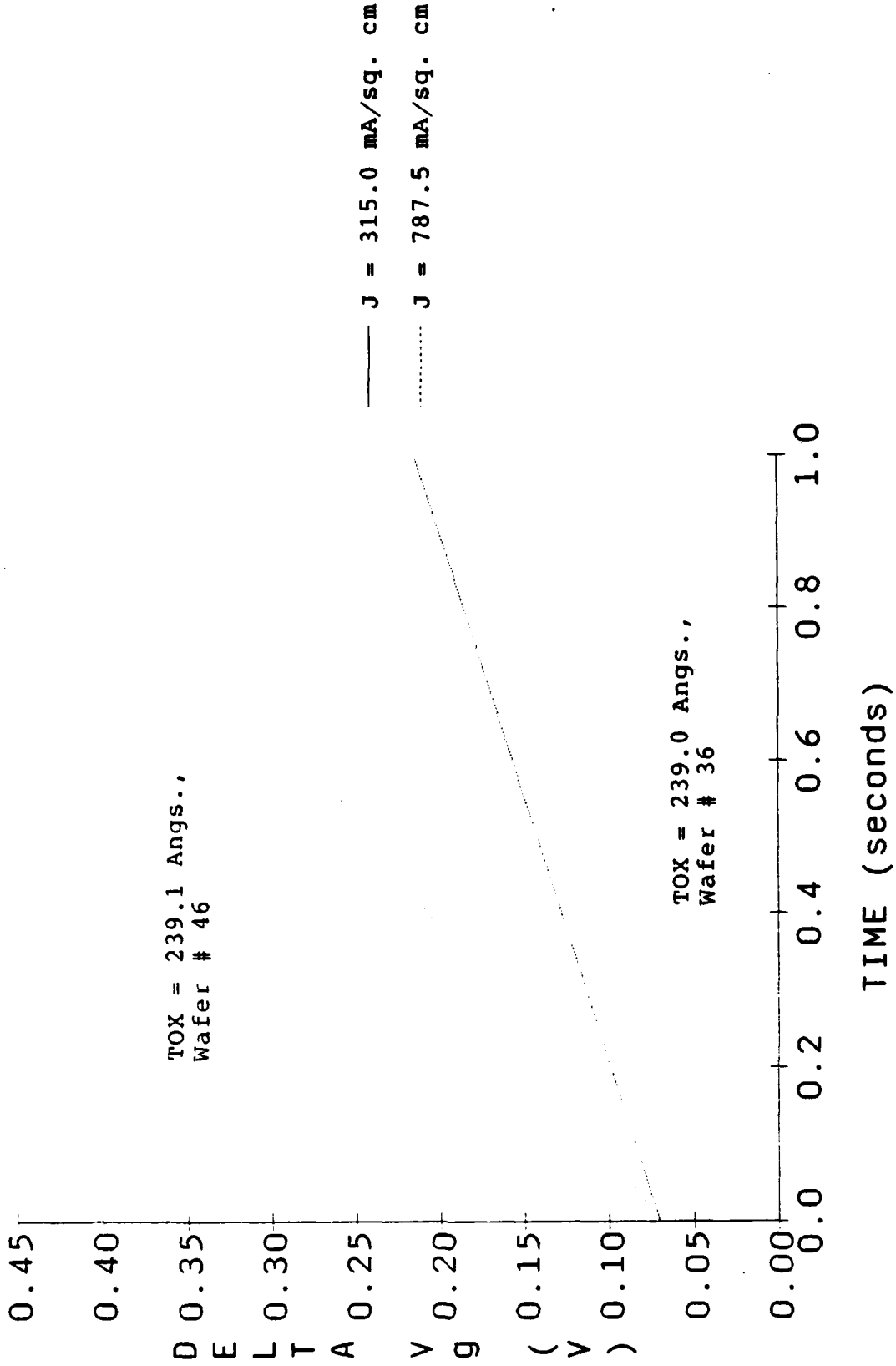
Tox = 54.3 Angs.,
wafer # 14



T = 125 C with 0KRAD for both wafers.

FIGURE 4.13. EFFECT OF INJECTED CHARGE DENSITY ON CHARGE TRAPPING OF 50 ANGSTROM OXIDES

Effect of Current Density on Positive Charge Trapping



T = 30 C with 0 KRAD for both wafers.

FIGURE 4.19. EFFECT OF INJECTED CHARGE DENSITY ON CHARGE TRAPPING OF 200 ANGS. OXIDES

A step by step discussion of how to analyze the data is given in 4.4.5, which will be followed by a brief discussion of the design and analysis of screening experiments in 4.4.6. This is necessary because, although our experiment was designed as a fractional factorial screening experiment, it will be discussed and shown why we eventually came to use the full factorial analysis methods.

We will then use the previously described background information and analysis methodology as applied to cumulative percent fails in time in 4.4.8, and as applied to charge trapping in 4.4.9. Finally, a summary of the statistical results will be given with some common observations from the data as backing evidence.

4.4.1 Factorial Matrices

Discrete factors have the property of being able to assume only a limited number of values. On the other hand, continuous variables (like those which we are dealing with) may take on any value within a numerical range. For a specific experiment, there will usually be an upper and lower limit of interest specified. Nevertheless, within the limits, the factor could be set to any value. In most factorial experiments only two levels for each factor are actually applied. The two levels are coded low (-) and high (+). For the case of continuous factors (as is ours) the two levels should be sufficiently separated so that a significant response can be easily and clearly distinguished from any experimental error in the measured response. By using widely spaced (+) and (-) levels the chances of identifying significant effects with an experiment, or to conclude that no effect other than experimental error occurs is improved.

4.4.2 Characteristics of Factorial Experiments

In factorial experiments, the use of factorial arrangements for the factors in an experiment makes each run yield information concerning every factor. Thus, not only are factorial experiments highly efficient in the number of runs utilized, but the efficiency is increased by multiple use of each response. The term factorial is used to indicate that a factorial experiment permits the simultaneous estimation of several factors, as opposed to "one-at-a-time" experiments in which the measured effects are due to the change of independent variables only. In other words, as the factorial $(n!)$ of an integer is its

product with all of the positive integers smaller than itself, in factorial experiments, each factor effect is based on all the individual measured responses. The term factor is chosen (in lieu of independent variable), to emphasize the fact that in factorial experiments, every run will produce information concerning the effect of every independent variable. In full factorial experiments, a set of runs in which all possible combinations of factors at the levels specified by the experiment are conducted. Thus, for a 2-level full factorial experiment, with k factors, 2^k runs are required. Since the (+) and (-) levels of each factor can represent the extremes of the ranges over which the factors of the experiment will be set, the complete experimental space of the experiment is covered by a full factorial experiment. Full factorial experiments, as opposed to one-at-a-time experiments, not only give a complete exploration of the experimental space, but they also offer the additional advantages of hidden replication, and information about interaction effects among factors. The terms factor effect, main effect, and interaction effect need to be defined at this point. A factor effect is the difference in the two measured responses when two different levels of a factor are applied in an experiment. An example of a factor effect is $(Y_1 - Y_2)$, where Y_1 is the response due to a factor set to level 1, and Y_2 is the response due to the same factor set at level 2. In the ideal case, only the difference in the factor levels plays a role in determining the value of the difference in responses, but in actual experiments, the value of the factor effect also depends on the experimental error. To reduce the role of the random experimental error, replication of the measurement must be performed. As noted, in the one-at-a-time approach, such replications must be direct. That is, identical experimental runs need to be repeated in order to get average values for Y_1 and Y_2 .

In factorial experiments, on the other hand, every run produces information concerning the effect of each factor. Therefore, an average value for each response at a given factor level can be calculated from the data of a full-factorial experiment, without having to replicate the entire factorial experiment (or even any of its individual runs). This ability of factorial experiments to intrinsically produce average values of factor effects without having to directly replicate experimental runs is referred to as a "hidden replication" capability. Information about two types of factor effects are also available from factorial experiments: a) main effects, and b) interaction effects.

On the other hand, in one-at-a-time experiments, no information about interaction effects can be extracted. Main effects for each individual factor are defined to be the difference between two average responses Y_+ and Y_- , or EQUATION 4.9:

$$\text{Main Effect} = (Y_+) - (Y_-) \quad (4.9)$$

average response at the (-) level.

Main effects can be easily visualized with the aid of a cube that represents a 2-level, 3 factor factorial experiment as shown in FIGURE 4.20. The main effect of factor A is based on a comparison of the response values at the left and right faces of the cube. Now, examine the lower-rear edge of the cube. Along this edge are two corners, each of which represents a set of factor values. The only difference between the sets is in the values of A. By taking the difference of the responses for the sets of values of these two corners we get an estimate of the effect of factor A (one-at-a-time estimate). However, there are also three other edges along which B and C will remain constant as A is varied. Basically, there are four edges that allow us to estimate the effect of A. The main effect of A is the average of the difference in the responses measured from these four edges, and is a measure of the effect that the varying of A alone will have on the response.

On the other hand, two or more factors are said to interact if the effect of one, say B, is different at different levels of other factors. Such interactions show up as interaction effects and they can be estimated from full factorial experimental data just as well as the main effects. To better illustrate a factor effect, consider a 2-level, 2 factor experiment with factors A and B shown in FIGURE 4.21 A. The interaction effect is defined as EQUATION 4.10

$$\begin{aligned} \text{Interaction Effect} &= [(Y_4 - Y_3) - (Y_2 - Y_1)]/2 \\ &= [(Y_1 + Y_4) - (Y_3 + Y_2)]/2 \quad (4.10) \end{aligned}$$

and it becomes apparent that the result involves the comparison of responses at diagonally opposite corners.

The presence of an interaction can also be shown by examining the responses of a 2-level, 2-factor experiment (for factors A and B). The graph of Y versus A is plotted with B being low. If the graphs have different slopes

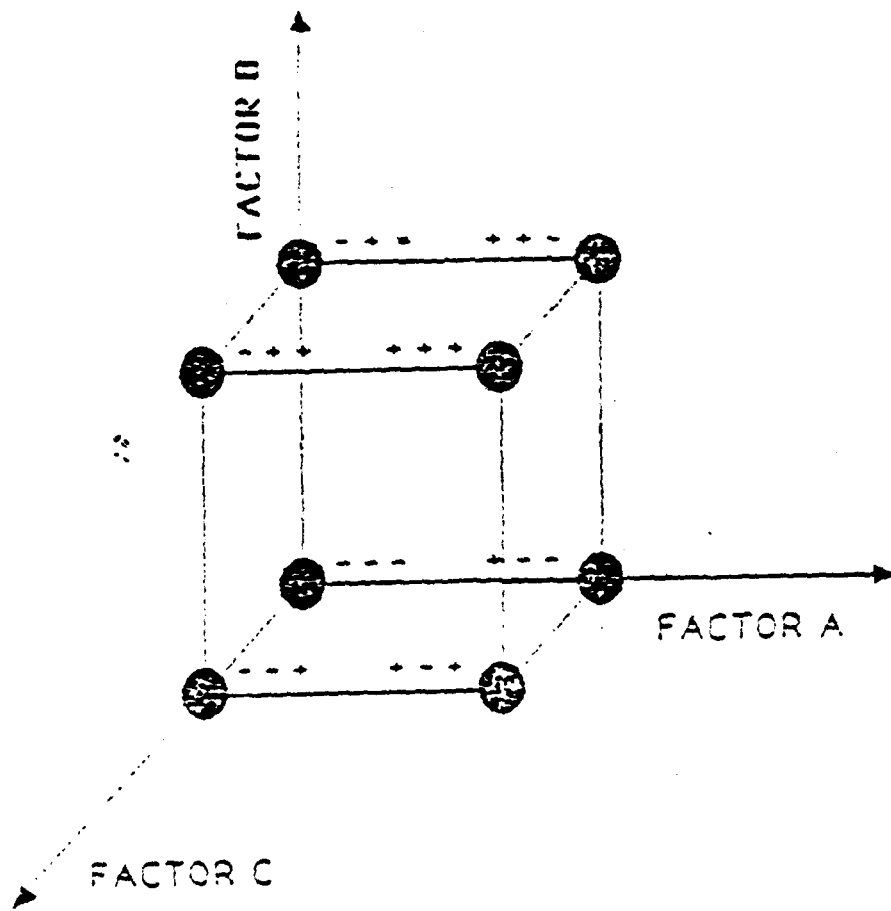
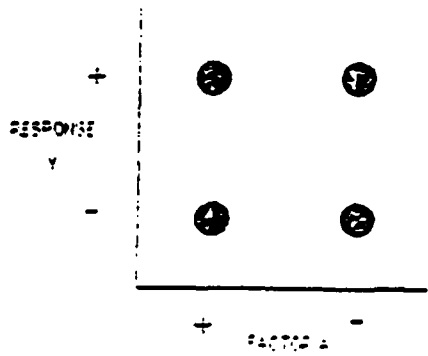
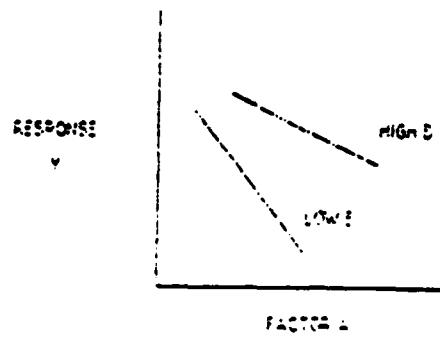


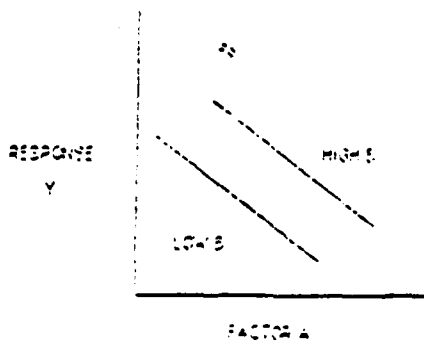
FIGURE 4.20. DEPICTION OF THREE FACTOR EXPERIMENT IN THREE DIMENSIONS



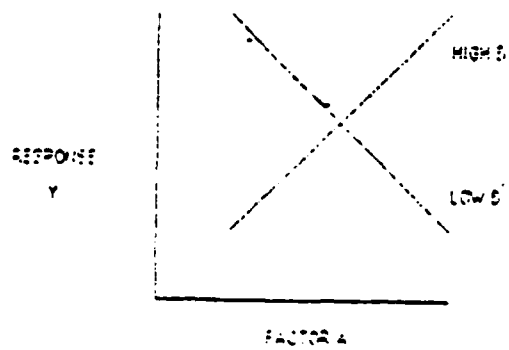
a). EXPERIMENT SPACE



c). MILD INTERACTION



b). NO INTERACTION



d). STRONG INTERACTION

FIGURE 4.21. TWO FACTOR EXAMPLE SHOWING INTERACTION EFFECTS

(FIGURE 4.21(B and C), there is no interaction effect between A and B. However, for the case of different slopes (FIGURE 4.21 D), this indicates the presence of an interaction effect.

Obviously, one of the roles of statistical analysis is to determine if the measured effects in an experiment (both main and interaction), are primarily due to the factors being investigated or are just due to fluctuations (more commonly known as errors) of the measured environment. Those effects which are determined in the analysis of experimental data as being greater than the expected error effects are referred to as significant (or more appropriately, statistically significant).

As was previously shown, even 2-level full-factorial experiments can easily require a very large number of runs, as the number of factors increase. In many circumstances, by making careful and appropriate selections, a smaller set of runs can provide some useful and efficient information. If an experiment is designed in such a way that only a fraction of all the runs of a full-factorial experiment are to be performed, it is designated as a fractional-factorial experiment. Reduced-run experiments of this sort find wide applicability in the early stages of an experimental project, where a large number of factors are cataloged, but knowledge about their relative importance on the process being optimized is not known. At that point, screening experiments designed to identify the significant factors of the group, are utilized. If the other factors are determined to have no significant effects on the process being investigated, then further experimental time and effort need not be expended. Such experiments, when the factor levels are carefully and methodically chosen, can make effective use of fractional-factorial experiments.

4.4.3 The Design and Analysis of Two-Level Full Factorial Experiments

As previously described, full factorial experiments allow the complete factor space of an experiment to be covered, and also to produce factor effects (main and interaction effects) that are based on response information from every run of the experiment. The main effect and interaction effect information can be used to generate limited response surfaces, or a linear polynomial equation that will allow response predictions to be interpolated within the ranges of the factor space. The latter of these

possibilities will be our goal in using this technique.

At this point it is useful to discuss a method for estimating any curvature that might exist within the factor space being investigated. That is, since only factor values at the extremes of their ranges are investigated with 2-level factorial experiments, no information about response values in the interior of the experimental space is provided. Thus, only linear (straight-line) variations can be used to predict the values of response within the limits of the factor space. To perform an economical check on the validity of such straight-line assumptions, a small number of additional runs with the factor values all set at their middle points, should also be conducted. It is usually recommended that 4 replicates of this run be conducted, so that an average value is obtained. The severity of any curvature present is estimated by calculating the difference between the average value of the design points and the average value of the center points (FIGURE 4.22). Unfortunately, if the curvature is found to be severe, the prediction model derived from the full-factorial data is not likely to give accurate results except near the experimental points.

4.4.4 Guidelines for Designing 2-Level Full-Factorial Experiments

In this section, a step-by-step approach to the design of 2-level full-factorial experiments is presented. Any number of responses may be measured for each set of factor values. The steps of the method are as follows (it is assumed that the factors to be investigated have already been selected):

1. The values of the limits of the factors to be applied in the experiment should first be determined. These limits will identify the two levels of each factor that will be applied in the experiment. The upper level is encoded as (+), and the lower level as (-). As noted earlier, these levels should be sufficiently separated so that a significant response to the variation in factor levels can be clearly distinguished from any experimental error.

2. Any number of responses can be measured at each experimental point. As discussed in an earlier section, the two-level factorial method will yield best results when the responses are continuous and have uniform independent errors. Uniform errors are those which have approximately the same magnitude at all experimental points.

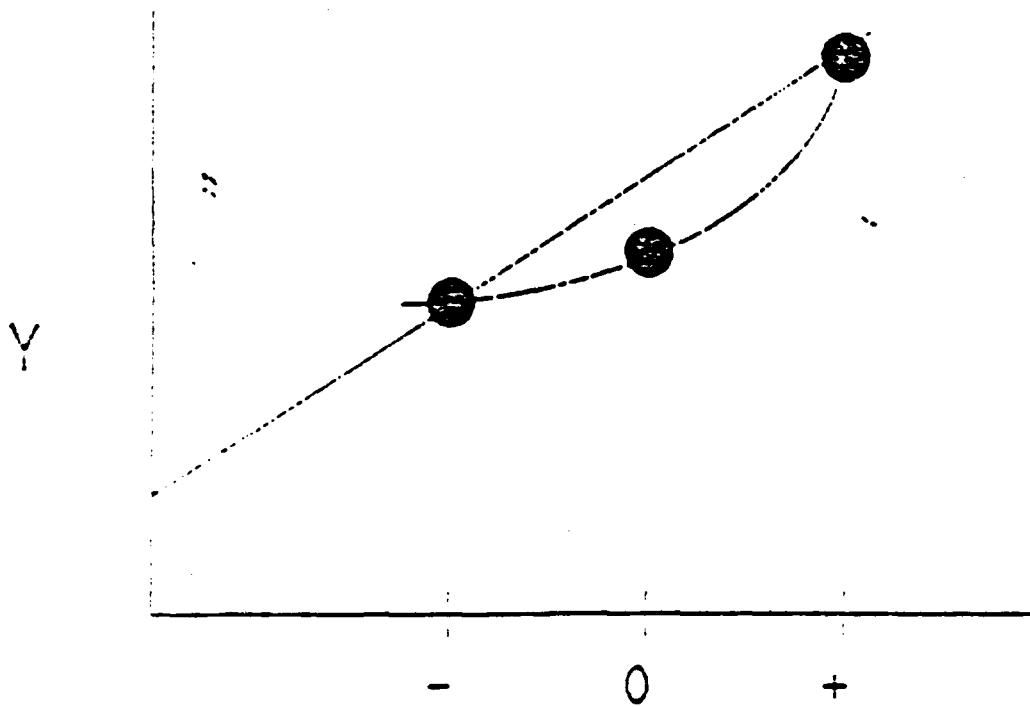


FIGURE 4.22. EXAMPLE OF CURVATURE

3. The design pattern, which specifies the level of each factor for every trial is then obtained from TABLE 4.2 (which gives this pattern for five factors, where the fifth factor is set equal to the product of the previous four). Such a Coded Design Table, as well as a Decoded version of the Design Table (in which the (+)'s and (-)'s in the Table are replaced with their actual values) should be prepared for the experiment file as illustrated, by our Decoded Design Table, in TABLE 4.3.

4. The order of running the trials should be randomized. Randomization reduces bias error. A new order should be selected each time a complete set of runs is replicated. Persons performing the experiment need to understand that runs must be conducted in the randomized order specified.

5. The number of necessary replicates should next be determined. The hidden replication of full-factorial experiments assists in reducing the variance of the average measured values, by effectively increasing the number of measurements used to calculate the mean. However, it must be determined if any additional direct replication is needed to estimate the variance of the random error, and to thus satisfy the confidence level requirements when deciding to identify a factor effect as being significant or not. If the experiment in question has 3 factors (8 runs for a full-factorial), and detection of significant factors greater than 2 sigma is acceptable, two full factorial groups carried out as a single experiment would have to be conducted (16 runs).

6. In order to use the full-factorial experiments to obtain information about the response within the experimental space, without significantly expanding the number of runs in an experiment, an additional group of runs can be added at a middle value for all factors. Four replicated runs with factor values set at their midpoints are suggested to increase the precision of middle point measurement. The degree of curvature can be estimated by the difference between the average of the measured response at the middle points and the average of all the other experimental points. If this turns out to show that the curvature is severe, the prediction model generated from the full-factorial is likely to be quite inaccurate except near the design points (FIGURE 4.22).

7. The experiment is then conducted and the responses for each run are recorded.

A	B	C	D	E	(0)	EFFECTS
-	-	-	-	-	?	TOTAL
+	-	-	-	+	?	A
-	+	-	-	+	?	B
+	+	-	-	-	?	AB
-	-	+	-	+	?	C
+	-	+	-	-	?	AC
-	+	+	-	-	?	BC
+	+	+	-	+	?	ABC
-	-	-	+	+	?	D
+	-	-	+	-	?	AD
-	+	-	+	-	?	BD
+	+	-	+	+	?	ABD
-	-	+	+	-	?	CD
+	-	+	+	+	?	ACD
-	+	+	+	+	?	BCD
+	+	+	+	-	?	ABCD

ABCD--E
 -----> A--BCDE
 B--ACDE
 AB--CDE
 C--ABDE
 AC--BDE
 BC--ADE
 ABC--DE
 .
 .
 .
 etc.

TABLE 4.2 CODED DESIGN TABLE

FACE CONTACT HOMOGENEOUS MATRIX

<u>CELL</u> <u>(#)</u>	<u>THICKNESS</u> <u>(Angstroms)</u>	<u>GVMA DOSE</u> <u>(MRAD)</u>	<u>STRESS</u> <u>CURRENT</u>	<u>TEMPERATURE</u> <u>(Celsius)</u>	<u>STRESS</u> <u>TIME</u>
16	50	0	-2.47	30	1.88
12	200	0	-2.47	30	6.88
15	50	500	-2.47	30	6.88
1	200	500	-2.47	30	1.88
7	50	0	4.47	30	6.88
2	200	0	4.47	30	1.88
13	50	500	4.47	30	1.88
9	200	500	4.47	30	6.88
11	50	0	-2.47	126	6.88
8	200	0	-2.47	126	1.88
14	50	500	-2.47	126	1.88
6	200	500	-2.47	126	6.88
10	50	0	4.47	126	1.88
4	200	0	4.47	126	6.88
5	50	500	4.47	126	6.88
3	200	500	4.47	126	1.88
17*	100	50	-3.47	70	1.88

TABLE 4.3 DECODED DESIGN TABLE

4.4.5 The Analysis of the Measured Data

1. The factor effects are first computed from response data in the following manner:

a) Create a Computation Table (CT). To assist in tabulating the analysis, use the design from TABLE 4.2.

b) List the averages of the replicate runs in a column at the right of the CT labeled (0). (Follow the run order listed at the left of the CT, and not the random run order.)

c) Total the values of the run averages for the lines that have a "+" sign for each column. Put this total under the correct column of the line SUM +.

d) Repeat the process for the lines with "-" signs. Enter their totals under the appropriate columns in the line called SUM -.

e) Add the values of SUM + and SUM -. Enter the total on the line OVERALL SUM. This step is a check. The value of the OVERALL SUM should be identical for all columns.

f) Subtract SUM + from SUM -. Place the difference on the line called DIFFERENCE.

g) Finally, divide the difference by the number of + signs in that column, and enter on the line EFFECT. This number is a main effect, or interaction effect (depending on the particular column). For column one, the result on the EFFECT line is the average of the responses of all the experimental points.

2. The curvature is then calculated. This is done by:

a) Computing the average value of responses of the runs carried out with all the factors set at their middle values (average value of center points).

b) Then computing the difference between
(1) the average of the responses all the experimental points and

(2) the average value of the center points. This difference is entered on the CURVATURE line of the CT

3. The significance of the main effects, interaction effects, and curvature are then determined. That is if any of the computed main factors or interaction effects is found to be larger than a minimum significant factor effect, MSF (which we will demonstrate how to calculate), it can be concluded that the effect is indeed non-zero. On the other hand, if the value is smaller, it is likely that no significant effect exists, and the variation in experimental

response for that effect is just due to experimental error fluctuations. By the same token, if the curvature is greater than the minimum significant curvature, MSC, it can be concluded that at least one response has non-zero curvature associated with it. The MSF and MSC are computed from EQUATION 4.11:

$$MSF = p * Spooled * (2 / (r * k)) ** 0.5 \quad (4.11)$$

and EQUATION 4.12

$$MSC = p * Spooled * [(1 / (r * k)) + (1 / c)] ** 0.5 \quad (4.12)$$

where: p is the value of the t -distribution at the desired probability level $(1 - \alpha)$ for the number of degrees of freedom used to calculate the standard deviation (S); $Spooled$ is the pooled standard deviation of a single response; r is the number of + signs in the column (note that the main and interaction effect columns have $2^{*(q-1)} + 1$ signs, where q is the number of factors in the experiment); k is the number of replicates of each trial; and c is the number trials conducted with factors set at middle value.

Note that the number of degrees of freedom, $d.f.$, is determined by EQUATION 4.13:

$$d.f. = n - (\text{number of main effects} + \text{number of interaction effects}) - 1 \text{ (for calculating the average)} - 1 \text{ (for calculating curvature)} \quad (4.13)$$

where n is the total number of runs in the experiment.

Thus, if a 3-factor experiment was designed to be replicated twice (16 runs) and to have an additional four center point runs, a total of 20 runs would constitute the experiment. There would be 11 degrees of freedom available for calculating S , since 3 would be used to calculate the main effects, 4 for the interaction effects, and one each for the average of all the responses and average of the center point responses.

4. The main and interaction effects are compared with MSF, and those that are larger are concluded to be significant. The curvature effect is compared with MSC, and if it is larger, the response is acknowledged as having significant curvature within the factor space being studied.

5. A linear model, in the form of an equation, that will predict the value of the response for any value of the

factors within the factor space, from the data of the factorial experiment, can then be formulated. The equation is of the form EQUATION 4.14:

$$\begin{aligned} \text{YPR} = & A_0 + A_1 X_1 + A_2 X_2 + \dots + A_n X_n + A_{12} A_1 A_2 + \dots \\ & \dots + A_{q-1, q} X_{q-1} X_q + \text{higher order interactions} \end{aligned} \quad (4.14)$$

where: YPR is the predicted response; q is the number of factors; $A_0 = \bar{Y}$; $A_j = 0.5 \times (\text{factor effect for } x_j)$; $a_{jj} = 0.5 \times (\text{factor effect for } x_j \times x_j)$; and: $X_j = [(\text{factor level at the experimental point}) - 0.5 \times (\text{high} + \text{low factor level})] / 0.5 \times (\text{high} - \text{low factor levels})$

4.4.6 The Design and Analysis of Screening Experiments

In many processes it is possible to identify a variety of factors that may impact the process responses. The number of runs necessary to perform a 2-level full-factorial experiment with k factors is 2^k , and for more than about 4 factors, this number may become excessive. In such cases, a more effective strategy than conducting full-factorial experiment would be to carry out a less extensive experiment designed to identify the most important factors, and then perform the full-factorial experiment using only these. Such preliminary experiments that eliminate unimportant factors are called screening experiments, and can substantially reduce the number of runs that must be used to separate out significant factors. Such screening experiments are still based on the principles which underlie full-factorial experiments (e.g. hidden-replication and full coverage of the experimental space), but use a smaller number of runs for a given number of factors.

There is a price that is paid for the reduced number of runs. When the results from analysis of the Computation Table are calculated, the values obtained no longer necessarily contain information about a single main or interaction effect, but instead contain information from two or more effects. This is known as confounding. For example, if a screening experiment was performed with three factors and only four runs were conducted (instead of the 8 needed for a full-factorial experiment), the value calculated in each of the EFFECT rows would no longer result from a single main effect or interaction effect, but would have contained response information from a main effect and an interaction effect. Such confounding is due to the fact that the same factor level combination is used to produce the factor effect of more than a single factor or interaction of factors.

As the fraction of the total number of runs compared to the number required for a full-factorial experiment gets smaller, the larger the number of effects that are confounded. That is, if half the number of runs is conducted (and in which the experiment is known as a half-factorial), each EFFECT value confounds only two effects, while each EFFECT value in an experiment with only one-fourth the number of runs confounds four effects. The reason that such confounding is generally tolerable is that interactions involving three or more factors (higher order interactions), are almost always less important than main or two-factor interactions. Thus, by properly designing a screening experiment such that each main effect (and if possible, each two-factor effect) is confounded only with effects due to higher order interactions (i.e. by being careful that two main effects do not confound each other), it is still highly probable that the most important main and two-factor interaction effects will be found.

Here is a rough guideline for obtaining the most information from the least number of screening experiment runs, while paying the least penalty (in the form of losing key information from confounding effects):

a) For screening experiments containing 5 factors, use a 16 run experiment (half-factorial of a 5-factor full-factorial experiment), and take the product of the coded values (+ and -) of the first four factors (for the first 16 runs of a 5-factor full-factorial table), and assign the resulting product level to the fifth factor (i.e. this product value will be either "+" or "-"). Using this design, the main effect of the fifth factor would be the same as the four-way interaction, and thus the main effects are confounded with the four-way interaction. In addition, the two-way interactions will be confounded with three-way interactions;

b) For screening experiments of 6 to 8 factors, a 16 run experiment can still be used in which the main effects are all confounded with third and higher order interactions, and the two-factor interactions are likewise confounded only with such higher order interactions [7].

4.4.7 The Matrix Applied to Cumulative Percent Fails and Charge Trapping

It is necessary at this time to explain some things about our specific matrix and its factors. Due to the lack

of time and equipment, it was necessary to design the test so that a statistically valid number of fails in time would occur, while keeping that time as short as possible. In order to do this, the current density had to be increased. However, such a wide distribution of fails in time existed that there was no way to obtain data for every cell for any common time to a certain percentage of fails. It was for the following two reasons that we decided to drop time as a factor: 1) There was too much of an error in failure distributions to even consider only total fails in time and, 2) It has been reported that the injected charge (i.e. current multiplied with time of injection) is the important factor and this renders time no longer an independent variable.

What we did was look at the cumulative percent fails at one second. This data was common to all cells in the test matrix, and also eliminated time as a matrix factor because even if a cell was stressed to sixty seconds, it would have the same characteristics at one second. This enabled us to use the matrix as a full-factorial matrix, thereby reducing the amount of confounding.

As explained earlier, in order to remain consistent, we examined the charge trapping characteristics at one second after stress also. This brought about a need to further reduce our matrix and split it into two separate 3 factor fullfactorial matrices: one for the fifty angstrom thickness, and one for the two-hundred angstrom thicknesses. This was done because the trapping mechanisms for the two thicknesses are completely different at one second; one is trapping positive charges, and the other is trapping negative charges.

4.4.8 Analysis of Cumulative Percent Fails in Time as an Output

Using the method of analysis outlined in section 4.4.5, we can derive the equation to relate the cumulative percent fails at one second to the stressing factors in the matrix. TABLE 4.1 is the computation table for this analysis. The average values obtained from the cumulative percent fail plots for each cell is shown to the right of the table. For each column, the sum of all the outputs corresponding to a "+" sign in that column have been tabulated and placed on the line marked SUM +. This was repeated for the corresponding "-" signs and those values were placed in SUM -. As a check, the values for SUM + and SUM - were added

COMPUTATION TABLE FOR FACTOR EFFECT RELATED TO CUMULATIVE PERCENT FALLS AT 1 SECOND

FA	D	ToxD	I	ToxI	DI	ToxDI	T	ToxT	DT	ToxDI	IT	ToxIT	DIT	ToxDIT	(O)(%)
-	-	+	-	+	+	-	-	+	+	-	+	+	-	+	4.5
+	-	-	-	+	+	+	-	+	-	+	+	+	+	-	13.1
+	+	-	-	+	-	+	-	+	-	+	+	+	+	-	4.8
+	+	+	-	+	-	+	-	+	-	+	+	+	+	+	23.0
-	-	+	+	-	-	+	-	+	+	-	-	+	+	+	26.0
-	+	-	+	+	-	+	-	+	+	-	-	+	+	+	50.0
-	+	-	+	+	+	-	-	+	-	+	-	+	+	+	5.0
+	+	+	+	+	+	+	-	+	-	+	-	+	-	-	43.5
-	-	+	-	+	+	+	+	-	-	+	-	+	+	-	17.5
+	+	-	-	+	+	+	+	+	+	-	-	+	+	+	13.0
+	+	-	-	+	-	+	+	+	-	+	-	+	-	+	20.0
+	+	+	+	-	-	+	+	+	-	+	+	+	-	+	18.3
-	-	+	+	+	-	+	+	+	-	+	+	+	-	+	77.5
-	+	-	+	+	+	-	+	+	+	-	+	+	+	-	41.0
+	+	-	+	+	+	+	+	+	+	-	+	+	+	-	85.0
+	+	+	+	+	+	+	+	+	+	+	+	+	+	+	38.8

SUM + 240.7 238.5 249.1 366.8 220.2 220.4 236.8 311.1 164.6 242.6 225.1 287.8 166.3 276.3 257.8

SUM - 240.1 242.6 232.2 114.3 268.9 260.7 244.3 170.0 316.5 238.5 256.0 193.3 314.8 204.8 223.3

TOTAL 481.1 481.1 481.1 481.1 481.1 481.1 481.1 481.1 481.1 481.1 481.1 481.1 481.1 481.1 481.1

DIFFERENCE 9.3 -4.1 16.9 252.5 -40.7 -40.3 -7.5 141.1 -151.9 4.1 -30.9 94.5 -148.5 71.5 34.5

EFFECT 0.038 -0.5 2.1 *31.6 -5.1 -5.0 -0.9 17.6 -22.2 3.8 -3.9 11.8 -14.0 4.4 -2.2

CENTER POINT AVERAGE = 3.75 TOTAL AVERAGE = 30.1 NSC = 55.9 CURVATURE = 30.1 - 3.75 = 26.35 < 55.9

* Significant Factor Because MSF = 27.1

Tox = oxide thickness (Angs.), D = gamma dose (KRAD), I = current (A), T = temperature (degrees Celcius)

TABLE 5.4. COMPUTATION TABLE FOR FACTOR EFFECTS RELATED TO CUMULATIVE PERCENT FALLS AT 1 SECOND

but at the time used for evaluation (1 second) no significant effect was observed.

The equation relating current to the cumulative percent fails at 1 second can be derived using the method described earlier. From section 4.4.5,

$$\text{Cumulative \% Fails @ 1 second} \\ AI*(I(\mu A) + 350)/150 \quad (4.14)$$

where,

$$AI = 0.5 * \text{CURRENT EFFECT} = 0.5 * 31.6 = 15.8$$

so that one obtains EQUATION 4.15:

$$\text{Cumulative \% Fails @ 1 second} = -15.8 * \\ (I(\mu A) + 350)/150 \quad (4.15).$$

The MSC was found from equation (4.12) to be 55.9 and the curvature was determined to be 26.4. This would seem to indicate that no significant curvature exists, however, care should be used in interpreting this since the points we used as centerpoints are not actually centerpoints. For instance, 100 Angs. is not in the center of 50 and 200 Angs., so that curvature may exist where none is predicted.

4.4.9 Analysis of Charge Trapping Properties using Nt and G as Outputs

Section 4.3 explained the method of analysis used to determine Nt and G, therefore, we will avoid any redundancy and present only the results as determined using the Hadamard matrix. First, we will present the results for the 50 Angs. oxides (both Nt and G), then we will present the findings for the 200 Angs. oxides in the same manner.

Using the method of section 4.4.5. and in the same way as was done for the TDDB analysis, TABLE 4.6 was generated. TABLE 4.6 A shows the results tabulated for Nt and TABLE 4.6 B shows the results tabulated for G both of which are for the 50 Angs. oxides. In order to determine the minimum significant factor effect, we calculated the pooled standard deviations and resulting MSF's to be,

$$\text{Spooled(for Nt)} = 1.89 \quad \text{=====} \quad \text{MSF} = 1.64 \\ \text{Spooled(for G)} = 1.45 \quad \text{=====} \quad \text{MSF} = 1.26$$

so that we could then eliminate the insignificant factors. Referring to TABLE 4.6 A, it is obvious that the significant

COMPUTATION TABLES FOR FACTOR EFFECTS RELATED TO CHARGE TRAPPING FOR 50 ANG. OXIDES

	<u>D</u>	<u>I</u>	<u>DI</u>	<u>T</u>	<u>DT</u>	<u>IT</u>	<u>DIT</u>	<u>(0)(x10¹¹/cm²)</u>
-	-	-	+	-	+	+	-	0.2
+	+	-	-	-	-	+	+	0.54
-	+	-	-	-	+	-	+	1.9
+	+	+	+	-	-	-	-	1.99
-	-	+	+	+	-	-	+	1.2
+	-	-	-	+	+	-	-	1.0
-	+	-	-	+	-	+	-	5.1
+	+	+	+	+	+	+	+	5.2
SUM +	8.64	14.1	8.5	12.5	8.3	11.04	8.84	
SUM -	8.4	2.94	8.54	4.54	8.74	6.0	8.2	
TOTAL	17.04	17.04	17.04	17.04	17.04	17.04	17.04	
DIFFERENCE	0.24	11.2	-0.04	7.96	-0.44	5.04	0.64	
EFFECT	0.06	*2.8	-0.01	*2.0	-0.11	1.3	0.16	

* Significant Factor Because MSF = 1.64

A). FACTOR EFFECTS FOR DENSITY OF NEGATIVE TRAPPED CHARGE

	<u>D</u>	<u>I</u>	<u>DI</u>	<u>T</u>	<u>DT</u>	<u>IT</u>	<u>DIT</u>	<u>(0)(x10⁻⁰⁸/electron)</u>
-	-	-	+	-	+	+	-	1.0
+	+	-	-	-	-	+	+	2.8
-	+	-	-	-	+	-	+	3.8
+	+	+	+	-	-	-	-	3.8
-	-	+	+	+	-	-	+	5.9
+	-	-	-	+	+	-	-	5.1
-	+	-	-	+	-	+	-	10.0
+	+	+	+	+	+	+	+	10.0
SUM +	21.7	27.6	20.7	31.0	19.9	23.8	22.5	
SUM -	20.7	14.8	21.7	11.4	22.5	18.6	19.9	
TOTAL	42.4	42.4	42.4	42.4	42.4	42.4	42.4	
DIFFERENCE	1.0	12.8	-1.0	19.6	-2.6	5.2	2.6	
EFFECT	0.25	*3.2	-0.25	*4.9	-0.65	*1.3	0.65	

* Significant Factor Because MSF = 1.26

B). FACTOR EFFECTS FOR THE ACCEPTOR TRAP GENERATION RATE

TABLE 4.6. COMPUTATION TABLE FOR FACTOR EFFECTS RELATED TO CHARGE TRAPPING FOR 50 ANG. OXIDES

factors for Nt are: current, and temperature. From TABLE 4.6 B, the significant factors for G are: current, temperature, and the interaction between the two. From these results and the method discussed previously, the equations relating the factors to the responses were derived. For the density of trapped charge the equation was

found to be EQUATION 4.16,

$$Nt(X10E11/cm2) = 2.1 - 1.4*(I(uA) + 350)/150 + 1.0*(T(C) - 77.5)/47.5 \quad (4.16)$$

and regarding the trap generation probability the equation was found to be EQUATION 4.17,

$$G(X10E-08/electron) = 5.3 - 1.6*(I(uA) + 350)/150 + 2.5*(T(C) - 77.5)/47.5 - 0.7*((I(uA) + 350)/150) * (T(C) - 77.5)/47.5 \quad (4.17)$$

These are consistent with the results as discussed previously in section 4.3. The results for the 200 Angs. oxides are presented next.

The method is repeated for the 200 Angs. oxides with the Computation tables for Nt and G shown in TABLES 4.7 A and B. The pooled standard deviations and resulting MSF's were found to be,

$$\text{Spooled(for Nt)} = 0.73 \text{ =====> MSF} = 0.64$$

$$\text{Spooled(for G)} = 1.88 \text{ =====> MSF} = 1.64$$

so that the significant factors were identified and all other factors were eliminated. From the Computation tables it was determined that the significant factors related to Nt were : current and temperature, and that the only significant factor related to G was: temperature. Again using the method for deriving the equations relating the factors to the responses, the equations were derived. For the density of trapped charge the equation was determined to be EQUATION 4.18:

$$Nt(X10E12 cm2) = 1.8 - 0.74*(I(uA) + 350)/150 + 0.59*(T(C) - 77.5)/47.5 \quad (4.18)$$

and for the trap generation probability the equation was determined to be EQUATION 4.19,

$$G(X10E-07 electron) = 5.3 + 1.7*(T(C) - 77.5)/47.5 \quad (4.19)$$

COMPUTATION TABLES FOR FACTOR EFFECTS RELATED TO CHARGE TRAPPING FOR 200 ANG. OXIDES

	<u>D</u>	<u>I</u>	<u>DI</u>	<u>T</u>	<u>DT</u>	<u>IT</u>	<u>DIT</u>	<u>(0)(x10¹²/cm²)</u>
-	-	-	+	-	+	+	-	0.62
+	-	-	-	-	-	+	+	0.80
-	+	-	-	-	+	-	+	2.20
+	+	+	-	-	-	-	-	1.30
-	-	+	+	-	-	-	+	1.80
+	-	-	-	+	+	-	-	1.10
-	+	-	+	+	-	+	-	3.40
+	+	+	+	+	+	+	+	3.30
SUM +	6.50	10.20	7.02	9.60	7.22	8.12	8.10	
SUM -	8.02	4.32	7.50	4.92	7.30	6.40	6.42	
TOTAL	14.52	14.52	14.52	14.52	14.52	14.52	14.52	
DIFFERENCE	-1.52	5.88	-0.48	4.68	-0.08	1.72	1.68	
EFFECT	-0.38	*1.47	-0.12	*1.18	-0.02	0.43	0.47	

* Significant Factor Because MSF = 0.64

A). FACTOR EFFECTS FOR THE DENSITY OF POSITIVE TRAPPED CHARGE

	<u>D</u>	<u>I</u>	<u>DI</u>	<u>T</u>	<u>DT</u>	<u>IT</u>	<u>DIT</u>	<u>(0)(x10⁰⁷/electron)</u>
-	-	-	+	-	+	+	-	3.1
+	-	-	-	-	-	+	+	4.2
-	+	-	-	-	+	-	+	4.5
+	+	+	-	-	-	-	-	2.7
-	-	+	+	-	-	-	+	8.9
+	-	-	-	+	+	-	-	5.7
-	+	-	+	+	-	+	-	6.9
+	+	+	+	+	+	+	+	6.7
SUM +	19.3	20.8	21.4	28.2	20.0	20.9	24.3	
SUM -	23.4	21.9	21.3	14.5	22.7	21.8	18.4	
TOTAL	42.7	42.7	42.7	42.7	42.7	42.7	42.7	
DIFFERENCE	-4.1	-1.1	-0.1	13.7	-2.7	-0.9	5.9	
EFFECT	-1.0	-0.3	-0.03	*3.4	-0.7	-0.2	1.5	

* Significant Factor Because MSF = 1.64

B). FACTOR EFFECTS FOR THE DONOR TRAP GENERATION RATE

TABLE 4.7. COMPUTATION TABLE FOR FACTOR EFFECTS RELATED TO CHARGE TRAPPING FOR 200 ANGS. OXIDES

4.4.10 Summary of Statistical Results

We found that in analyzing the cumulative percent fails at 1 second, only the current was significant. Although temperature does decrease the time to fail, the factor effect associated with it is insignificant. This is believed to be due to such a large current density used in the testing. The current density is probably masking any other effects which might have been observed at lower current densities, because it is actually "blasting" the oxide with electrons.

In reference to charge trapping, we found that both thicknesses trap holes initially and eventually trap electrons. However, due to the difference in trap saturation times, we observe different polarities of trapped charge at 1 second. Therefore, we needed to split the matrix into two full-factorial matrices with three factors each.

The 50 Angs. oxides showed densities of trapped charge on the order of $\sim 10E11$ sq. cm, or trap generation rates on the order of $\sim 10^{*-08}$ electron. Also, both temperature and the amount of injected charge density are first order effects. With an increase in both of these factors comes a corresponding increase in both responses. This was illustrated earlier in FIGURES 4.16 and 4.17.

The 200 Angs. oxides had densities of trapped charge about 10X higher than the 50 Angs. oxides ($\sim 10E12$ /sq. cm, positive polarity), or trap generation rates on the order of $\sim 10E-07$ (also about 10X higher than the 50 Angs. oxides). Injected charge density and temperature also were first order factors in the determination of the responses, but temperature appears to play a more important role than in the 50 Angs. oxides. In fact, it appeared to be of higher importance than the injected charge density. It could be possible that the high current density is causing some detrapping of positive charge in this thickness which makes temperature seem to be a more dominant factor, however, this would need to be studied further to determine physically what is occurring.

5.0 PHYSICAL ANALYSIS

The following sections describe sample preparation, results and conclusions of the physical characterization performed on each cell with a scanning and transmission electron microscope.

Following all electrical testing, a wafer from each cell was delivered for physical characterization. Each cell (wafer) was cleaved parallel to the wafer flat. One half of the wafer was used for TEM and the other for SEM characterization.

5.1 ELECTRON BEAM INDUCED CURRENT ANALYSIS

Electron signal current with negative bias (EBIC) was used in an attempt to image areas on the capacitors drawing high current.

5.1.1 Introduction

The electron-beam-induced current technique is one of several techniques which can be used to localize defects in MOS capacitor structures. This technique makes use of a rastered and focused electron beam striking the surface of the sample while monitoring the substrate current. This substrate current is used to control the video image being displayed. An external bias can be used to enhance this image and photographic records can be made of the EBIC image, recording dark and bright spot locations on the structure under inspection [19].

In this analysis, a scanning Auger microscope (Perkin-Elmer PHI 600) was used in an electron microscope mode. This system was used only because of the availability of the sample current preamplifier attached to this system. The samples were mounted on a miniature probe station (Ernest F. Fullam No. 18154) and then attached to a modified sample mounting stub, enabling biasing of the structures from the external vacuum chamber. A battery and a simple voltage divider circuit was used to apply bias to the structures. See FIGURE 5.1 for an illustration of the technique.

5.1.2 Analysis

Each sample used for the EBIC analysis was broken apart from the wafer and subjected to a metal etch. A

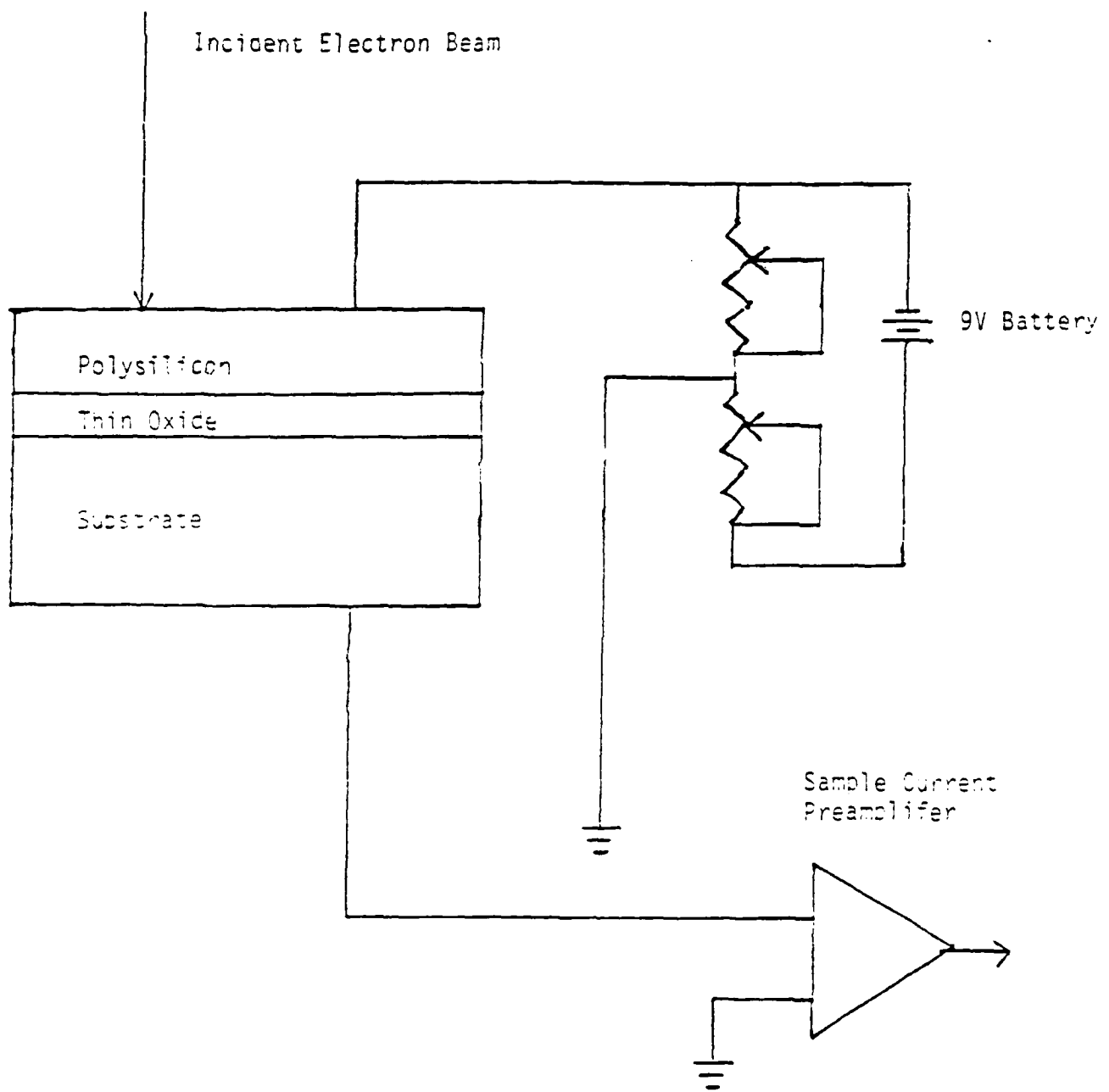


FIGURE 5.1 SIGNAL CURRENT CIRCUIT

concentrated solution of KOH was used at room temperature for approximately 5 minutes. After the metal was removed the samples were mounted on the probe station, as described above, inspected with both a secondary image and an EBIC image and then the findings were recorded. The secondary image was used primarily to locate and position the capacitor under the rastered electron beam and then the instrument was switched to the EBIC image. With the EBIC image selected, the voltage across the capacitor structure was varied from 0V to the peak battery voltage, approximately 9V. The voltage, at which a contrast change was identified, was recorded and the location of the contrast change/defect was also recorded.

While performing the analysis, the electron beam accelerating voltage and spot size were varied along with the bias across the capacitor. Best results were obtained with 10-15KV accelerating potential rather than 5-10KV. Larger beam spot sizes and higher bias voltages across the capacitors were also found to improve resolution of the EBIC technique. No significant advantages were found with changes in the incident beam angle or the working distance. TABLE 5.1 lists the instrument parameters used.

Accelerating voltage	3-15KV
Electron Beam Spot Size	1000 Ang.
Magnification	~3,000X
Incident Beam Angle	0-30 degrees
Working Distance	10-12 mm

TABLE 5.1 Instrument Parameters

5.1.3 Observations

Defects were only found when the capacitor was biased with the battery circuit. Cells 16, 8 and 10 were examined using only the electron beam as a current source and no visual contrast changes defects were found. Examination of other structures from these cells found contrast changes defects when using the battery bias circuit. See TABLE 5.2 and 5.3 for a summary of the observations and

OBS.	50ANG. OX. (%)	>200ANG. OX. (%)
DF-C	33	13
DF-NE	21	33
DF-E	4	21
NVD	42	33

total	100%	100%

TABLE 5.3 EBIC OBSERVATION SUMMARY

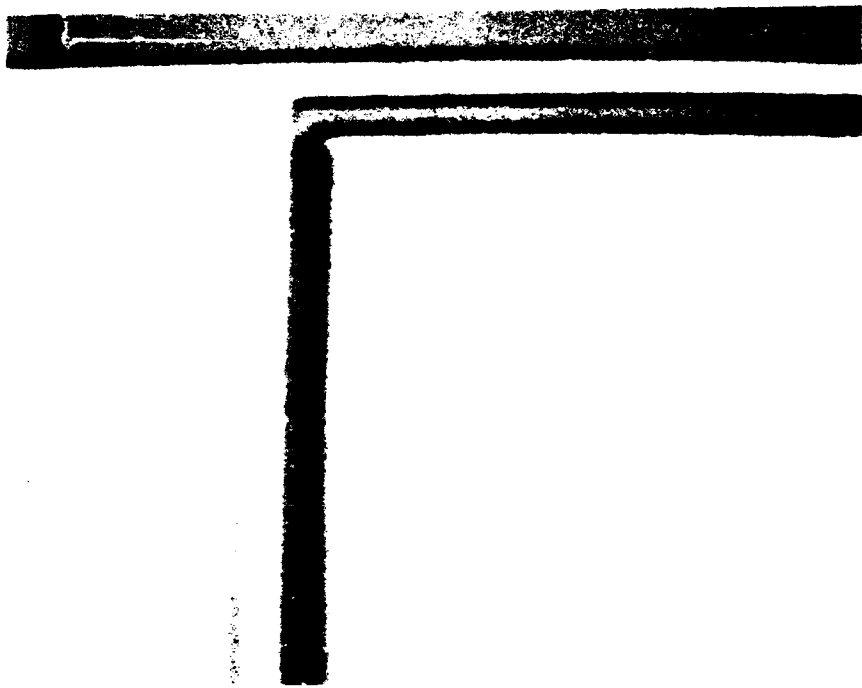


FIGURE 5.2

PHOTO 1 CELL 4 WAFER 27
SECONDARY ELECTRON IMAGE

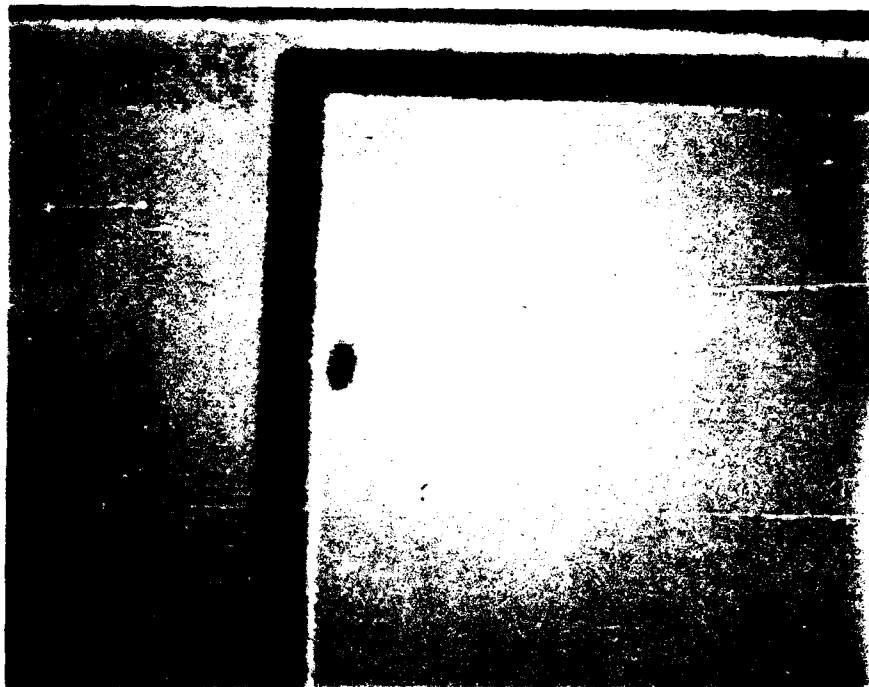


FIGURE 5.3

PHOTO 2 CELL 4 WAFER 27
SAMPLE CURRENT (EBIC) IMAGE

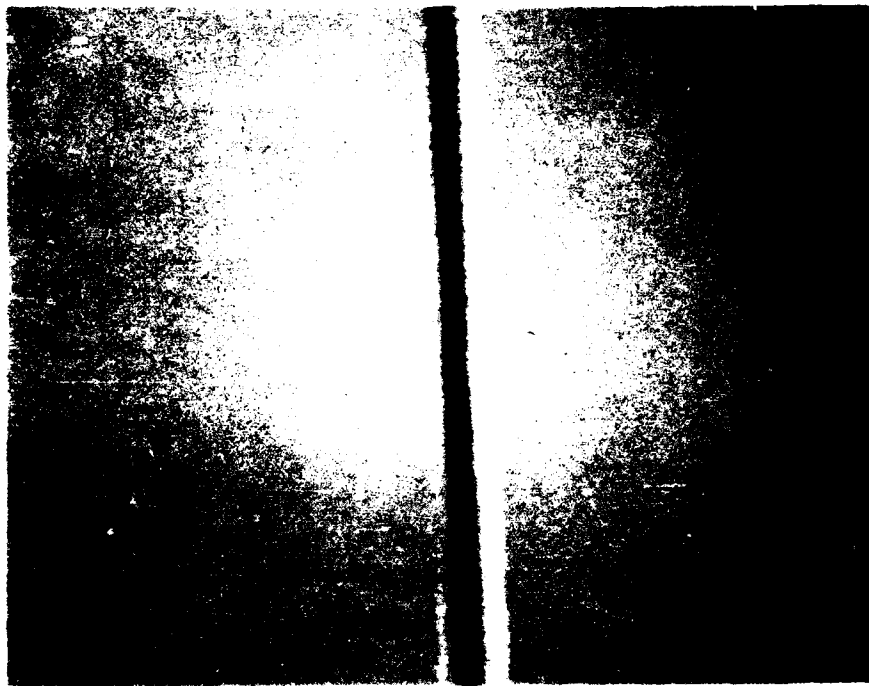


FIGURE 5.4

PHOTO 3 CELL 3 WAFER 37
SECONDARY ELECTRON IMAGE

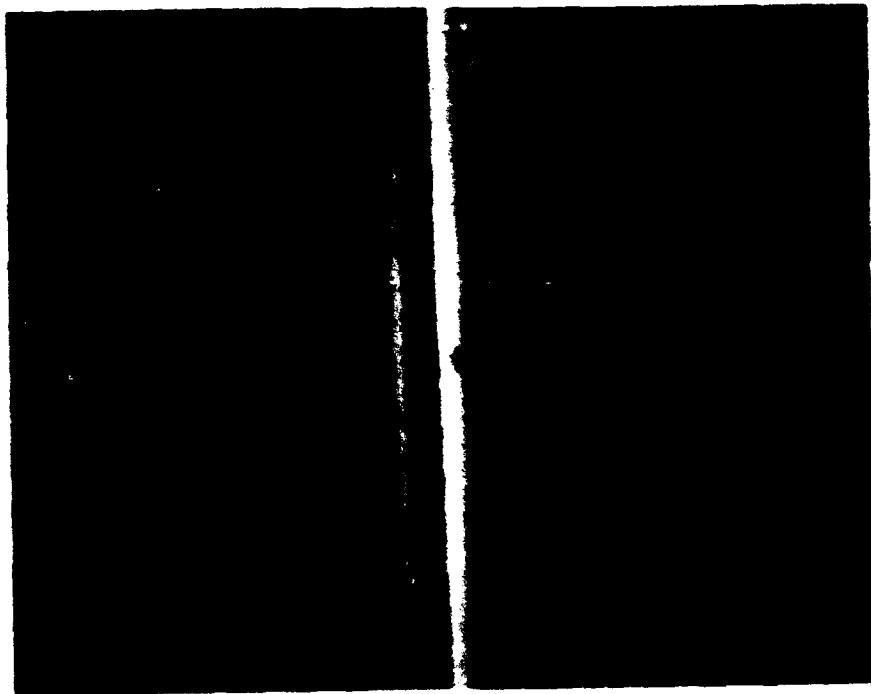


FIGURE 5.5

PHOTO 4 CELL 3 WAFER 37
SAMPLE CURRENT (EBIC) IMAGE

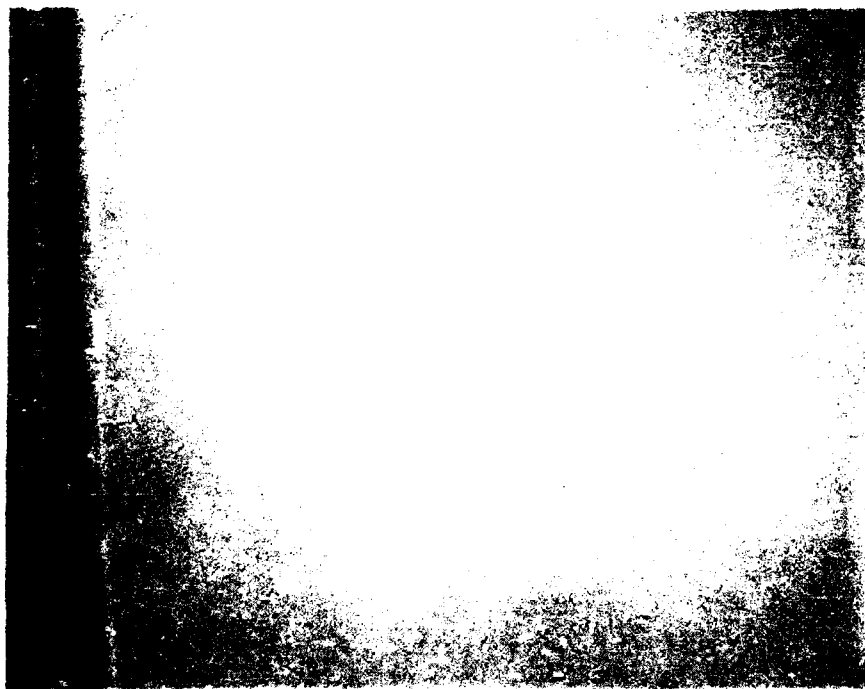


FIGURE 5.6

PHOTO 5 CELL 5 WAFER 1
SECONDARY ELECTRON IMAGE



FIGURE 5.7

PHOTO 6 CELL 5 WAFER 1
SECONDARY ELECTRON IMAGE



FIGURE 5.8

PHOTO 7 CELL 1 WAFER 23
SECONDARY ELECTRON IMAGE



FIGURE 5.9

PHOTO 8 CELL 1 WAFER 23
SAMPLE CURRENT (EBIC) IMAGE

photos 1-8 (FIGURES 5.2-5.9) showing the secondary electron image and the EBIC image.

The defects found were classified into three groups. One group of defects were away from the edge and labeled as center defects. The second group were defects which were localized to near the edge of the capacitor and were approximately 1 to 3 microns away from the edge. The third group were defects which were located at the edge of the active area of the capacitor.

5.1.4 Results and Discussions (Signal Current)

The signal current (EBIC) data showed that the oxides on the order of 50 Angstroms thick, took higher negative bias voltages to produce a signal current image and the thicker oxides, in general, tended to show a lower signal current "turn-on" voltage; thus possibly indicating more latent defects; as for example in two samples from cell 10 where the signal current "turn-on" voltage was 1.26 volts and 1.79 volts for two of the samples with oxide thicknesses on the order of 50 Angstroms and a "turn-on" voltage of 0.50 volts for a sample from cell 1 with an oxide thickness on the order of 250 Angstroms. It is thought that a higher "turn-on" voltage may indicate a stronger oxide; however, "turn-on" voltage may also be a function of the quality of the contact to the sample under test through the experimental set-up using the small probe station and each time the small probe station was used, the contact resistance may have been different.

The signal current data seems to indicate that latent defects in the oxides can be imaged using this technique; with more work, the technique could be refined and more information gained.

One general trend was that signal current detection in the 50 Angstrom oxides tended to occur in random areas; while signal current detection in the thicker oxides tended to occur at the edges of the capacitors.

Several ideas as to what the "whole-plate-contrast" detection indicated have been discussed within the group. It was suggested that "whole-plate-contrast" might occur because of Al from the metallization changing the resistivity of the polysilicon top electrodes of the capacitors by diffusion into the polysilicon when shorts caused heating of the metallization; however, it seems that the "whole-plate-contrast" is too even and if Al did diffuse

into the polysilicon, localized areas would show a signal current.

5.2 OXIDE/Si SURFACE MORPHOLOGY EXAMINATION BY TEM MICROSCOPY

The TEM replica technique was used to image the surface of the oxides and some of the silicon substrates in an attempt to gain information on defects in the oxides.

5.2.1 Introduction

The use of two-stage carbon replicas is a convenient method for observing detailed surface morphology with a transmission electron microscope. Replication is an alternative to cross-sectional and planar material samples.

The decision to use this technique was based on successful results of earlier data of replication of thin oxide surfaces that had been stressed using a ramped voltage. Results of experiments involving the vitrification of oxides also indicated that the technique is useful for elucidating fine surface morphology.

Briefly, the technique involves application of a highly conformal acetate film to the surface of interest, coating this film with carbon (actual replica), shadowing with evaporated metal (for contrast) and finally removal of the original acetate.

5.2.2 Analysis

To prepare the oxide surface morphology replicas [20] from each cell, the metalization was removed with a dip in 55 degree Celsius Metal Etch II (73 % phosphoric acid, 6.6 % acetic acid and 0.83 % nitric acid) until the metal was cleared. The removal of the polysilicon layer was accomplished with a 40-50 second dip in 95 % polysilicon etch. The variation in etch time was required because of the slight variances of poly thickness encountered. Each etch step was followed by a thorough rinse and dry. After all oxide surface samples had been prepared and examined under TEM, the piece of wafer used for TEM work was split in half and one half was subjected to a 20 second HF (49%) dip to remove all thin oxide. This half was then replicated to examine the Si surface morphology.

5.2 OXIDE/Si SURFACE MORPHOLOGY EXAMINATION BY TEM MICROSCOPY

After etching, each cell was scribed in five separate locations to denote the five study sites as per the statement of work. Each cell was then rinsed and dried to remove gross silicon particles created by scribing. Thick acetate replicating tape (.127 mm) then was applied to each marked capacitor cluster, allowed to dry and removed. This process was repeated two more times. These cleaning steps greatly reduced artifact-producing foreign matter. It should be noted that all poly/oxide replicas were from failed caps.

The actual surface replicas were produced with thin acetate replicating tape (.022 mm) and were produced immediately after the third piece of "cleaning" tape was removed to further reduce the possibility of particle contamination. The surface replication was achieved by soaking a cotton swab in acetone, daubing the capacitor cluster of interest and immediately applying the thin tape. (NOTE: Soaking thin tape in acetone will render it useless.). The replicas were then allowed to dry overnight. Each replica was carefully removed (minimal tensile force) and excess material was trimmed off. Each was then placed on a clean microscope slide with double sided tape with the replicated surface facing up in preparation for carbon coating.

Carbon coating was performed at a vacuum of 5.0 E-6 torr. Once vacuum conditions were achieved, a 1/16 inch carbon rod was evaporated at 38 amps for 30 seconds (no sparking) while rotating the specimens. This resulted in a carbon film of approximately 250-300 Angstroms [21]. A Denton Vacuum DV-502 evaporator was used for this procedure. Without breaking vacuum and with the specimens stationary, Pt/Pd shadowing material was applied at an approximate 15 degree angle in a 48 amp., 1 second flash. The carbon coated replicas were again carefully removed to avoid any tensile stress to the carbon film. The coated specimens were washed in an acetone reflux condensation apparatus in groups of three in order to remove the acetate substrate.

The washing apparatus consisted of a round bottom flask 1/4 filled with clean acetone (semiconductor grade), a vertical condensation tube and a cold arm maintained at 21-23 degrees Celsius by recirculating tap water. TEM grids (200 mesh, Ni) were then placed on a stainless steel screen attached to the cold arm. The unwashed replicas were strategically placed on the grids, carbon side up. The acetone was brought to a boil with a heating mantle around the flask. Washing continued for approximately 1.5 hours.

The replicas were allowed to dry in ambient air and placed in a replica box. After washing 6 replicas, the acetone was replaced with fresh solvent.

At this point each individual replica was inspected and mapped optically under a Polyvar metalograph. A 4"x 5" Polaroid photograph was taken at low magnification showing the entire replica. A subsequent examination at a higher magnification allowed the location of each tested capacitor to be marked by grid square on the low magnification photographs. Both unstressed and stressed to fail capacitors were mapped from each individual cell in all locations. This procedure eliminated time-consuming searches under the transmission electron microscope for the specific areas of interest.

Observation conditions on the Philips EM-420 microscope were as follows: 120 KeV accelerating voltage, condenser aperture (50 micron Pt/Th), objective aperture (70 micron Au). Two randomly selected areas from the unstressed capacitor were photographed at 30,000x and a third area at 60,000x. The same sequence of photographs was used for the stressed to fail areas. Only the 30,000x negatives were printed. The prints were enlarged to a standard magnification of 122, 144x, giving a standard area of 4 square microns.

5.2.3 Results

Cell 1, wafer 23 had an oxide thickness of 247 Angstroms, was radiated with 500 Krad of gamma radiation and was stressed at a temperature of 30 degrees Celsius at 200 micro-amps for 1 second. The oxide surface morphology from the unstressed area exhibited a medium degree of roughness and 2-3 pit anomalies for every 2 study sites. The stressed oxide surface exhibited a medium roughness with 4-5 pit anomalies for every study site. Silicon surface morphology showed a shallow, raised mottling from one cell area and a smooth surface from the alternate area from both stressed and unstressed areas.

Cell 2, wafer 25 had an oxide thickness of 280 Angstroms, did not receive radiation and was tested at 30 degrees Celsius at 500 micro-amps for 1 second. The unstressed oxide morphology showed a low degree of roughness with a concentration of 3-5 pit anomalies (250 Angstroms in diameter) per study area whereas the stressed oxide indicated a higher concentration of 5-7 pit defects per site

with the same overall surface roughness as the unstressed areas. The Si surface indicated very low roughness in both the unstressed and stressed areas.

Cell 3, wafer 38 with a measured oxide thickness of 234 Angstroms was stressed at the elevated temperature of 125 degrees Celsius for 1 second at 500 micro-amps after receiving a 500 Krad dose of radiation. Surface texture through the 5 sites of unstressed oxide ranged from smooth to a medium roughness, with only 1 pit anomaly found at 1 site. Two shallow projections were seen in another study area. From the stressed oxide, a similar roughness trend was seen with no obvious pitting detected. Both the stressed and unstressed Si surfaces were generally smooth.

Cell 4, wafer 27 with a measured oxide thickness of 269 Angstroms was stressed at 125 degrees Celsius for 60 seconds at 500 micro-amps with no radiation dose. Surface texture of the unstressed oxide ranged from a low to a medium roughness with 1-2, 200 Angstrom pit anomalies found in 2 study areas. In this case, the stressed oxide surface showed low surface roughness with the pitting density increasing to 2 pit anomalies in 3 sites. Both Si morphology samples indicated a uniform low roughness trend.

Cell 5, wafer 1 with a measured oxide thickness of 58 Angstroms was stressed at 125 degrees Celsius for 60 seconds at 500 micro-amps after receiving a 500 Krad radiation dose. Unstressed oxide surfaces ranged from a low to a medium roughness through the 5 sites. No blatant pitting was detected, but analysis of one site indicated 30-40 shallow projections (800 Angstroms in diameter). The stressed oxides showed the same range of roughness again with one site showing 30-40 shallow projections that were only 500 Angstroms in diameter. One pit anomaly was seen on two study sites. The stressed Si surface was low in roughness while the unstressed was smooth in texture.

Cell 6, wafer 33 had a measured oxide thickness of 232 Angstroms. This cell was tested for 60 seconds at 200 micro-amps with a temperature of 125 degrees Celsius after a 500 Krad dose of gamma radiation. Unstressed oxide surfaces exhibited a high degree of roughness in some areas and a medium roughness in other areas; 1 pit anomaly was seen in every site. The stressed areas showed the same roughness trend with the pitting increasing to 2 for every site. Again the trend of the Si surface was smooth for both stress conditions.

Cell 7, wafer 2 had a measured oxide thickness of 51 Angstroms. It was stressed for 60 seconds at 30 degrees Celsius with 500 micro-amps without being irradiated. Unstressed oxide surfaces showed low to medium roughness trends with 3 pit anomalies seen in 3 locations, while the stressed oxide surface ranged from low to medium to high degrees of roughness with 2 pit anomalies seen in two sites. Si surfaces under all conditions were smooth.

Cell 8, wafer 34 turned in an oxide measurement of 238 Angstroms and was stressed for 1 second at 200 micro-amps (125 degrees Celsius) with no pre-test radiation. Its unstressed oxide surface was found to be in a range from low to medium roughness with possible propagated Si defects which appear to be "decorated" stacking faults (FIGURE 5.10) on 2 locations with 1-2 pit anomalies seen in every study site. The stressed oxide was generally smooth with 2 locations showing the same type of previously described "crystal defect". Pitting was observed to be at the same density as the unstressed areas. The Si surfaces were both smooth under each condition except for 1 stressed area which showed some mottled projections.

Cell 9, wafer 35 had a measured oxide thickness of 240 Angstroms. It was stressed at 30 degrees Celsius for 60 seconds at 500 micro-amps after being exposed to 500 Krads of gamma radiation. Its unstressed oxide regions showed low roughness with no pitting. The stressed oxide showed a medium roughness with 4 pits seen in 1 study site. All Si surfaces in all cases were smooth and defect free.

Cell 10, wafer 3 had a measured oxide thickness of 56 Angstroms. It was stressed for 1 second at 125 degrees Celsius with 500 micro-amps of current; it was not irradiated. The unstressed oxide was shown to have a medium roughness trend with only 1 defect seen on 1 site. The stressed oxide surface had a medium roughness with 3 pit anomalies seen in 1 site. All Si surfaces were smooth in all cases.

Cell 11, wafer 4 had a measured oxide thickness of 55 Angstroms. Its stressing parameters were: 60 second stress of 200 micro-amps at a temperature of 125 degrees Celsius. It was not irradiated. The unstressed oxide surface had a medium roughness texture for all study sites as did the stressed oxide. The difference was seen in the presence of pitting anomalies. Three pits were seen in 2 separate locations in the stressed oxide, while no pitting was seen

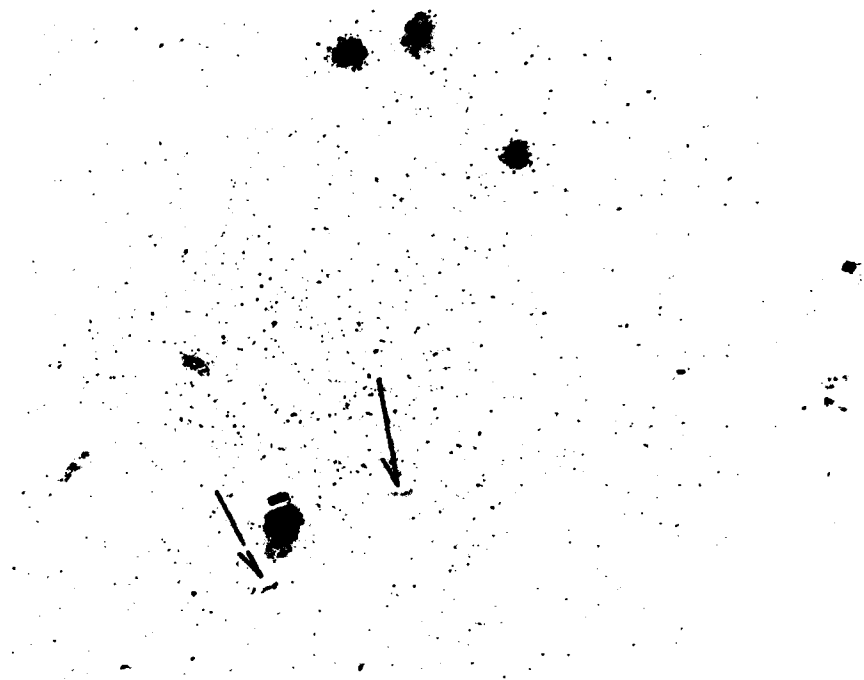


**FIGURE 5.10 POSSIBLE PROPAGATED CRYSTAL DEFECTS
REPLICA - 55,714X**

in the unstressed locations. In this cell, the Si surface was found to be uniformly smooth except in one location in the stressed region where 1 or 2 small pit anomalies were detected.

Cell 12, wafer 36 had a measured oxide thickness 239 Angstroms and was not radiated. It was stressed for 60 seconds at 200 micro-amps at 30 degrees Celsius. All surfaces associated with all stressed and unstressed conditions were not useful due to a proliferation of preparation-induced artifacts. This proliferation made accurate surface analysis of both the Si/oxide and Poly/oxide impossible.

Cell 13, wafer 5 had a measured oxide thickness of 58 Angstroms and was irradiated with a 500 Krad dose of gamma radiation. It was stressed for 1 second at 500 micro-amps at 30 degrees Celsius. Unstressed oxide surfaces showed no pit anomalies with medium roughness. Stressed oxides tended to be a low-medium texture, with 3 pit anomalies seen in one study site. Both stressed and unstressed Si surfaces were generally smooth with a few (500 Angstrom in diameter) projections seen in the stressed Si and 2 pits seen on the one study site from the no stress area.

Cell 14, wafer 6 had a thin oxide measured at 57 Angstroms and was irradiated with 500 Krad of radiation. It was stressed at 125 degrees Celsius for 1 second at 200 micro-amps. Unstressed oxide surfaces tended to be generally smooth to low roughness with no pitting. One site had 15-20 shallow projections that were 1000 Angstroms in diameter. The stressed oxide followed the same trend except for 3 pit anomalies seen in 2 study sites. The Si surface morphology was generally smooth with 1-2 shallow projections seen on 1 site from both stressed and unstressed areas.

Cell 15, wafer 8 had a thin oxide thickness measured at 60 Angstroms with a dose of radiation of 500 Krads. It was stressed for 60 seconds at 30 degrees Celsius with 200 micro-amps of current. Unstressed oxide surfaces tended to show low roughness with 2 pit anomalies seen in one study area and 2 irregular shaped pits in a separate site. Stressed oxides were rougher with a medium texture. On 4 of 5 sites, a few shallow projections (450-1000 angstroms in diameter) were found. On two study sites 2 pits were found on each. Both Si surfaces were determined to be smooth under all conditions.

Cell 16, wafer 9 with a thin oxide thickness of 63 Angstroms and no radiation exposure was stressed for 1 second at 200 micro-amps at 30 degrees Celsius. The unstressed oxide surface showed a medium roughness with only 2 pit anomalies for every 2 study sites. Likewise the stressed oxides were of a medium texture with pit density increasing to 1-2 pits for every study site. Again Si surfaces were generally smooth, and there were no detectable differences.

Cell 17, wafer 20 had an oxide thickness of 124 Angstroms and a 50 Krad dose of radiation. Its stress conditions consisted of 10 second stress time, at 350 micro-amps with a 70 degree Celsius temperature. Both the unstressed and stressed oxides showed a low degree of roughness with no pitting. The stressed Si surface morphology was generally smooth as was the unstressed areas except on one site which indicated a few very shallow projections and depressions.

5.2.4 DISCUSSIONS AND SUMMARY

The data pointed to several general conclusions. Possible trends existed in several different categories and groupings of cells. (NOTE: All wafers were irradiated at room temperature.)

Comparing radiation effects between 50 Angstrom thick unstressed oxide cells the following observations were made. Less pitting was seen in cell 15 (radiated) as opposed to cell 16 (non-radiated). The same trend was also seen between cell 13 (radiated) and cell 7 (non-radiated), both 50 Angstrom unstressed oxides.

Comparing radiation effects between 200 Angstrom thick unstressed oxides, a similar trend is noticed. No pitting was observed on cell 9 (radiated), but cell 2 (non-radiated) exhibited a fairly high degree of pitting.

Two other 200 Angstrom oxide cells, cell 6 (radiated) and cell 8 (non-radiated) continued to support this trend. Cell 6 showed roughly half as much pitting as was seen in cell 8. FIGURES 5.11-5.14 show this difference between unstressed oxide surfaces of radiated and non-radiated cells (both 50 and 200 Angstrom Tox).

Comparing the effect of stress temperature on unstressed oxides, TEM results indicate another possible correlation between degree of pitting.

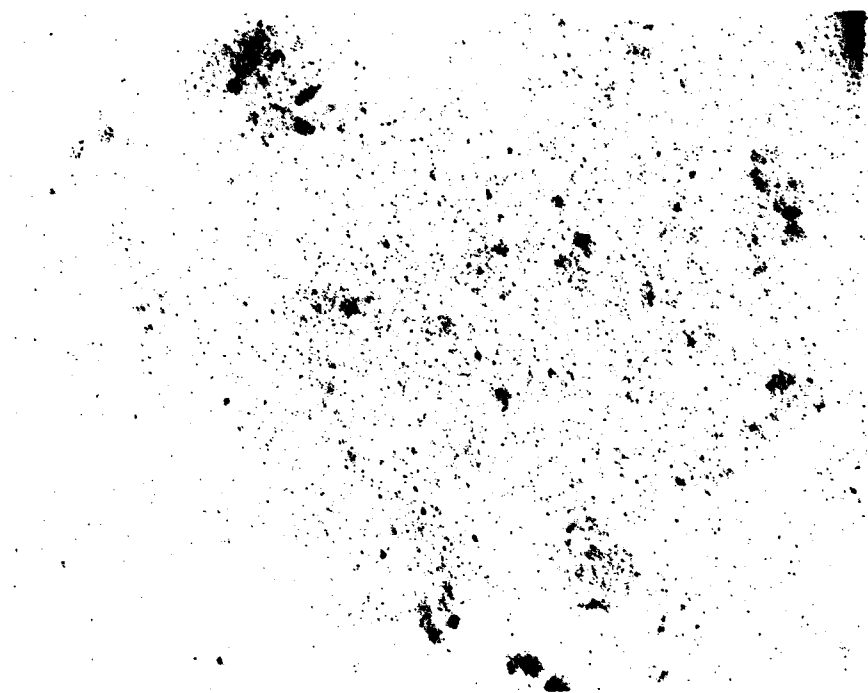


**FIGURE 5.11 CELL 7 UNSTRESSED OXIDE NON-RADIATED
50 ANGSTROM TOX - MORE PITTING**



FIGURE 5.12 CELL 13 UNSTRESSED OXIDE RADIATED
50 ANGSTROM TOX - LESS PITTING
REPLICA--55,714X

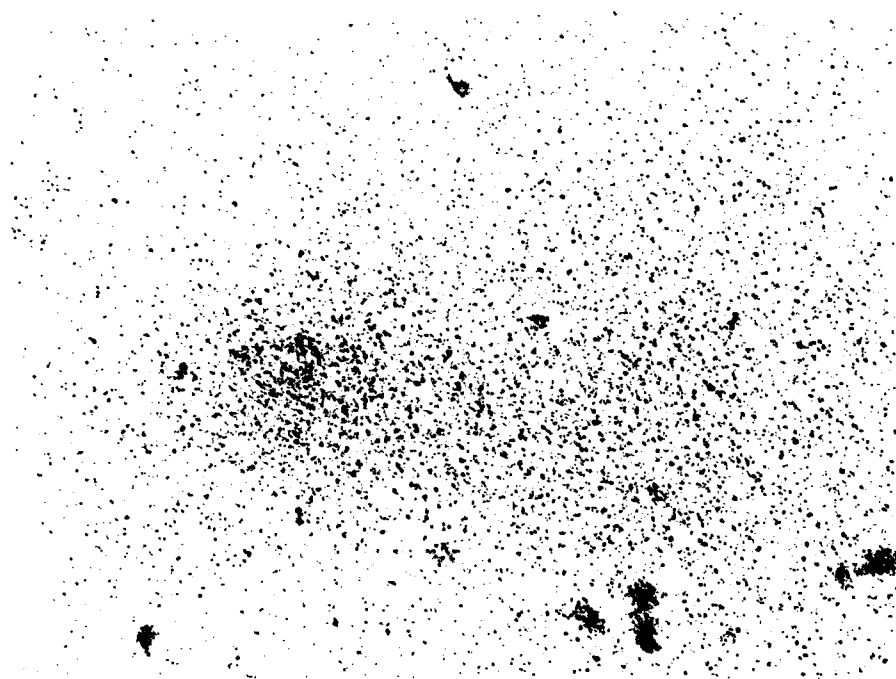


FIGURE 5.13 CELL 02 UNSTRESSED OXIDE NO RADIATION
200 ANGSTROM TOX - MORE PITTING
REPLICA--55,714X

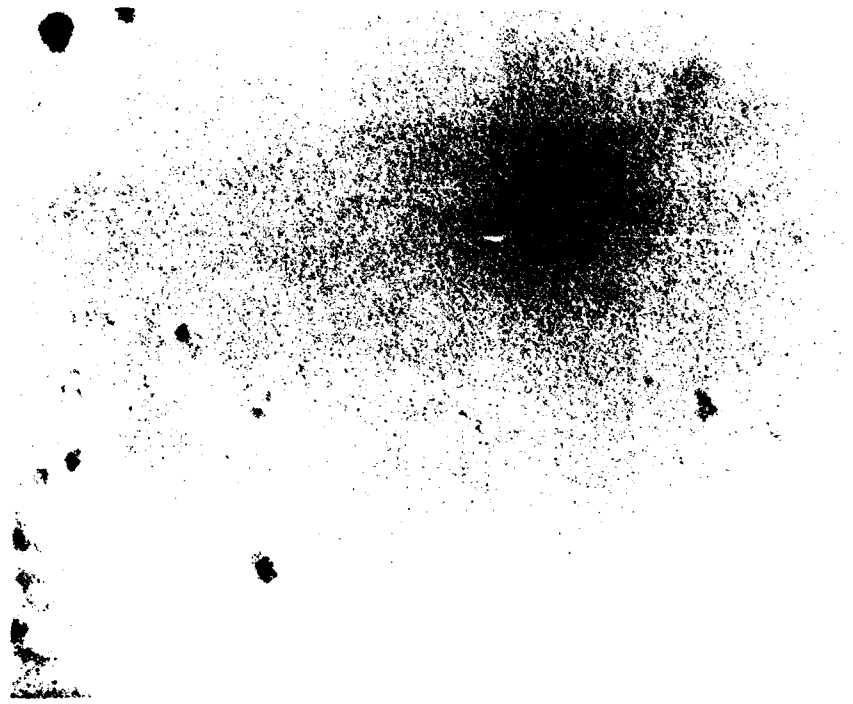


FIGURE 5.14 CELL 09 UNSTRESSED OXIDE RADIATED
200 ANGSTROM TOX - LESS PITTING
REPLICA--55,714X

Cell 7 was tested at 30 degrees Celsius and cell 10 at 125 degrees Celsius. Pitting was found to be more extensive at the lower temperature, both of these cells had 50 Angstrom oxides. Cells 11 and 16 (also 50 Angstrom oxides) were tested at 125 and 30 degrees respectively and found to follow the same trend. An oxide surface comparison between cells with 200 Angstrom oxides stressed at different temperatures is not possible between cell 12 and cell 8 because of the de-processing of cell 12; however, continued support of the above trend is found between cell 2 and cell 4 (200 Angstrom oxides) tested at 30 and 125 degrees Celsius. Cell 2 shows more pitting than cell 4. This trend is illustrated in FIGURES 5.15-5.18. The effect of temperature may have to do with a slight annealing effect from the elevated temperature.

These observed trends are not completely conclusive and no obvious trends were seen between the different current conditions. An overall trend in the degree of pitting seems to exist between the stressed and unstressed capacitor oxide surfaces (more pitting in stressed surfaces); This may be and probably is inherent to stressing the capacitor with the method used in the study, however, because of the multitude of different test parameters and wafer conditions this trend should be approached with caution. TABLES 5.4 and 5.5 are summaries of the observed TEM data. It also must be noted that, all stressed oxides were from failed capacitors.

It was determined from the beginning that the original surfaces were affected by the wet etch deprocessing. It was assumed that if de-processing was kept to a standard methodology all effects on the sample surface (Si and SiO₂) would be equal in all cells. Nevertheless some enhancement of the micro-surface has occurred and should be taken into consideration. For this type of study, however, there is no way to avoid such enhancement.

A way of "reading" the various structures seen in the micrographs was developed. It was known that the actual replicas of holes or deep "pitted" areas on the wafer surface (Si or SiO₂) would be vertical projections in the carbon film. Likewise, projections on the wafer surface replicated as vertical depressions on the carbon replica. This difference caused the results of the contrast shadowing (Pt/Pd) to be unique for each structure. The projections on the replica (pits on the original surface) possessed a shadow (light areas in micrographs) that at the point of origin conformed to the general shape of the projection.



FIGURE 5.15 CELL 16 UNSTRESSED OXIDE 30 DEGREE CELSIUS STRESS
50 ANGSTROM TOX - MORE PITTING
REPLICA--55,714X

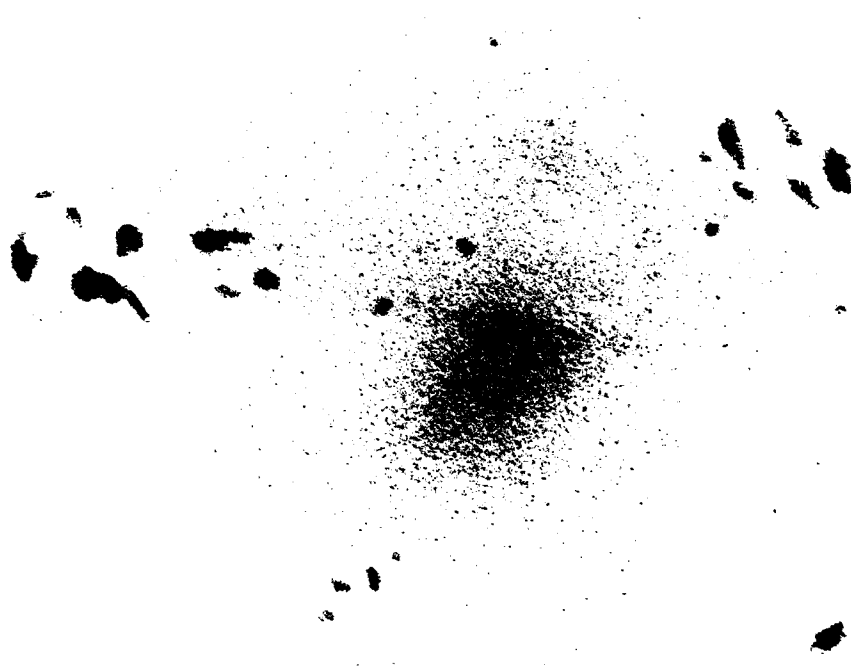


FIGURE 5.16 CELL 11 UNSTRESSED OXIDE 125 DEGREE CELSIUS STRESS
50 ANGSTROM TOX - LESS PITTING
REPLICA - 55,714X

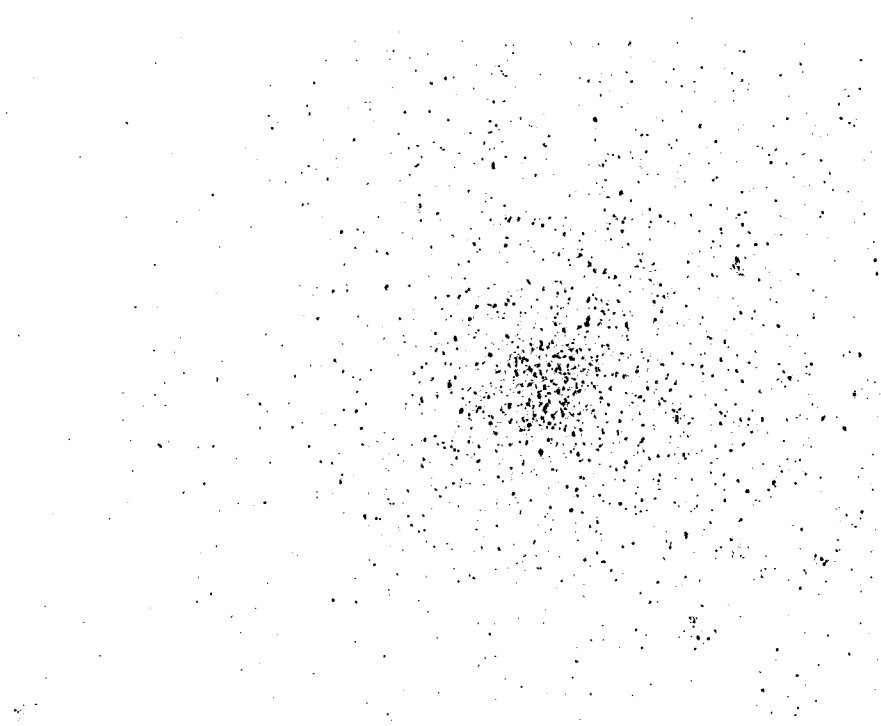


FIGURE 5.17 CELL 02 UNSTRESSED OXIDE 30 DEGREES CELSIUS STRESS
200 ANGSTROM TOX - MORE PITTING
REPLICA--55,714X

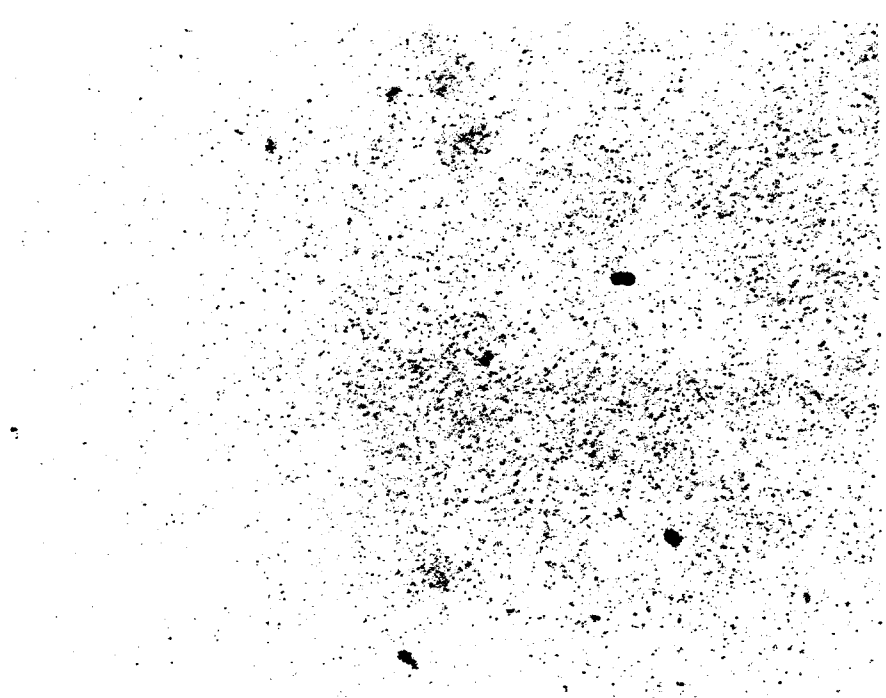


FIGURE 5.18 CELL 04 UNSTRESSED OXIDE 125 DEGREES CELSIUS STRESS
200 ANGSTROM OXIDE - LESS PITTING
REPLICA--55,714X

Cell	Roughness		Pitting Anomaly	
	Unstressed	Stressed	Unstressed	Stressed
#01 W23 275 ang. 200 uA, 30, 500 Krad 1 second	P medium-low S mottled-smooth	P medium-high S mottled-smooth	2-3 pit/2 sites (All pits 250 ang. in dia.)	4 pit/site
#02 W25 280 ang. 500 uA, 30, no radiation 1 second	P low S low	P low S low	3-5 pit/site (All pits 250 ang. in dia.)	5-7 pit/site
#03 W38 234 ang. 500 ua, 125, 500 Krad 1 second	P low-medium S smooth	P low-medium S smooth	1 pit/1 site 2 bump/1 site (All pits 200-250 ang. in dia.)	no pits
#04 W27 269 ang. 500 uA, 125, no radiation 60 seconds	P low-medium S low	P low S low	2 pit/2 sites (All pits 200-250 ang. in dia.)	2 pits/3 sites
#05 W01 58 ang. 500 uA, 125, 500 Krad 60 seconds	P low-medium S smooth	P low-medium S low	1 site-30 800 ang. diameter bumps (All pits 200-250 ang. in dia.)	1 site-30 500 ang. diameter bumps 1 pit/2 sites
#06 W33 232 ang. 200 uA, 125, 500 Krad 60 seconds	P medium/high S smooth	P medium/high S smooth	1 pit/site	2 pit/site (pits 250 ang. in dia.)
#07 W02 51 ang. 500 uA, 30, no radiation 60 seconds	P low-medium S smooth	P low-medium-high S smooth	3 pit/3 sites (All pits 200-350 ang. in dia.)	2 pit/2 sites
#08 W34 238 ang. 200 uA, 125, no radiation 1 seconds	P low-medium S smooth	P smooth S smooth/ mottled	2 pit/site possible crystal defect propagation into oxide in 2 locations	2 pit/site same crystal defect phenomenon in two locations
#09 W34 240 ang. 500 uA, 30, 500 Krad 60 seconds	P low S smooth	P medium S smooth	no pits (All pits 250 ang. in dia.)	1 pit/1 site

TABLE 5.4 TEM DATA AND TREND SUMMARY

		<u>Unstressed</u>	<u>Stressed</u>	<u>Unstressed</u>	<u>Stressed</u>
#10	56 ang.	P medium	P medium	1 pit/1 site	3 pit/1 site
W03	500 uA, 125, no radiation 1 second	S smooth	S smooth	(All pits 250 ang. in dia.)	
#11	55 ang.	P medium	P medium	no pits	3 pits/2 sites
W04	200 uA, 125, no radiation 60 seconds	S smooth	S smooth	(All pits 250-300 ang. in dia.)	
#12	239 ang.	not useable	not useable	de-processing problem	
W36	200 uA, 30, no radiation 60 seconds	not useable	not useable		
#13	58 ang.	P low-medium	P low-medium	no pits	3 pit/1 site
W05	500 uA, 30, 500 Krad 1 second	S smooth/1site 2 pits/1 site	S smooth/1 site 500 Ang. proj./1 site	(All pits 250-300 ang. in dia.)	
#14	57 ang.	P smooth-low	P smooth-low	no pits	3 pit/2 sites
W06	200 uA, 125, 500 Krad 1 second	S smooth with 1-2 shallow proj./1 site	S smooth with 1-2 shallow proj./1 site	15-20 1000 ang. diameter bumps/1 site	(All pits 250 ang. in dia.)
#15	60 ang.	P low	P medium	2 pit/1 site	2 pit/2 site
W08	200 uA, 30, 500 Krad 1 second	S smooth	S smooth	2 irregular pits/ 1 site	few shallow bumps 450-1000 ang. diameter bumps on 4 sites. (All pits 250 ang. in dia.)
#16	63 ang.	P medium	P medium	2 pit/2 sites	1-2 pit/site
W09	200 uA, 30, no radiation 1 second	S smooth	S smooth	(All pits 250-300 ang. in dia.)	
#17	124 ang.	P low	P low	no pits	no pits
	350 uA, 70, 50 Krad 10 seconds	S smooth	S smooth A few shallow proj./1 site + depressions		

SITE = 4 SQUARE MICRONS

TABLE 5.4a TEM DATA AND TREND SUMMARY (CONT'D)

50 Angstrom Oxide
Average # Pits/Site/Cell

Cell #05 - 0 pit/site
 Cell #07 - 1.8 pit/site
 Cell #10 - 1 pit/site
 Cell #11 - 0 pit/site
 Cell #13 - 0 pit/site
 Cell #14 - 0 pit/site
 Cell #15 - 0.4 pit/site
 Cell #16 - 0.8 pit/site

4.0 total average
 for 8 Cells

$$4.0 \text{ pit}/8.0 \text{ Cells} = x$$

$$x = .5 \text{ pit}/\text{site}$$

200 Angstrom Oxide
Average # Pits/Site/Cell

Cell #01 - 1 pit/site
 Cell #02 - 4 pit/site
 Cell #03 - 1 pit/site
 Cell #04 - 0.8 pit/site
 Cell #06 - 1 pit/site
 Cell #08 - 2 pit/site
 Cell #09 - 0 pit/site
 Cell #12 - N/A

9.8 total average
 for 7 Cells

$$9.8 \text{ pit}/7.0 \text{ Cells} = x$$

$$x = 1.4 \text{ pit}/\text{site}$$

Total Sites = 80

Site = 4 micron square

TABLE 5.5 OVERALL PITTING TREND FOR
 UNSTRESSED 50 AND 200 OXIDES

50 Angstrom Oxide
Average # Pits/Site/Cell

Cell #05 - 0.4 pit/site
 Cell #07 - 0.8 pit/site
 Cell #10 - 0.6 pit/site
 Cell #11 - 0.6 pit/site
 Cell #13 - 0.6 pit/site
 Cell #14 - 1.2 pit/site
 Cell #15 - 0.8 pit/site
 Cell #16 - 1.5 pit/site

6.5 total average
 for 8 cells

6.5 pit/8.0 cells = x

x = .8 pit/site

200 Angstrom Oxide
Average # Pits/Site/Cell

Cell #01 - 4 pit/site
 Cell #02 - 5.8 pit/site
 Cell #03 - 0 pit/site
 Cell #04 - 1.2 pit/site
 Cell #06 - 2 pit/site
 Cell #08 - 2 pit/site
 Cell #09 - 0.8 pit/site
 Cell #12 - N/A

15.8 total average
 for 7 cells

15.8 pit/7.0 cells = x

x = 2.2 pit/site

Total Sites = 80

Site = 4 micron square

TABLE 5.5a OVERALL PITTING TREND FOR
 UNSTRESSED 50 AND 200 OXIDES

From the source, this shadow tapered into a point, looking much like a comet tail. If the projection was low enough, the point of the tail was less pronounced. The tails of all replica projections pointed in the same direction on any one micrograph. (Whether the pit anomalies seen in the micrographs are actual pin-holes or latent defects in the oxide is not known because of problems with surface enhancement (previously mentioned) and the possible enlargement of such pin-holes.)

Depressions on the actual replica (vertical projections on the surface of interest) acted as bowls, with the shadowing material building up on the face directly opposite of the point of metal evaporation. This left the shadows of replica depressions pointing in the opposite direction of shadows from replica projections. Depression shadows also tended to be more rounded in the end point of their tails and less conformal to the actual replicated structure. The shadowing differences are seen in FIGURE 5.19 .

FIGURE 5.20 indicated a possible artifact produced during replication. The extremely round and well defined projection indicated by the arrow was thought to possibly be a micro-bubble produced by either trapped air or out-gassing of the sample surface. This effect was seen on a totally random basis and infrequently which lended to suspicion that they were preparation artifacts [22].

FIGURE 5.20 also illustrates the effect of overshadowing. Overshadowing slightly reduced the resolving power of a few replicas; some finer detail was lost. Over-shadowing was possibly caused by the timing of the 1 second flash of Pt/Pd being off a fraction of a second. It may have also been caused by the temperature of the replica substrate (acetate) being too warm as a result of the carbon evaporation. Later in the study, this factor was eliminated by allowing the chamber to cool for 2.5 minutes after carbon evaporation. The same FIGURE 5.20 also illustrates the appearance of left over acetate. The undissolved acetate takes on the appearance of dark blotches.

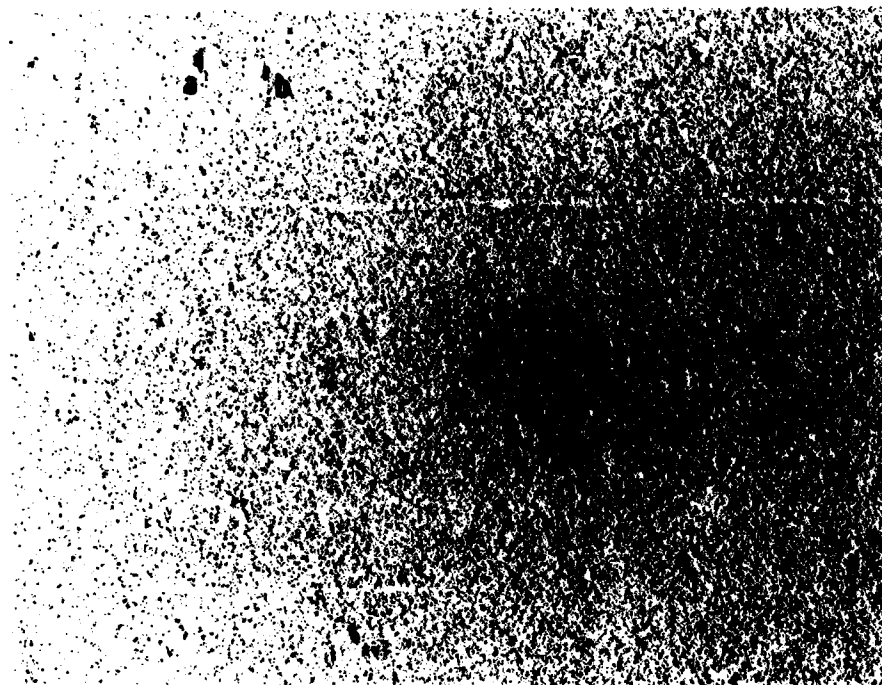


FIGURE 5.19 SHADOWING DIFFERENCE REPLICA - 55,714X
A. PROJECTION B. DEPRESSION

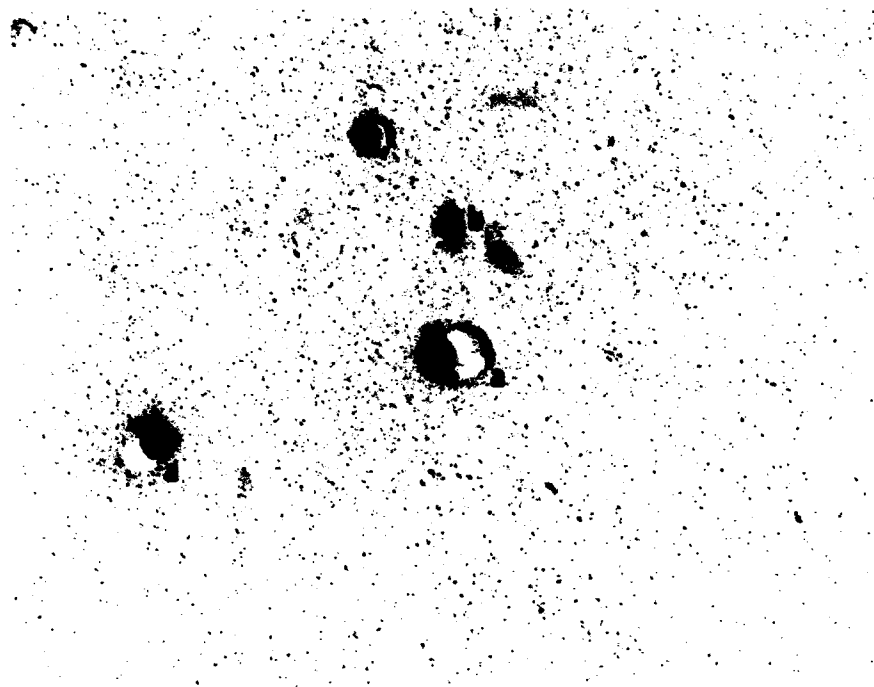


FIGURE 5.20 A. BUBBLE ARTIFACT B. ACETATE CONTAMINANT
GENERAL VIEW OF OVERSHADOWING
REPLICA - 55,714X

6.0 CONCLUSIONS

The use of the half factorial Hadamard matrix technique in the evaluation of the stress factors involved in this experiment using constant current stress has provided some general directions for further study in the area of oxide reliability and the relationship between the stress factors, charge trapping and oxide quality.

The effects of oxide thickness, stress current, temperature, stress time and radiation effects on oxide breakdown, charge trapping and generation rates have been investigated.

6.1 CONCLUSIONS FROM THE ELECTRICAL DATA

It was concluded from the electrical data that stress current density has a strong first order effect on time dependent breakdown of ultra-thin oxides. The data indicated that for 200 micro-amp (0.3 amp/cm^2) the oxide time-to-fail is about ten times longer than for the oxides stressed with 500 micro-amp (0.8 amp/cm^2). Stress current shows important effects on Nt; oxides stressed with 500 micro-amp stress currents show several times higher Nt than those stressed with 200 micro-amp. Stress current effects on G only show an important effect for 50 Angstrom oxides but not in the case of the 200 Angstrom oxides. Statistical analysis also confirms that stressed current density has a strong effect on oxide time-to-fail, Nt and G.

Stress temperature also shows some effect on oxide breakdown; however, it is rather second order compared to stress current density. Stress temperature shows significant impact on both Nt and G. Oxides stressed at 125 degrees showed several times higher Nt and G than the oxides stressed at 30 degrees. Statistical analysis shows that temperature effect is the second most important factor next to current density for Nt, and it is the most important factor for G. Equations for time-to-fail, Nt and G as functions of stressed current and temperature were generated from statistical analysis.

Oxide thickness shows little effect on the the time-to-fail of the oxides under constant current stress; however, the breakdown fields are around 14-16 MV/cm for oxides thickness of around 50 Angstroms and 11-12 MV/cm for oxides with thickness of around 200 Angstroms with $0.3\text{-}0.8 \text{ amp/cm}^2$ stress current density.

Oxide thickness shows a strong first order effect on trapped charge density (Nt) and trap generation rate (G). Oxides with thickness around 200 Angstroms have around ten times higher Nt and G than oxides with thickness of around 50 Angstroms under constant current stress.

Radiation has little effect on oxide time-to-fail. The samples were not voltage biased for this experiment. Radiation has little effect on both Nt and G.

Stress time required to reach 50% cumulative failure (T50) is roughly ten times longer than required to reach 16% cumulative failure (T16) for 200 angstrom oxides. However, (T50) is roughly about two times (T16) for 50 angstrom oxides. Hole trapping dominates during early stress, while electron trapping dominates during later stress, for both the 50 angstrom and 200 angstrom oxides. The 50 angstrom oxides shift rapidly from hole to electron dominated trapping and the 200 angstrom oxides shift more gradually.

6.2 CONCLUSIONS FROM THE PHYSICAL DATA (TEM REPLICAS)

As indicated by the TEM micrographs, less surface pitting was observed on the oxide surface of oxides that had been exposed to radiation and oxides stressed at higher temperature.

No trends were detected when comparing cells stressed with different current densities.

6.3 CONCLUSIONS FROM THE PHYSICAL DATA (SEM SIGNAL CURRENT)

The signal current technique (EBIC) with bias was shown to be able to image latent defects in ultra-thin oxides. The signal current defect images were observed only for samples with voltage bias. Random latent defect locations were observed for all cells. Thicker oxides tend to have more latent defects near or at the diffusion edges. Stress current, temperature and radiation show little effect on the signal current data. The signal current data did indicate that thinner oxides around 50 Angstroms have lower latent defect densities when compared with the thicker oxides around 200 Angstroms.

6.4 RECOMMENDATIONS

In future research on this subject, it is recommended that a more intensive study using stress current (electric

field) and temperature splits in order to fully investigate the time dependent breakdown and charge trapping characteristics of ultra-thin oxides be done.

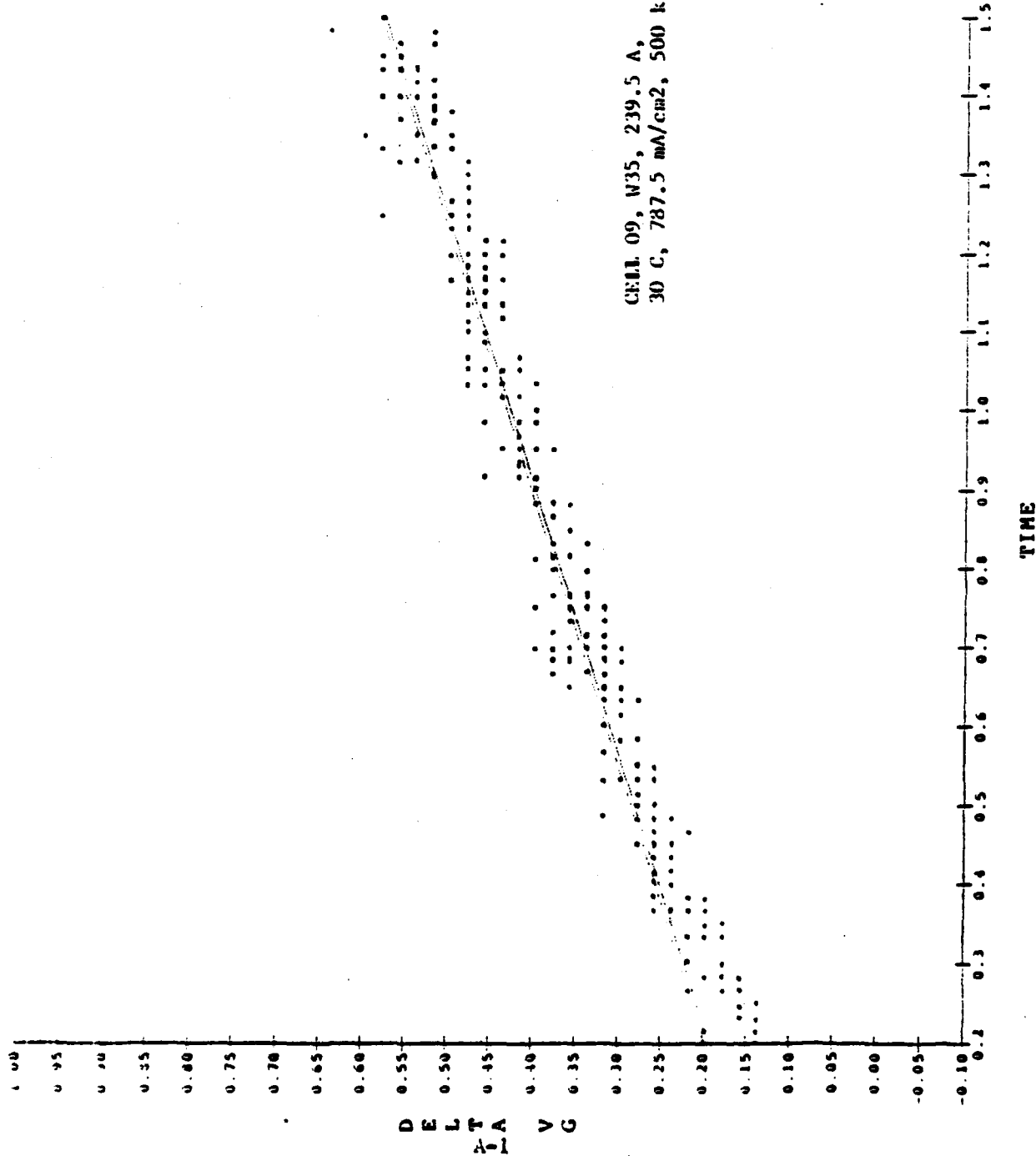
Further study of radiation effects should be done with test vehicles that are under voltage bias and future studies should include the biased signal current technique (EBIC).

REFERENCES

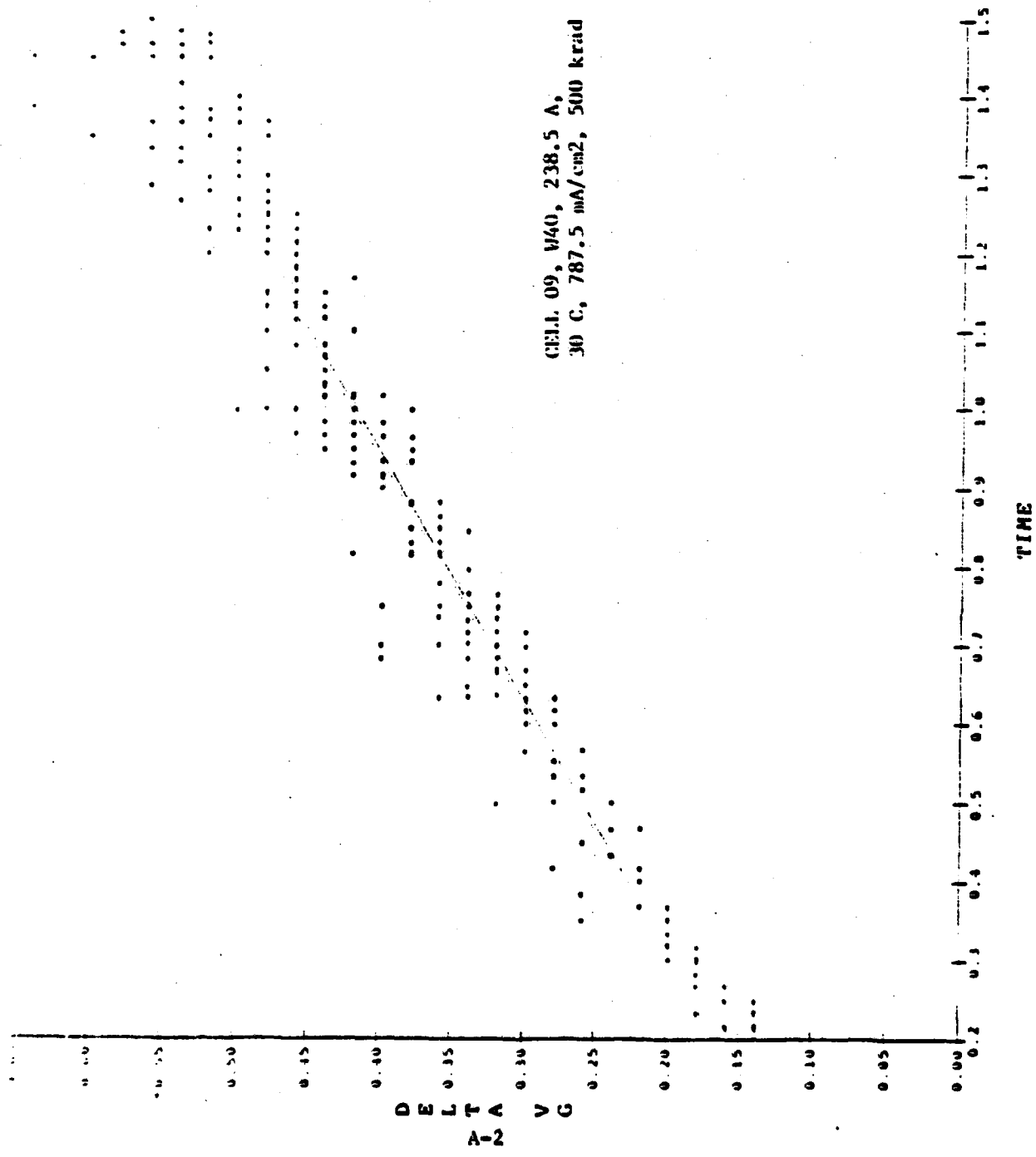
- [1] S.M. Sze, Edt., "VLSI Technology", McGraw-Hill, N.Y., 1983, page 1.
- [2] D.E. Bradley, "Replica and Shadowing Techniques", from Techniques for Electron Microscopy, Desmond Kay Edt., Chapter 5, pp 96-151, 1961.
- [3] Internal communications J. Michlowsky, SGS-Thomson Microelectronics.
- [4] Work completed at UTC-Mostek, Advanced Technology Group by Y. Limb, D.A. Tiffin, D.J. Bast, and J.W. Staman in 1984-85.
- [5] Presentations to RADC in 1987 on the status of work on this contract 1987 by Dave Fisch, Thomson Components-Mostek Corp.
- [6] Work completed at UTC-Mostek, Advanced Technology Group by Y. Limb, D.A. Tiffin, D.J. Bast and J.W. Staman in 1984-85.
- [7] Stanley Wolf and Richard N. Tauber, Silicon Processing for the VLSI Era Volume 1: Process Technology, Lattice, Sunset Beach (1986), Chap. 18.
- [8] Work at UTC-Mostek in 1981-82 in the Process R&D Group.
- [9] Communications from L.M. Beam, Texas A&M University, Cyclotron Institute via John Krohn, Texas A&M University, College Station, Texas 77843
- [10] D.E. Gray, Edt., "American Institute of Physics Handbook", McGraw-Hill Book Co., N.Y., 1982, D.T. Goldman, Ch. 8, page 17.
- [11] UTC-Mostek, Advanced Technology Group internal work, 1984-85.
- [12] Saks, et al; "Generation of Interface States by Ionizing Radiation in Very Thin MOS Oxides", IEEE Trans. Nuc. Sci., Vol NS-33 no. 6, Dec. 86.
- [13] Schwank, et al; "Radiation-Induced Interface-State Generation in MOS Device", IEEE Trans. Nuc. Sci., Vol NS-33 no. 6, Dec. 86.
- [14] Y. Cohen, "High Field Trapping in Gate Oxides", Intel Internal Memo, May 27, 1982.

- [15] Andre R. Leblanc and Wagdi W. Abadeer, " Behavior of SiO₂ Under High Electric Field//current Stress Conditions", IEEE/IRPS, 1986.
- [16] Y. Nissan-Cohen, J Shappir and D. Frohmen-Bentchkowsky, "Characterization of Simultaneous Bulk and Interface High-Field Trapping Effects in SiO₂", IEDM, 1983.
- [17] Masaharu Noyori and Takashi Hori, "Analysis of Instabilities by Fowler-Nordheim Injection into Thin SiO₂ Films in MOS Structures", INFOS, 1986.
- [18] K. Tatsuuma, M. Sugimoto, T Ajiki, "Electrical Characteristics of Very Thin Oxide Breakdown", VLSI Symposium, 1988.
- [19] Anjan Bhattacharyya, Jan D. Reimer and Kenneth N. Ritz "Breakdown Voltage Characteristics of Thin Oxides and Their Correlation to Defects in the Oxide as Observed by EBIC Technique," IEEE Electron Device Letters, Vol. EDL-7, No.2, pp 58-60, February 1986.
- [20] D.E. Bradley, "Replica and Shadowing Techniques," from Techniques for Electron Microscopy, edited by Desmond Kay Chapter 5, pp 96-151, 1961.
- [21] Unpublished internal memo on Carbon Coating from M.M. Matthews, Baylor College of Dentistry, Dallas, 1984.
- [22] Internal communication from John Staman to Don Tiffin on Possible Artifacts seen in Replicas, 1987.

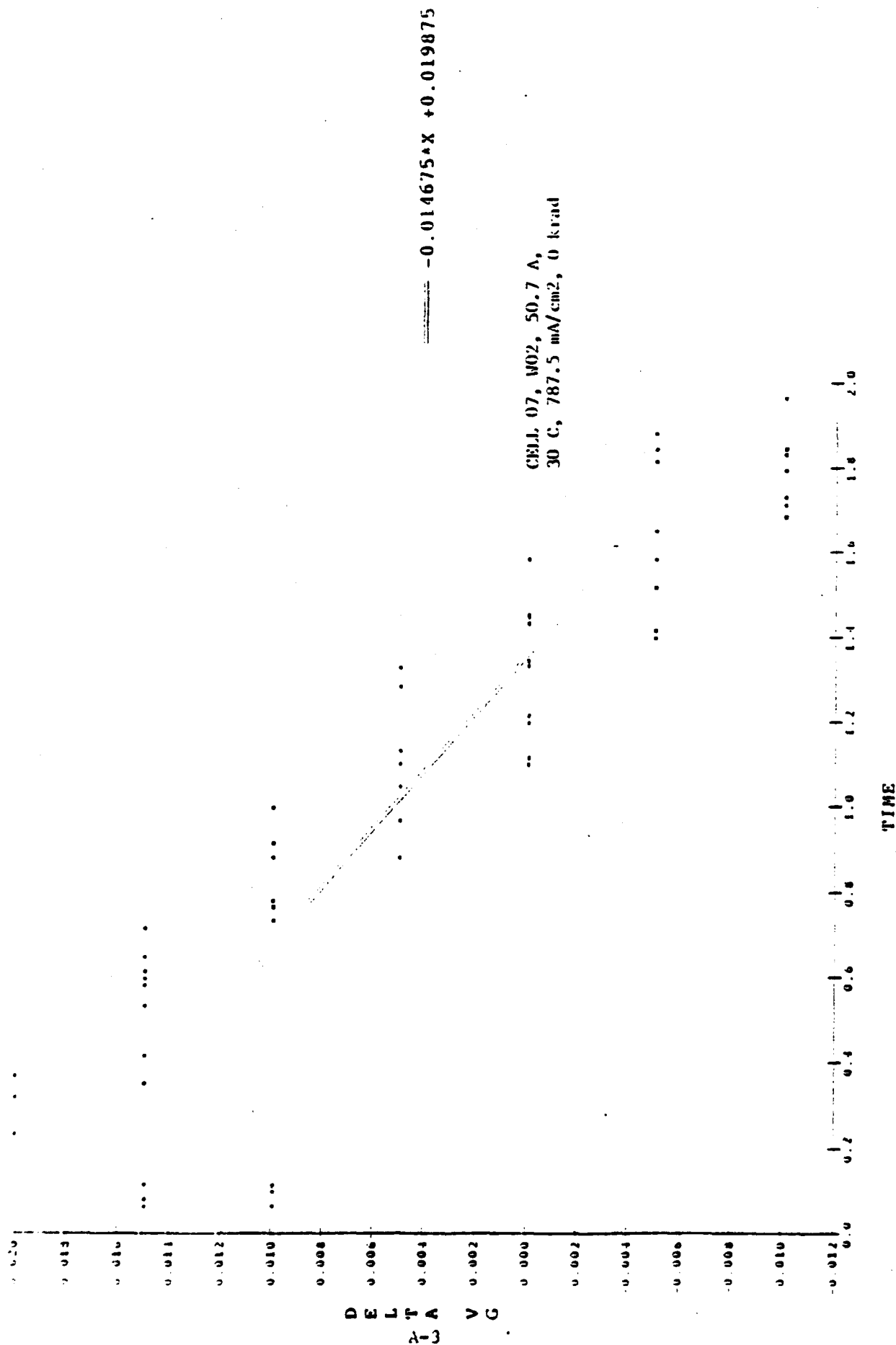
DELTA VG VS TIME FOR W35



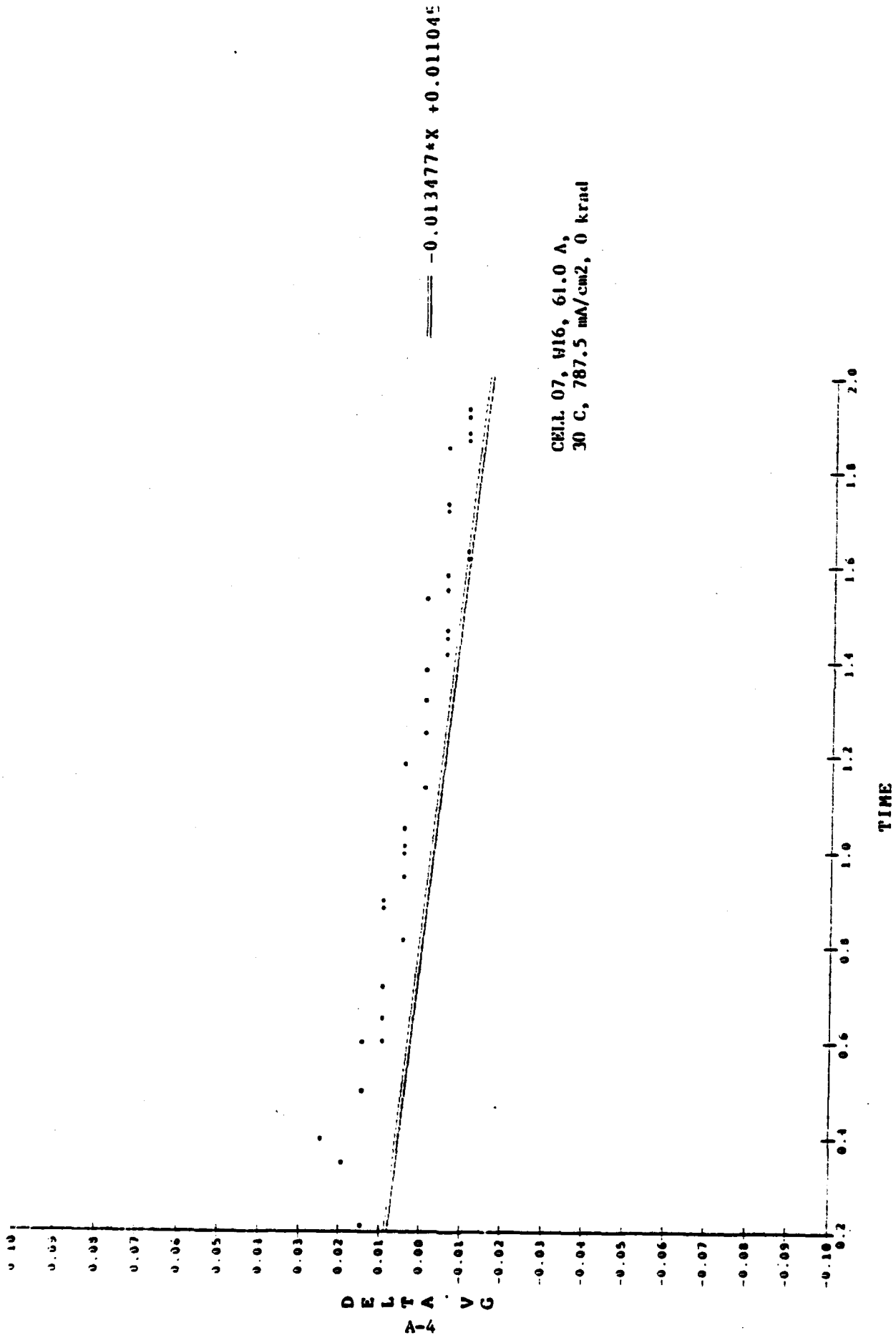
DELTA VG VS TIME FOR V410



DELTA VG VS TIME FOR W02

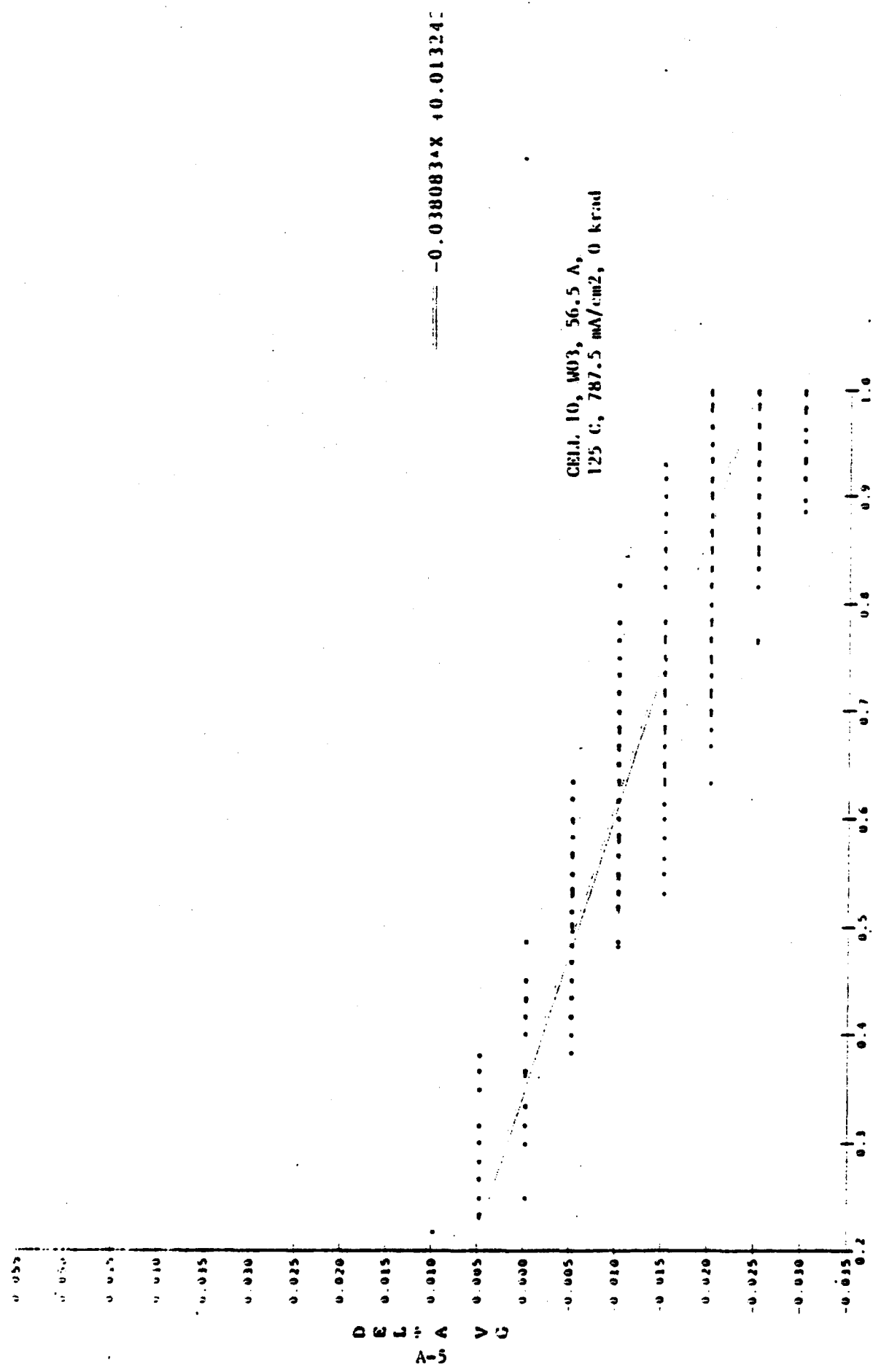


DELTA VG VS TIME FOR VI6

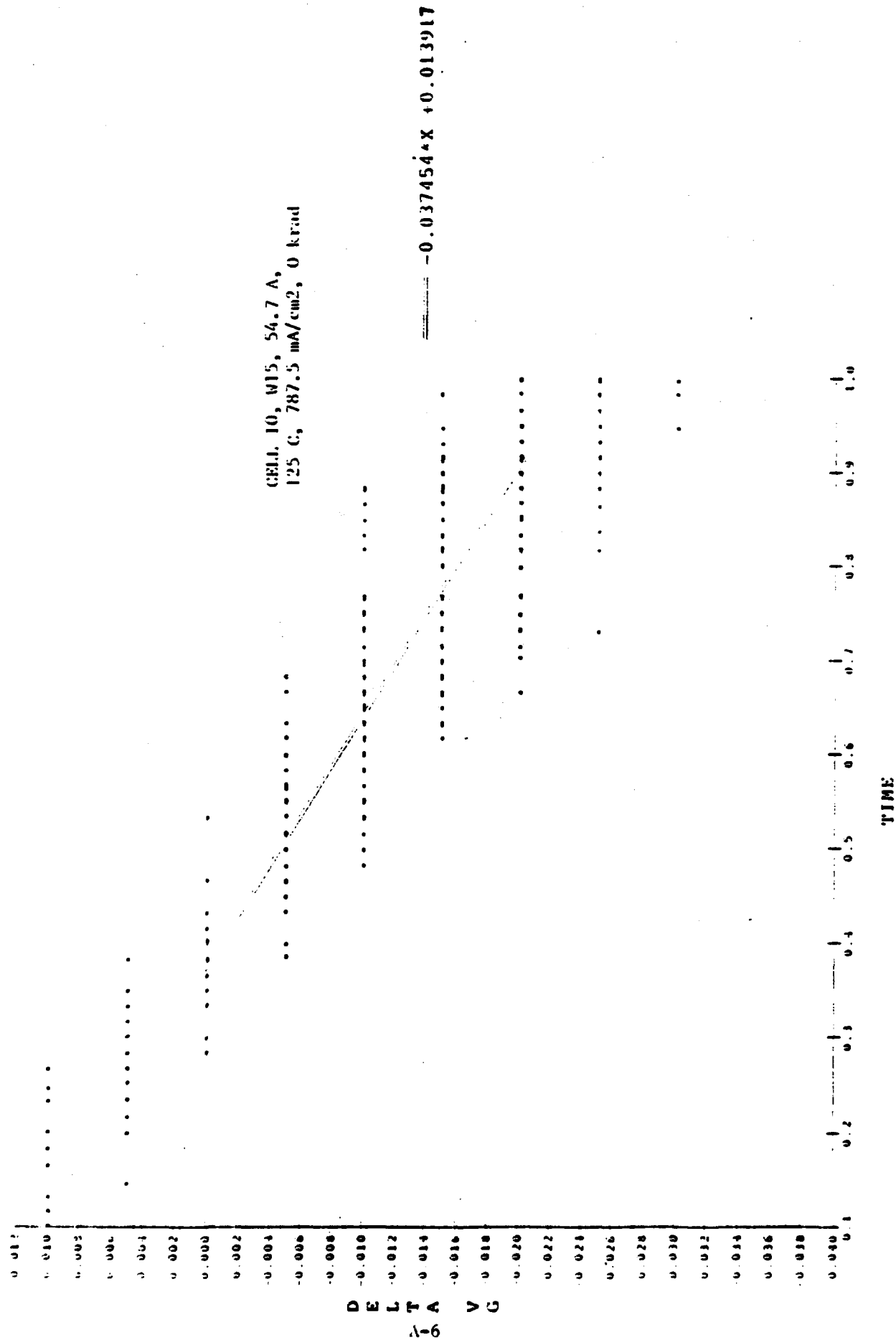


CELL 07, VI6, 61.0 A,
30 C, 787.5 mA/cm², 0 krad

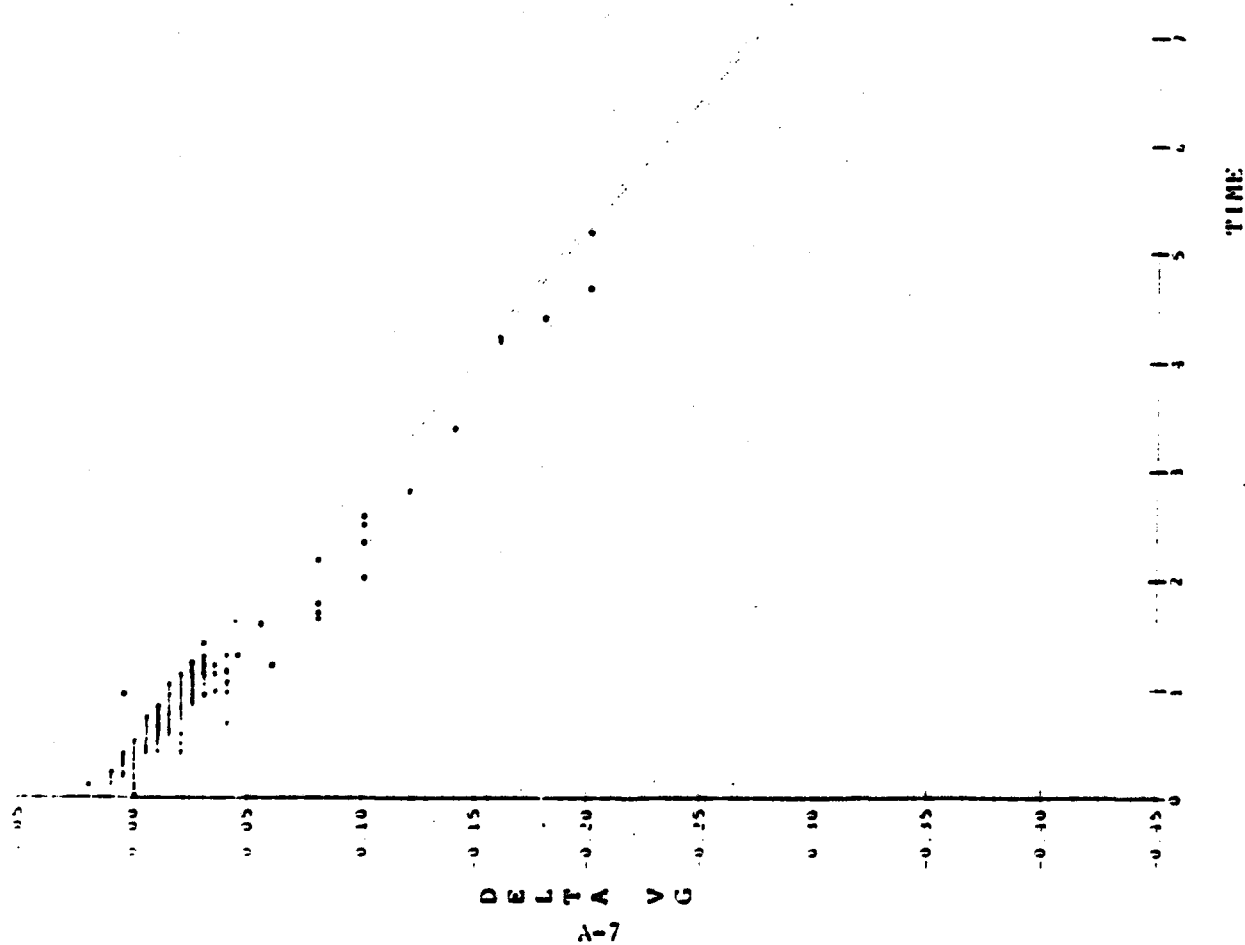
DELTA VG VS TIME FOR 503



DELTA VG VS TIME FOR W15



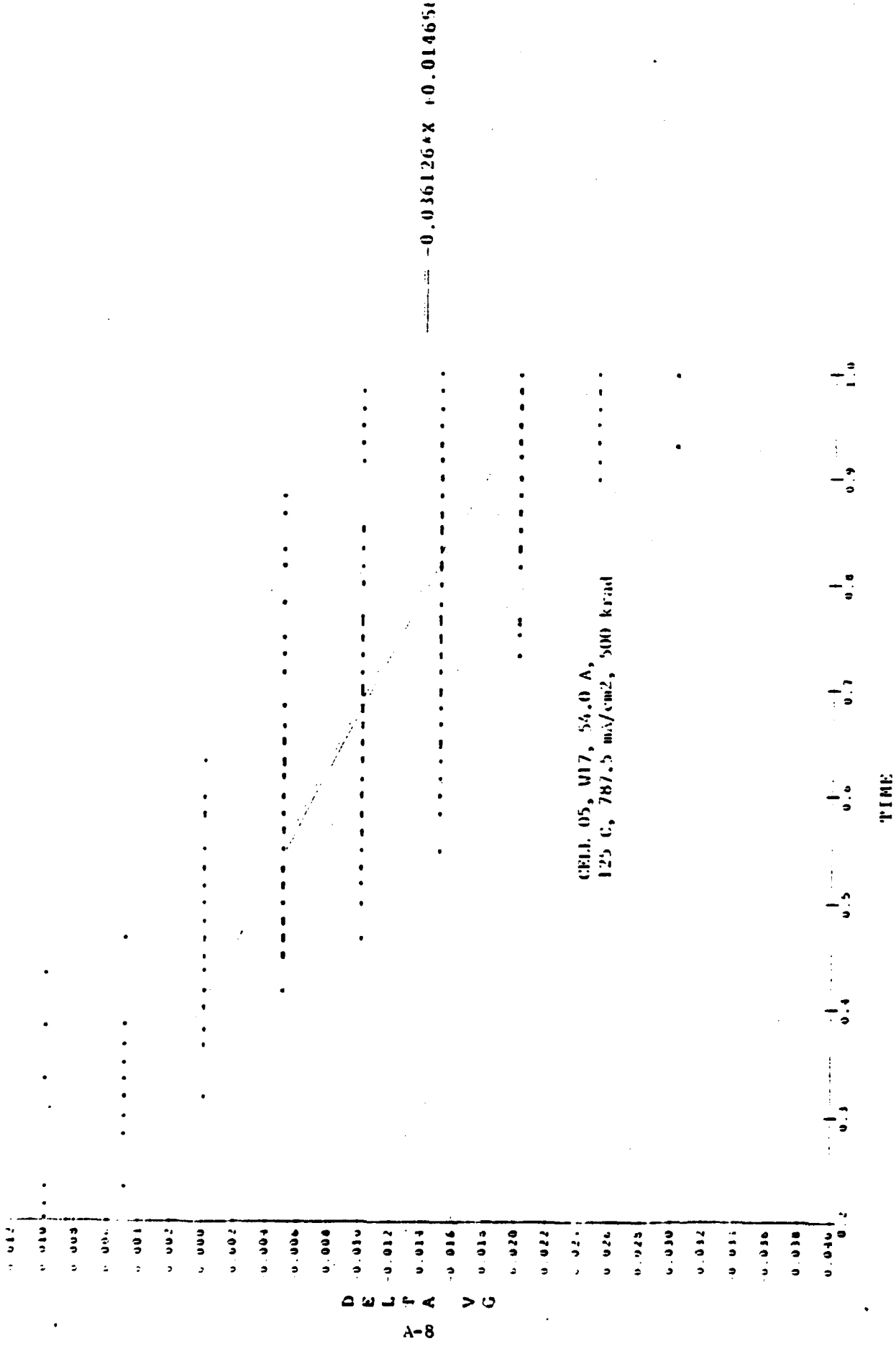
DELTA VG VS TIME FOR W01



CELL. 05, W01, 58.0 A,
125 C, 787.5 mA/cm², 500 krad

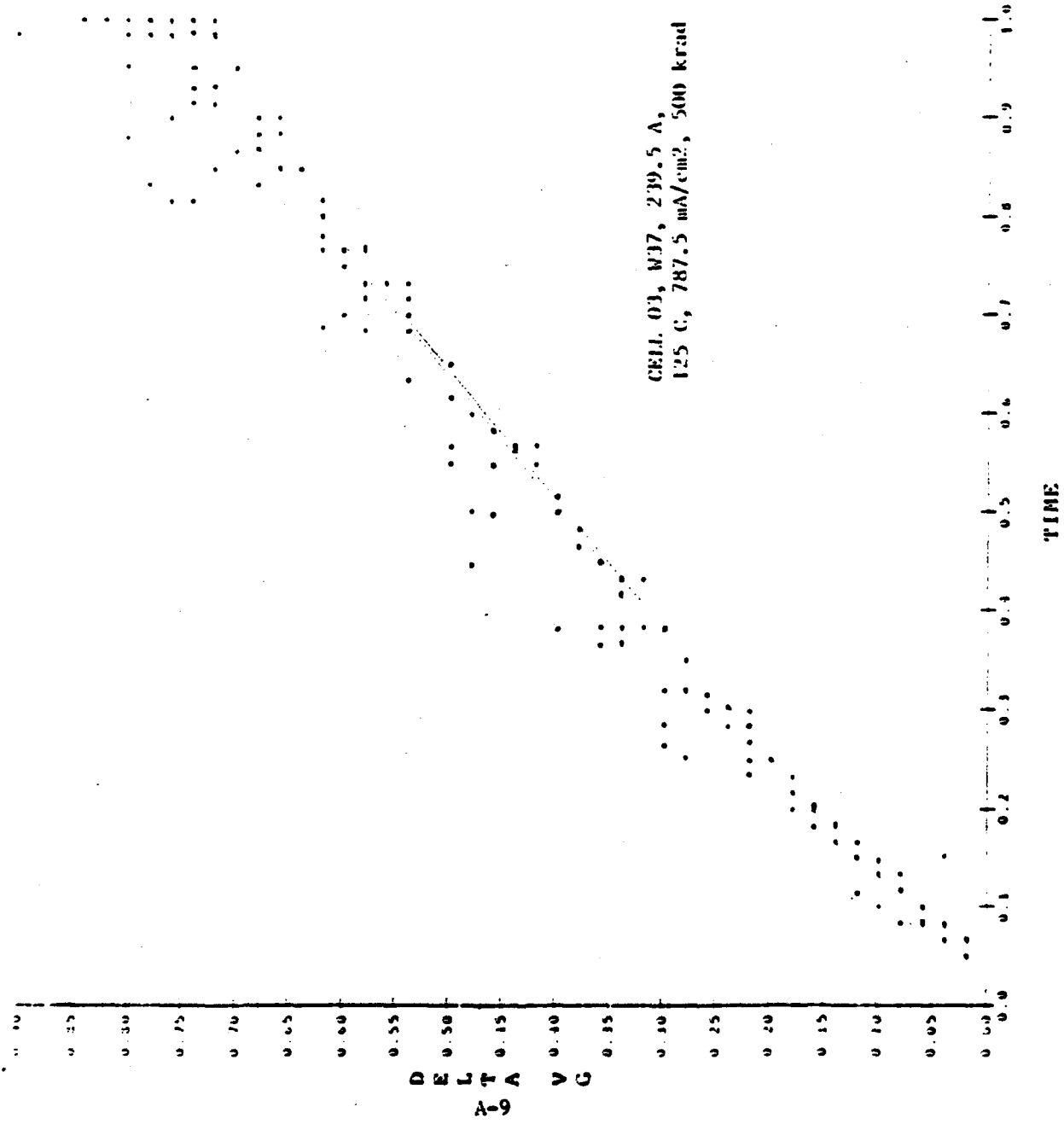
----- -0.041239 * X + 0.016322

DELTA V_G VS TIME FOR M17



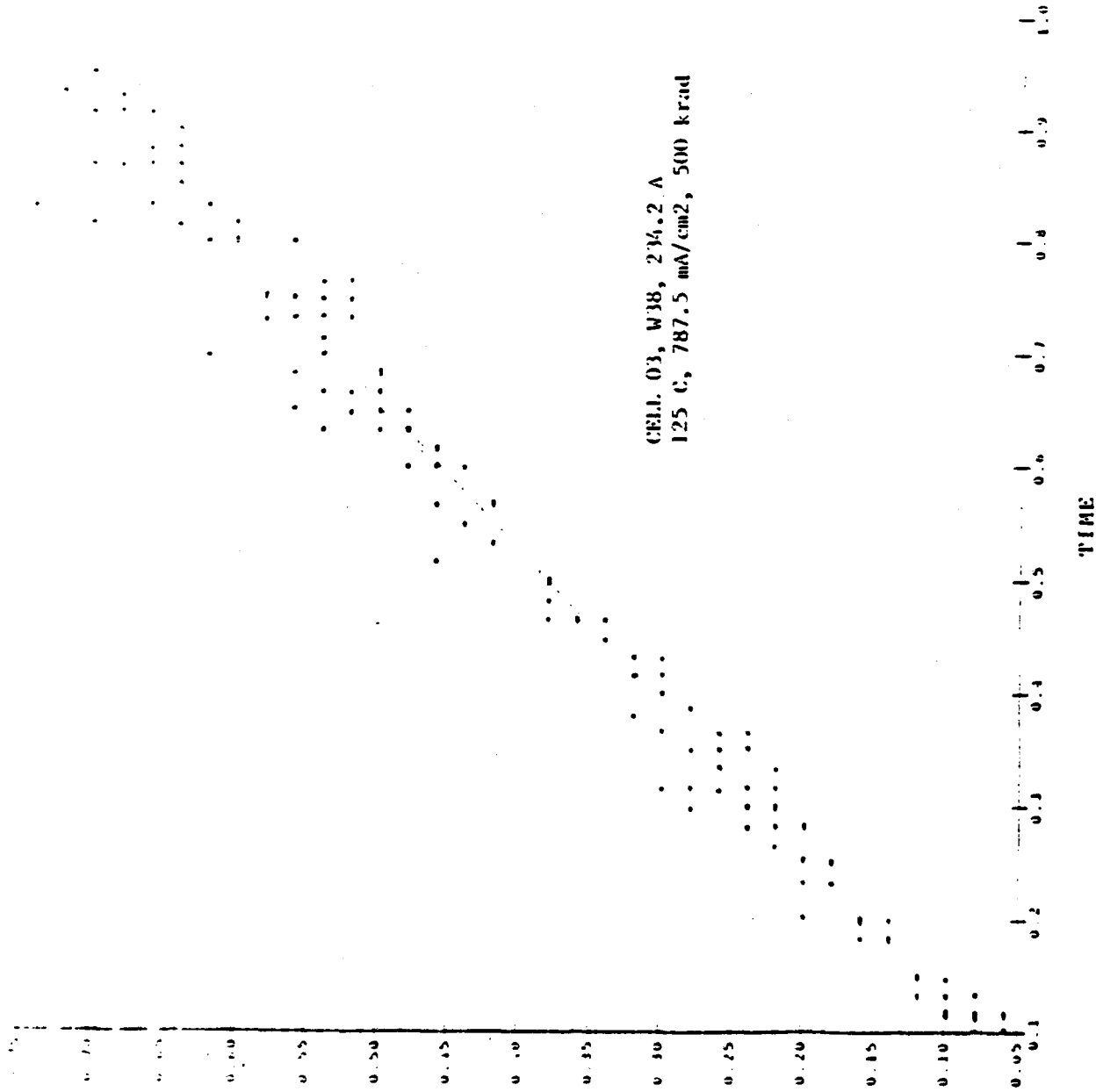
CELL 05, M17, 54.0 A,
125 G, 787.5 mA/cm², 500 krad

DELTA VG VS TIME FOR 937



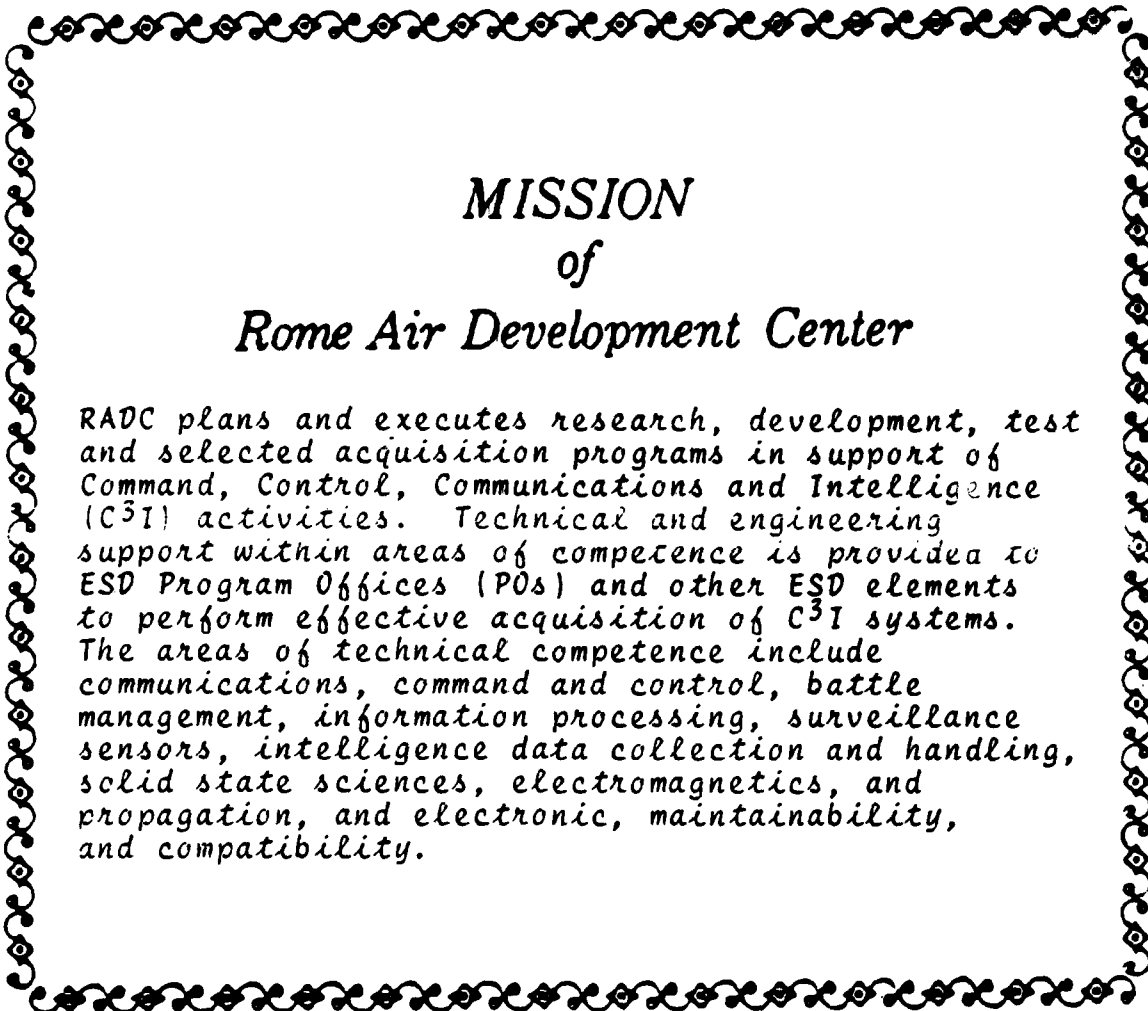
DELTA VG VS TIME FOR W38

DELTA
λ-10
VG



CELL. O3, W38, 234.2 A
125 C, 787.5 mA/cm2, 500 krad

----- 0.7594184X +2.067464e-03



*MISSION
of
Rome Air Development Center*

RADC plans and executes research, development, test and selected acquisition programs in support of Command, Control, Communications and Intelligence (C³I) activities. Technical and engineering support within areas of competence is provided to ESD Program Offices (POs) and other ESD elements to perform effective acquisition of C³I systems. The areas of technical competence include communications, command and control, battle management, information processing, surveillance sensors, intelligence data collection and handling, solid state sciences, electromagnetics, and propagation, and electronic, maintainability, and compatibility.